Water and chemical transport in limestone

Merging measurement and modelling concepts at different scales

Niels Claes

Master thesis:

2010-2011

Title: Water and chemical transport in limestone: Merging measurement and modelling concepts at different scales

Theme: Hydrogeological properties of a limestone aquifer

Project period: Autumn 2010 - Spring 2011

Project group: Niels Claes

Participant:

_____

Niels Claes

Supervisors:

Jacob Birk Jensen

Per Møldrup

Copies: 4
Page Numbers: 66
Appendixes: 15
Delivery date: 01.06.2011

Synopsis:

This master thesis analyses the hydrogeological properties that are determining the transport of water and solutes in a limestone aquifer. A closer look is been taken at the hydraulic conductivity and effective porosity of the limestone aquifer through experiments on small scale samples and an iterative process of in situ tests and numerical modelling.

This thesis provides a toolbox to investigate and describe the architecture of the dual porosity system in limestone by gas diffusion through small scale samples. The hydraulic conductivity and effective porosity of small scale samples are determined through indirect and direct measurement methods and visualisation techniques. These hydrogeological parameters are also defined for a limestone aquifer through an iterative process of in situ tests and modelling. These parameters for both scales are compared and connected to each other to conclude this thesis.

Acknowledgements and preface

This thesis is the result of the long master thesis project (60 ECTS) of Niels Claes during the Autumn semester 2010 and Spring semester 2011 within the Department of Civil Engineering at Aalborg University.

The chapters, sections and subsections in this master thesis are numbered in the order they occur in this thesis. The appendixes are alphabetically named, in the order they occur in the thesis. Whenever a reference to an appendix is made, this is done by only including their letter in the text, for example (Appendix B).
All figures, tables and equations in the text are numbered in the order they come in this thesis. The captions of all figures are given below the figure. The captions of the tables are placed above them. References in this thesis are made in parentheses, including the name of the author and the year of publication, for example (Claes, 2010). A reference that is made in the middle of a sentence refers to the information that is given directly before this reference.

I wish to thank my supervisors Jacob Birk Jensen and Per Møldrup for their supervision during the time of this thesis project and Kaj Henriksen for his advice. I also would like to thank Helle Blendstrup, Kim Mørkholt and Henrik Koch for their technical assistance with my experimental work.

This thesis has been made possible with the help of NIRAS and the Research Centre Foulum - Faculty of Agricultural Sciences – Aarhus University which I thank gratefully for their technical and logistical assistance. Furthermore I would like to thank the Soil-It-Is project for the opportunities that were given to me during the project period.

Contents

1 Introduction

The presence of fractured saturated zones such as limestone, sandstone and fractured clay may potentially pose significant environmental concerns due to the rapid, preferential migration of solute plumes through interconnected pore networks. Recent modelling studies related to fractured vadose and saturated zone processes are mostly limited to hydrogeological (water and solute) transport studies with very poor attention to the gaseous phase transport studies (Kristensen et al. 2010). A more detailed profile of the aquifer characteristics can be constructed through gas-diffusivity measurements, which can in turn be related to hydrogeological characteristics.

The main hydrogeological parameters that are considered in this thesis, because of their importance to water and solute transport in aquifers, are the saturated hydraulic conductivity and the effective porosity of the limestone. These parameters are analysed by three different groups of methods. The first group consists of indirect measurements through experiments in the gas phase on small scale samples (100 cm^3 samples) and by in situ experiments on a large aquifer. The second group consists of direct measurements on small scale samples. Next to these two groups of measurements direct visualisation of the limestone is performed through X-Ray CT-scans and IR image analysis as a last group of measurements.

The first three chapters of this thesis characterize the architecture of fractured limestone and its hydrogeological parameters on a small scale (100 cm^3 samples). The first chapter of this thesis provides a toolbox for characterising the limestone architecture in relation to tortuosity and pore connectivity. These two characteristics are vital towards the network that facilitates transport through the limestone network and are therefore also important in relation to the hydraulic conductivity and effective porosity. The second chapter of this thesis focuses on the liquid phase and flow of water in small saturated samples. Direct measurements of both hydraulic conductivity and effective porosity are performed on small scale samples and related to the earlier performed measurements in the gas phase. The third and last chapter that focuses on the small scale transport properties in this thesis handles visualisation of the limestone architecture. The effective porosity of the system is analysed through image analysis.

The second part of this thesis focuses on the hydrogeological parameters of a limestone aquifer on a larger scale. An iterative process between the modelling of the system and the performance of single-well tracer tests is carried out. This iterative process starts with a rough image of the hydrogeological situation and ends with a precise picture, established through changes and refinements that are carried out during this process.

A final comparison between the hydraulic conductivity and effective porosity on small and large scale concludes this thesis. The difference in values for these parameters based on the type of measurement group they belong to and the scale at what they are looked at is analysed and linked to risk analysis.

2 Characterisation of the limestone architecture through gas diffusion

Limestone can be considered as a dual porosity system (Figure 1). Fractures with a larger diameter (>10-20µm) are cutting through a denser matrix that is composed of a pore network with smaller pores (~1-10µm). This dual porosity is an important characteristic with respect to transport and flow through limestone aquifers or vadose zones.
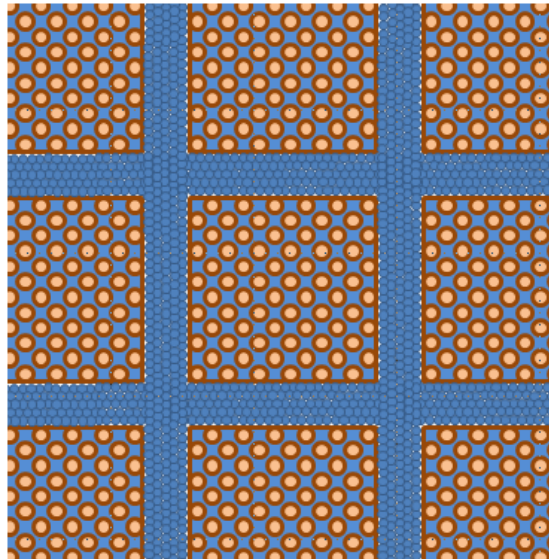
Figure 1: Dual porosity network in limestone (blue: water-filled fractures; brown: denser matrix)

The fracture network has the function of a highway for flow in both saturated and unsaturated conditions, while the denser matrix can be considered as a storage facility. Solutes can diffuse from the fractures into the matrix or the other way around, depending on the gradient that is present in the system. More information about these diffusion processes can be found in specialized literature (eg. (Janniche, Mouvet & Allbrechtsen 2010)) and are not discussed in this thesis.

One of the most important characteristics that influences the solute transport through the limestone is the tortuosity of this fracture network. The tortuosity, T, expresses the degree to which the actual travel distance deviates from the shortest distance between two points (Figure 2).
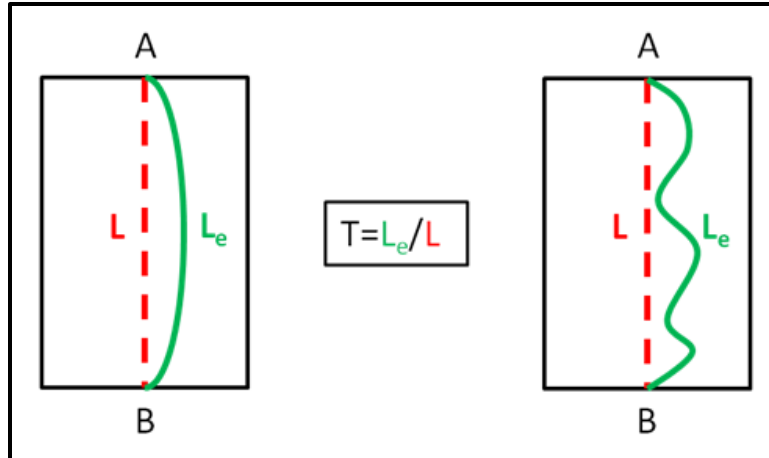
Figure 2: Example of Tortuosity, T (L is the shortest distance between A and B, Le is the effective travel distance); (Left) System with a low degree of tortuosity; (Right) System with higher degree of tortuosity

The time it takes to travel with the same velocity from one point to another point is longer in a system with a higher degree of tortuosity than in a system with a low degree of tortuosity. Hence a fracture network with lower tortuosity will facilitate the transport of water and solutes through the limestone aquifer.

A description about the tortuosity and the connection of pores, derived through gas diffusion experiments is given in the following part of this chapter. This description is given based on three different fingerprints. These fingerprints provide, just like fingerprints on a crime scene, a characterisation of the limestone architecture that is different for each individual sample.

These three fingerprints were presented on the CESAR (2010) conference during the poster sessions. The abstract of this presentation can be found in (Appendix O), together with the presented poster.

2.1 Materials and methods used in the analysis

2.1.1 Gas diffusion in limestone

Gas diffusion and diffusion in more general, is the movement of particles. In these gas-diffusion experiments, a closer look is been taken to the behaviour of gas particles that are diffusing trough the limestone sample as function of the air-filled pore-space: starting with a saturated sample and drying or draining it gradually. These experiments result in the curves that can be observed in Figure 3. Figure 3 shows the results of gas diffusivity (D_p/D_o, where D_p and D_o are, respectively, the gas diffusion coefficient in soil and in free air) against air content (ε).

A physical explanation behind the gas diffusion experiments is given in (Appendix A). The soil gas diffusivity increases with increasing soil-air content for all samples. This increase in D_p/D_0 occurs in 2 stages, which suggest that a dual-porosity model is more suited to describe this behaviour. The first stage is characterized by a linear increase, while in the second stage this increase shows a more exponential behaviour. The 2 different stages in the increase of D_p/D_0

are connected to the three fingerprints that are used to characterize the dual-porosity system in this section.

2.1.2 Data used in the analysis

In this section, a total of 13 fractured limestone samples which were sampled from two different vadose zone profiles in Denmark are considered: Gug limestone and Storvorde limestone (Figure 3) (data from (Kristensen et al. 2010)). From Gug limestone, two samples (ID 37 and ID38) taken vertically just below the ground surface, six samples (ID 28 and ID GKUG 1 to 5) taken vertically under the basement of a house, and two samples (ID 25 and 26) taken horizontally under the basement of the same house are analysed. Three Storvorde limestone samples were retrieved vertically about 2 m below the ground surface. For details on the sampling, preparation and measurements, see (Kristensen et al. 2010).
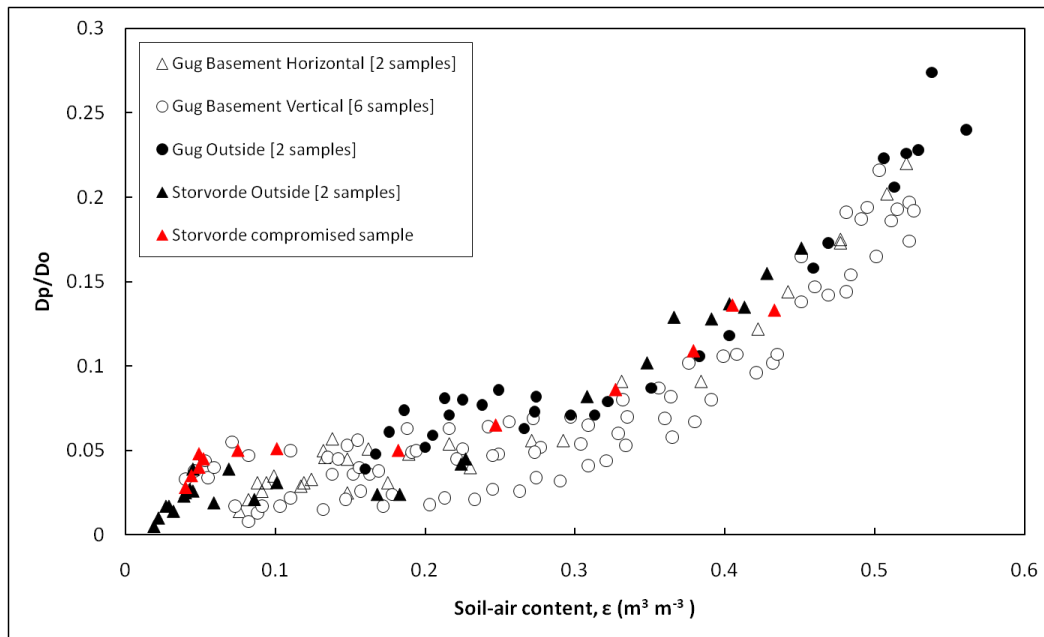
Figure 3: Obtained data from the gas-diffusivity experiments (data from (Kristensen et al. 2010))

Next to these 13 samples from which the data was recovered from literature, another 5 samples are measured on. These were sampled just under the ground surface at the Eternitten site in Aalborg. Details about their sampling and naming can be found in (Appendix C). The data from the measurements done on these 5 samples are enlisted in (Appendix D). The data from these measurements are not considered in the analysis of the tortuosity based on the three fingerprints that are presented in the following section but are used for further analysis in next chapters of this thesis.

2.1.3 Three Fingerprints describing Tortuosity and Pore Connectivity

A brief overview of the three used fingerprints to describe the limestone architecture is given together with an explanation how they relate to tortuosity and pore connectivity in limestone in this section. A more detailed explanation of each fingerprint, together with calculation methods and examples can be found in Appendix B.

Figure 4 situates the three fingerprints within the drainage process. On one side is the average angle of diffusion located. This fingerprint is based on gas diffusivity in the drained fracture network. On the other side of the drainage process is the modified Buckingham (1904) pore connectivity factor situated. This parameter describes the tortuosity and pore connectivity in the fully drained limestone matrix. In between these two fingerprints lies the two parameter exponential model, describing the tortuosity and pore connectivity inside the limestone matrix during gradually draining of the sample.
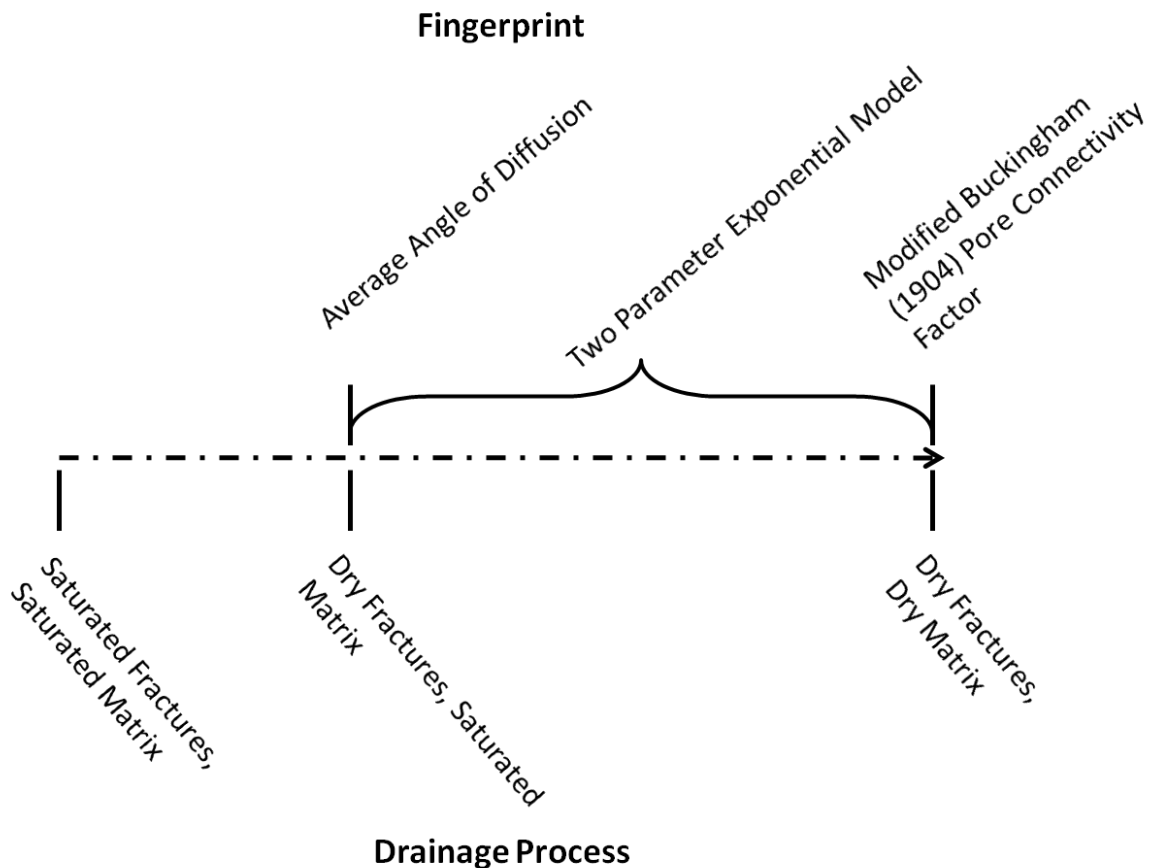
Figure 4: Overview of the fingerprints together with the phase in the drainage process they characterize

The average angle of diffusion, α

The orientation of fractures and the network they form is an important characteristic governing most of the fractured media transport processes. In this first fingerprint, therefore, the average angle of diffusion α within the fracture network (Moldrup et al. 2010) is observed for the selected

four soil groups. This fingerprint describes only the tortuosity in the fracture system that runs between the limestone matrix. The average angle of diffusion is determined by the diffusivity through the fully drained fractures (Figure 4). A higher angle of diffusion leads to a shorter pathway through the sample and less tortuosity.

The modified Buckingham (1904) pore connectivity factor, X*

For the second fingerprint of the fractured limestone, a modified Buckingham (1904) model for matrix diffusivity is adopted. This pore connectivity factor is a measure for the connectivity and tortuosity of the fully drained pore network in the limestone matrix (Figure 4). It is based on the Buckingham (1904) pore connectivity factor (see Appendix B) with a higher pore connectivity factor characterizing a system with a more tortuous pore network inside the limestone matrix. A modified version of the Buckingham model is suggested to describe the gas diffusivity in the matrix:

$$(D_p - D_{p0})/D_0 = (\varepsilon - \varepsilon_0)^{X^*} \qquad ; \varepsilon \geq \varepsilon_0 \tag{1.}$$

where D_{po} and ε_0 are, respectively, the gas diffusivity and air-filled porosity at the condition of fully drained fractures, and X^* is the modified Buckingham pore-connectivity factor. The average value of the three highest X^* factors for each sample is later used for comparison between the soil-groups to filter out any outliers

The two-parameter (A,B) exponential model

The non-linear increase in D_p/D_0 within the matrix (Figure 3) during the process of gradually draining of the sample can be described by a two-parameter exponential model by taking into account both the fracture connectivity and the matrix pore-connectivity as follows:

$$D_p/D_0 = Ae^{B\varepsilon} \; ; \varepsilon \geq \varepsilon_0 \tag{2.}$$

where A is the fracture connectivity factor, B is the matrix pore-connectivity factor, and ε_0 is the soil-air content at which all the factures are fully drained. Figure 5 illustrates the observed D_p/D_0 vs. ε in the matrix region for two selected samples together with the exponential model. Higher values of the fracture connectivity factor indicate a less tortuous and better connected network in the fractures.
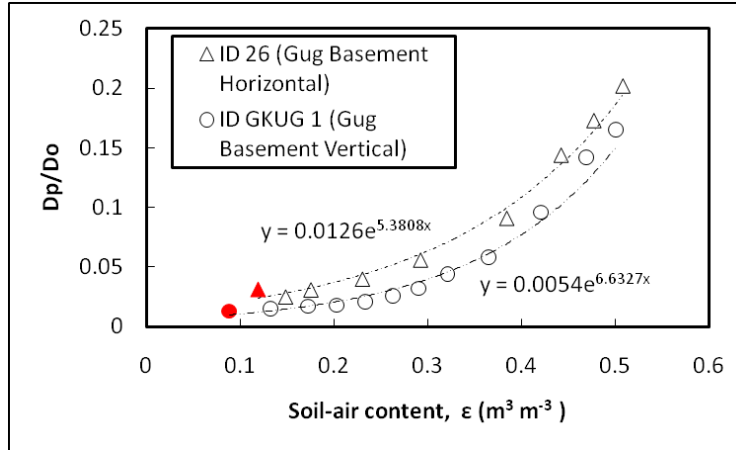
Figure 5: Example of the two-parameter (A,B) exponential model with the starting point in red; (upper) based on data from ID 26; (lower) based on data from ID GKUG 1

This exponential model that describes the behaviour inside the matrix during gas diffusion experiments is not only dependent on the behaviour inside the limestone matrix. As can be seen on Figure 5, the model is dependent on the starting point of the drainage in the matrix system. To obtain a model that is more independent of the behaviour in the fractures, an axis transformation is carried out (Figure 6). This results in following model:

$$\left(\frac{D_p - D_{p0}}{D_O}\right) = A^* \ e^{(B^*(\varepsilon - \varepsilon_0))} \tag{3.}$$

Where D_{p0} and ε_0 are respectively the gas diffusivity and air filled porosity at the moment that the matrix starts to drain. A^* and B^* are respectively the modified fracture and matrix pore-connectivity parameters, analogue to eq. (2).
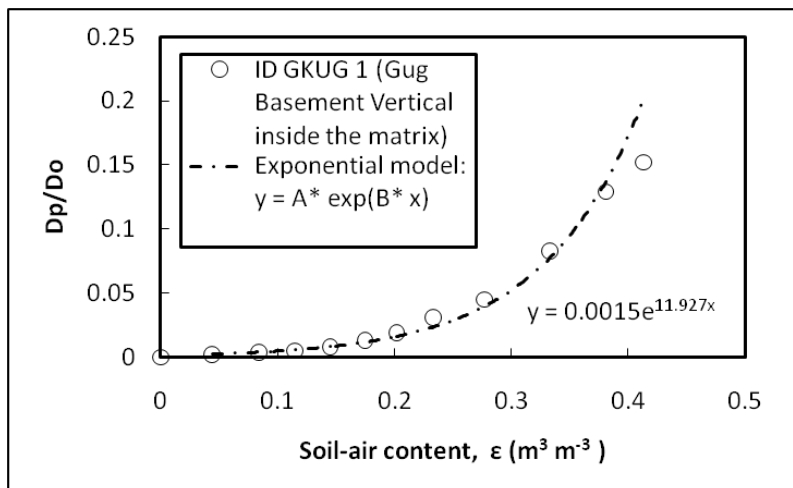
Figure 6: Exponential model (A*,B*) describing the behaviour inside the matrix for sample ID GKUG 1

2.2 Results and discussion

The obtained results for the three fingerprints are discussed individually in the next paragraphs after which they are merged together to give an overview of the internal matrix characteristics on one side and fracture characteristics on the other side. Before the results are analysed and discussed, a comment has to be made towards the analysis and the area on the border between the flow in the fractures and the matrix in the gas diffusion experiments.

The border between the fracture network and the matrix network, is an area that should carefully be approached (Figure 7). The slight drop in gas-diffusivity in the transition area between a complete drained fracture network and the start of the drainage of the matrix, can be explained by a reconfiguration in the solid-liquid phase. The thin film of microbial activity that might be present on the matrix border will go in solution and can potentially influence and hinder flow in the fractures. This can cause a drop in observed diffusivity (Figure 7 (red area)). The same definition for the start of matrix drainage has to be used for all the samples to take this effect into account during the analysis. In the analysis in this thesis, the drainage process in the matrix is considered started, after the decrease of diffusivity has occurred.
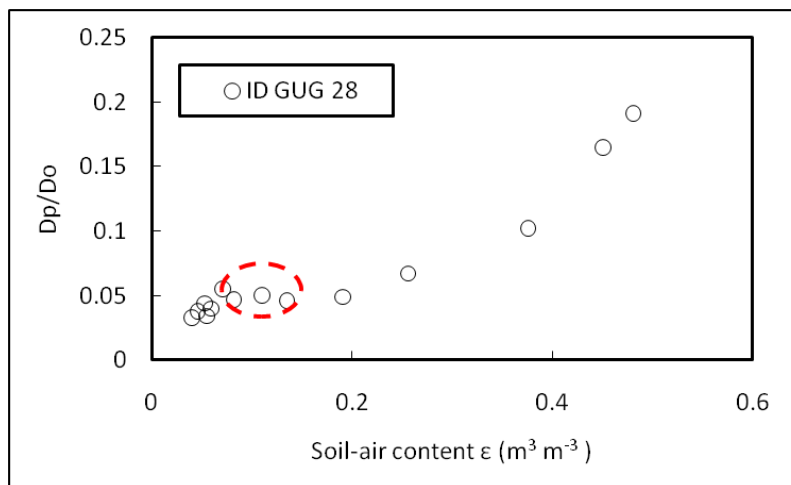
Figure 7: Example of a gas diffusivity curve with a small decrease in diffusivity on the border between matrix and fracture drainage (area circled in red)

2.2.1 The fingerprints separately

The results of this analysis are presented both with and without taking the percolation threshold of the fractures into account. The percolation threshold describes the phenomenon that the drainage of pores of a certain size not always results in an increase in gas diffusion through the sample. This percolation threshold is determined by the unconnected pores and series of pores of subsequent size that have to be drained before a connected path through the sample is drained (Appendix A). The reason of this dual analysis is that preceding this analysis, the hypothesis was that this percolation limit for these small samples would be completely random and have no physical meaning. Yet, after performing this dual analysis, this thought seemed to be incorrect.

The average angle of diffusion, α

The observed smaller average angle of diffusion for the samples taken below the basement compared to the samples taken from outside (Figure 8) can be attributed to the soil compaction that has been occurred under the building. A higher compaction will lead for the same soil type to a higher tortuosity and a lower average angle of diffusion in the fractures. The difference in angle of diffusion and tortuosity is clearer without taking the percolation into account. This indicates that the tortuosity in the fractures is dependent on how well the pores are connected and their size distribution.

Figure 8: Average angle of diffusion in the fractures for the different samples; (left) Analyses without percolation threshold; (right) Analyses with percolation threshold

*The modified Buckingham (1904) pore connectivity factor, X**

Figure 9 gives an overview of the maximum and minimum value for the modified Buckingham pore-connectivity for each sample-group, together with the average value. The maximum value for the modified Buckingham pore-connectivity is lower for the limestone in the surface layer in Gug due to a lower compaction of these samples, in comparison with the ones that were taken in Gug under the basement of the building. This absence of compaction will result in less tortuosity and a lower internal pore-connectivity factor.
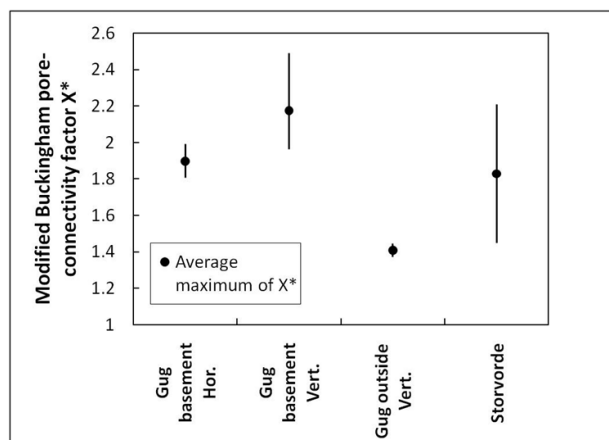
Figure 9: The interval and average of the maximum values for X*

Except for the uncompacted Gug limestone, other Gug and Storvorde limestones have an average X* factor close to 2, the value suggested by Buckingham (1904). Further, the slight anisotropy observed for the fractured region for Gug samples (under the basement) (Figure 3) could also be noticed in the matrix region (Figure 9).

The two-parameter (A,B) exponential model
Figure 10 (left) illustrates the observed D_p/D_o vs. ε in the matrix region for one selected samples together with a fitted exponential model (Eq. (2)). The same data, when presented in a log-normal plot, yield a linear relation (Figure 10 (right)).
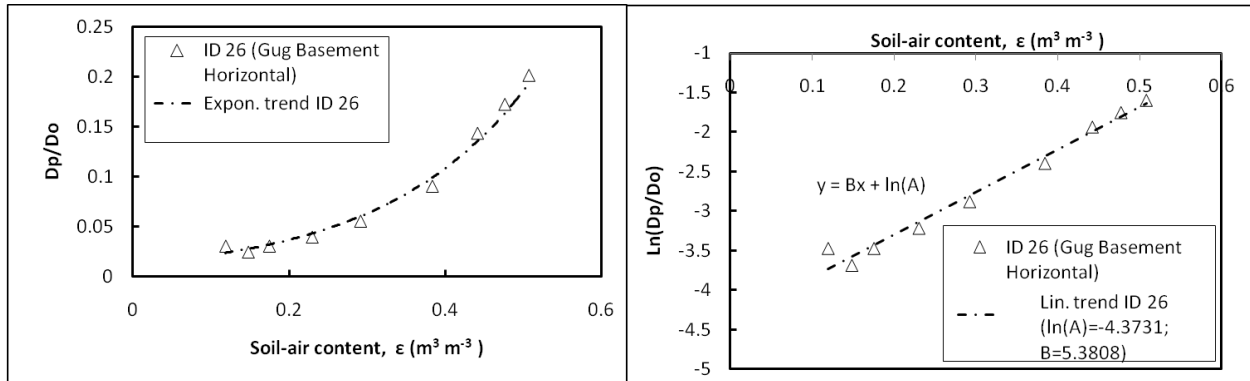
Figure 10: Gas diffusivity in the limestone matrix (left) D_p/D_0 vs. ε; (right) ln(D_p/D_0) vs. ε

An apparent overall linear relation between the parameters A and B (Figure 11) is observed, which can be adequately described by:

$$B = -117\,A + 6.94 \tag{4.}$$
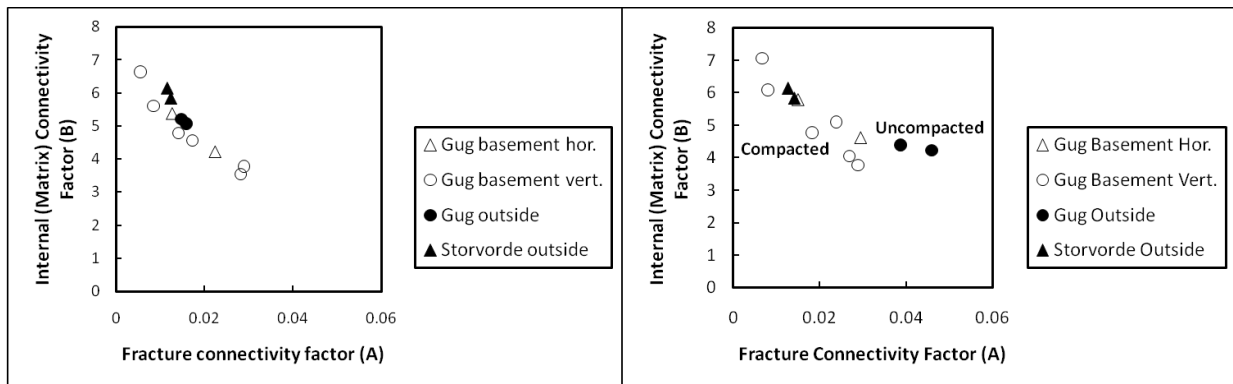
Figure 11: Relation between the fracture connectivity and the internal connectivity: (left) Analyses without percolation threshold (right) Analyses with percolation threshold

Taking the percolation threshold into account during the analyses results in a clear separation between the compacted and the uncompacted limestone structure. A clear correlation occurs between the matrix connectivity factor, the fracture connectivity factor and whether there is compaction of the limestone or not.

Figure 12 shows the values for the explicit connectivity factor, B*, after the transformation (eq. (3)) of the two parameter model. The more compacted samples have a lower value for the explicit matrix connectivity factor. This is different to the results of the internal connectivity factor B (Figure 11 (left)) which shows a less clear relation for between B and whether there is compaction. This less clear relation is due to the influence of the tortuosity of the dry fracture network. This influence of the fracture network has been eliminated in the modified two parameter model, which results in higher explicit matrix connectivity factor, B*, for less compacted samples (Figure 12).
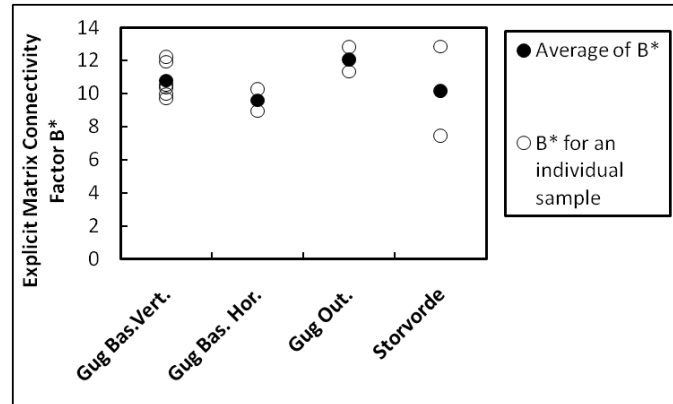
Figure 12: The individual and average value for B* for each sample group

2.2.2 Merging the fingerprints

The fracture network

It is clearly shown that compaction results in a more tortuous external network when the fingerprints which characterize the fracture (external) network are compared (Figure 13). The average angle of diffusion will decrease under the pressure by the compaction and the fracture connectivity will decrease.
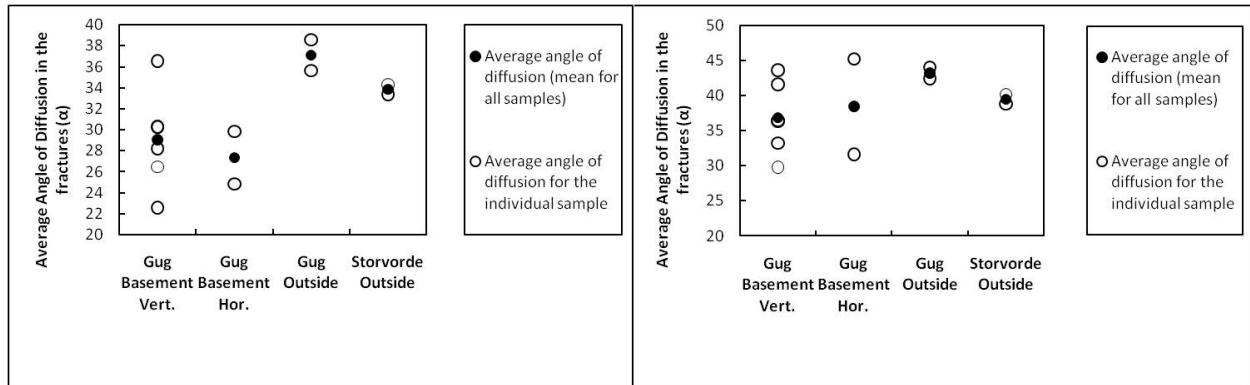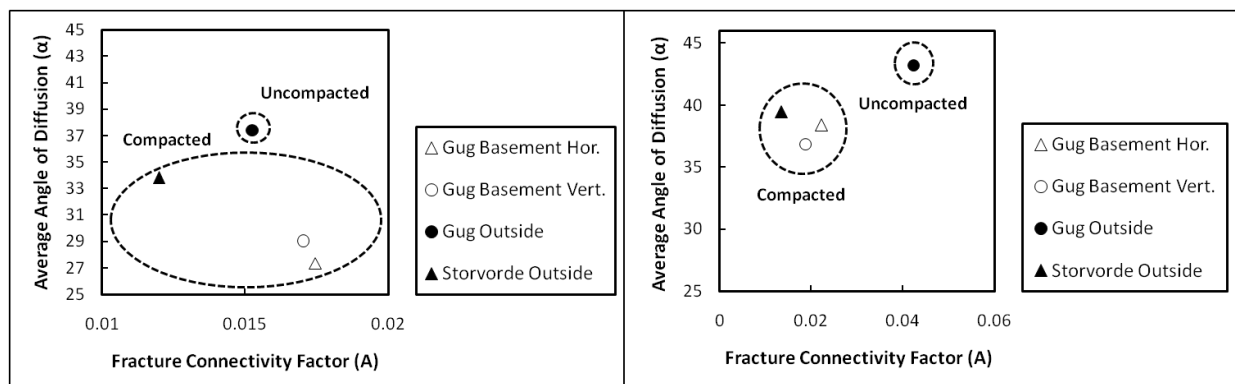

Figure 13: Relation between the fracture connectivity and average angle of diffusion in the fractures (left) Analyses without percolation threshold (right) Analyses with percolation threshold

The limestone matrix

The internal (matrix) connectivity factor and the modified Buckingham pore-connectivity factor both characterize the tortuosity inside the limestone matrix. As can be seen on Figure 14 results a lower compaction in a lower value for both fingerprints. The difference in both analyses (Figure 14) is caused by the correlation between the Internal (Matrix) Connectivity Factor, B, and the Fracture Connectivity Factor, A, as described in Eq. (4).
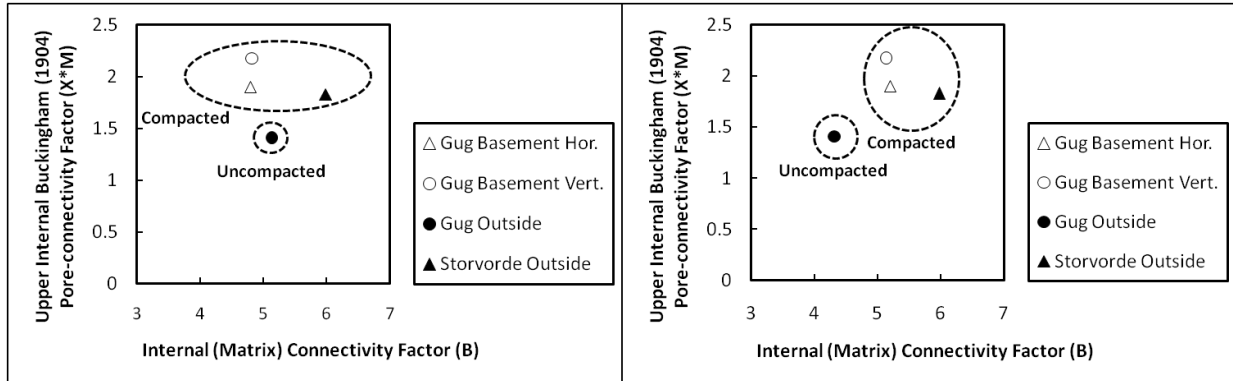
Figure 14: Relation between the internal (matrix) pore-connectivity factor and the modified Buckingham pore-connectivity factor; (left) Analyses without percolation threshold; (right) Analyses with percolation threshold

The description of the tortuosity inside the limestone matrix, without the influence of the fracture network, can be seen on Figure 15. Lower compaction results in lower tortuosity. This is expressed by both a higher explicit matrix connectivity factor and by a lower modified Buckingham (1904) pore-connectivity factor. The first expresses a better connected pore-network inside the matrix, while the second demonstrates a lower tortuosity in the limestone matrix.
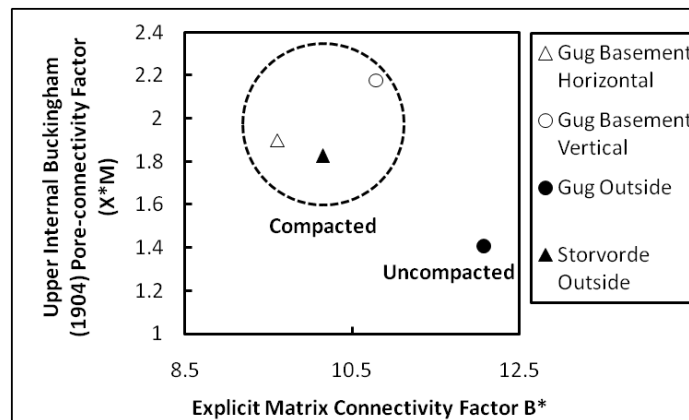
Figure 15: Relation between the modified Buckingham (1904) pore-connectivity factor and the explicit matrix connectivity factor

2.3 Conclusion

Gas diffusion measurements result in a non-destructive way to measure architectural fingerprints of intact limestone samples. The three presented fingerprints provide valuable insight into both the fracture tortuosity and connectivity on one side and the matrix pore-connectivity on the other side.

The fracture network within the limestone facilitates the transport of water and chemicals through the limestone. The average angle of diffusion, which describes the tortuosity and pore connectivity in the fracture network, shows that less compaction results in a less tortuous fracture network.

The modified Buckingham (1904) connectivity factor X^* gives a fingerprint of the limestone matrix. The tortuosity inside the limestone matrix is related to the compaction or stress that has been carried out on the limestone. A higher tortuosity (because of compaction) results in higher values for X^*.

The two-parameter exponential model shows that the diffusivity in the fracture network is related to the diffusivity within the limestone matrix. A lower diffusivity in the fracture network results in a lower diffusivity in the limestone matrix and hence connects the tortuosity in both networks with each other.

The inactive pore space, drained in the beginning of the drainage process (see Appendix A), should not be neglected in this analyses. This is demonstrated by the difference in results for both the average angle of diffusion and the fracture connectivity, which both characterise the fracture network and its tortuosity and pore connectivity.

3 Characterization of the limestone architecture in the liquid phase

The hydrogeological properties on a small scale can be determined by different methods. One method is by using the measurements that are obtained through gas diffusion experiments as have been performed in previous chapter. The other method is to perform direct measurements and fully saturate the samples before measuring the saturated hydraulic conductivity and effective porosity on them. This last method is more destructive than the method that uses gas diffusion. Erosion of the sample occurs when water is forced through the sample by applying a hydraulic gradient, while gas diffusion only induces water flow at a slow velocity during the process of draining. The results of these liquid phase experiments are connected to the earlier performed measurements and previous derived characteristics. The hydraulic conductivity that is referred to in this chapter is the saturated hydraulic conductivity.

3.1 Materials and methods used in the analysis

3.1.1 Direct measurements

Hydraulic conductivity measurements are performed on the samples after they have been saturated. Details about the saturation and the experimental setup can be found in (Appendix F). The effective porosity of the samples is determined next to the direct measurement of the hydraulic conductivity by measuring the weight difference between the saturated samples and their weight after draining at pF. 2.

The set of samples that is analyzed during this liquid phase experiment are the samples that are sampled at the Eternitten site. This is the same set as the second set, mentioned in the materials of the gas diffusion analysis. More details about the sampling of these samples can be found in (Appendix C). The set of samples is divided into 3 subsets, depending on their total porosity (Appendix E). The denser samples (2ETVC and 2ETHB) have a total porosity around 0.41, the looser samples (1ETVA and 1ETHB) around 0.51 and the fragile sample (1ETHC) has a total porosity of 0.55.

3.1.2 Indirect measurements

The flow of water and solutes will be governed by the larger pores or fractures in limestone. They are the more important flow paths when it comes both to flow in the gas phase as flow in the liquid phase. Hence their characteristics will contribute most to the permeability in the gas and liquid phase. The physical characteristics that are derived by gas-diffusion measurements can therefore be used to predict the saturated hydraulic conductivity (Poulsen et al. 1999).The data from the earlier performed gas diffusion measurements is analysed in this section.

Theoretical derivation

The saturated water permeability, $k_{l,s}$, can be estimated from the gas diffusivity at a pore water potential of -100 cm, $D_{g,100}$, when the larger pores up to 30 µm are drained (Poulsen et al. 1999):

$$k_{l,s} = \left(\frac{r_l^2}{8} \frac{D_{g,100}}{D_0} \right)^{\beta_l} \tag{5.}$$

Where r_l (=30 µm) is the equivalent tube radius for water flow and β_l (=1.05) is the pore connectivity parameter that corresponds to this. The hydraulic conductivity is determined from the saturated water permeability through following relationship:

$$K_{Sat} = k_{l,s} \frac{g}{\nu} \qquad (6.)$$

where K_{Sat} is the saturated hydraulic conductivity; g is the gravitational constant ; and ν is the kinematic viscosity.

The analysis of the hydraulic conductivity by means of gas diffusion is performed on two sets of samples. The first set of samples consists of the samples that are also used in the first chapter to describe the limestone matrix and its tortuosity (Gug & Storvorde samples). The second set of samples consists of 5 samples that were sampled at the site of Eternitten, located in Aalborg (Appendix C).

3.2 Results and discussion

3.2.1 Direct measurements

Hydraulic conductivity
Table 1 shows the measured saturated hydraulic conductivity for the 5 samples:

Table 1: Results of saturated hydraulic conductivity measurements

Sample	Saturated Hydraulic Conductivity [m/s] (1st run)	Saturated Hydraulic Conductivity [m/s] (2nd run)
1ETVA	3.39E-05	
1ETHC	2.56E-04	1.28E-04
1ETHB	1.18E-05	0.39E-05
2ETVC	3.44E-06	
2ETHB	1.38E-05	

The experiment is repeated for two samples to see whether the experiment is reproducible. This second run results in lower values for the hydraulic conductivity. Two phenomena are considered to cause a difference in values for the hydraulic conductivity between consecutive runs. These two phenomena that occur during the experiment are both induced by erosion of the larger pores. The erosion itself will enlarge and smoothen the larger pores or fractures which results in a network with a lower tortuosity. The erosion material will at the same time cause smaller pores to get clogged. This results in a more tortuous network. This last process is most likely the cause for the smaller hydraulic conductivity that is observed in the second run of the experiment.

Effective porosity

The values for the effective porosity for each sample are enlisted in (Table 2).

Table 2: Effective porosity of each sample (sample set from Eternitten)

Sample	Effective porosity, n [cm^3 air/cm^3 sample]
1ETVA	0.17
1ETHC	0.26
1ETHB	0.09
2ETVC	0.14
2ETHB	0.12

The higher effective porosity of sample 1ETHC can be linked to the higher hydraulic conductivity of this sample (Table 1). This higher effective porosity can be attributed to the gravel-like structure which can be noticed inside the sample (Appendix E). This gravel-like structure causes preferential flow-paths to occur more easily than in the samples with a denser structure. The larger diameter of the pores between the individual gravel blocks are causing a higher velocity of the water flowing through.

3.2.2 Indirect measurements

Calculated from the gas-diffusion measurements, earlier presented in this thesis, a saturated hydraulic conductivity is presented for both sample sets (Figure 16). Only the fracture network drained at pF. 2 is contributing to this hydraulic conductivity.
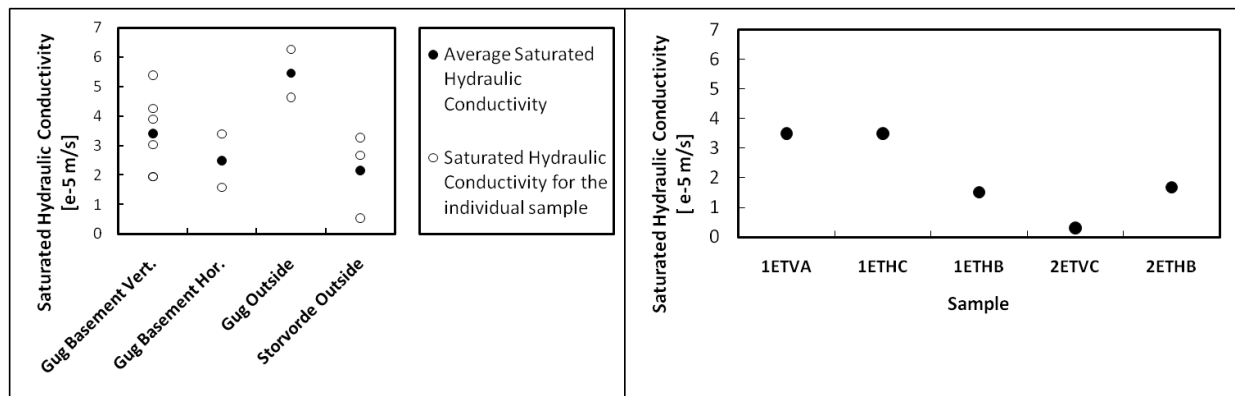
Figure 16: Saturated hydraulic conductivity values: (left) 1st sample set (Gug & Storvorde samples); (right) 2nd sample set (Eternitten samples)

Limestone with a fracture network that consists of smaller pores will have a lower hydraulic conductivity than the fracture network with bigger pores. As stated earlier, the saturated hydraulic conductivity is defined by the larger drained pores or fractures.

3.2.3 Merging the liquid phase characteristics with the gas phase

Figure 17 compares the hydraulic conductivity that is determined through indirect measurements with the tortuosity of the fracture network, expressed by the average angle of diffusion. The average angle of diffusion is a measure for the tortuosity of the complete fracture network, while the indirect method for the hydraulic conductivity only considers the larger fractures (>30µm). The same trend or relation between the hydraulic conductivity and the average angle of diffusion can be observed for samples that have a fracture network with larger well-connected pores. This relation is not observed for a fracture network that consists of smaller pores or larger unconnected pores, such as the samples from Storvorde Outside in Figure 17.
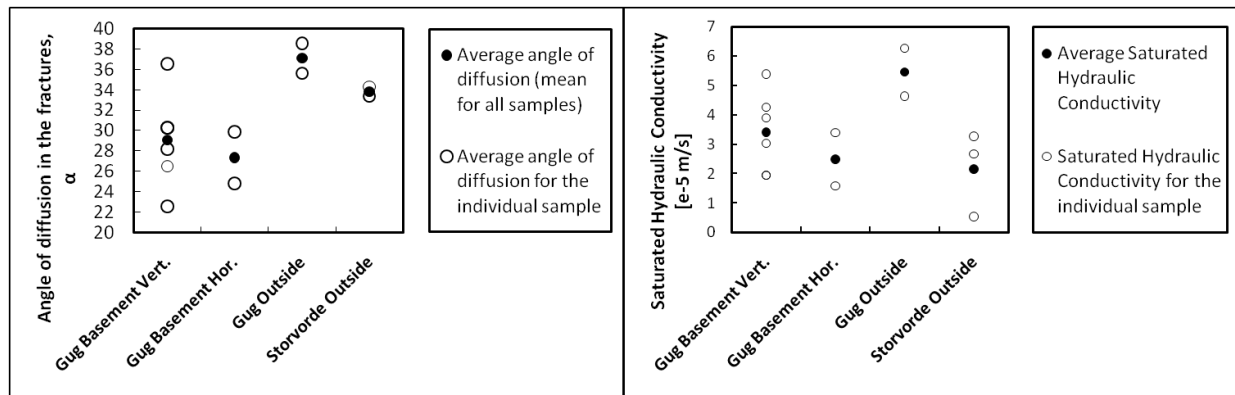
Figure 17: (left) Average angle of diffusion; (right) Saturated hydraulic conductivity (both for Gug & Storvorde samples)

Figure 18 gives an overview of the different parameters that characterise the limestone matrix and their relation towards the hydraulic conductivity for the samples taken from Eternitten. Figure 18(a) demonstrates the relation between the saturated hydraulic conductivity and the gas diffusivity in the samples when the larger pores (>30µm) are drained. Both gas diffusivity and saturated hydraulic conductivity are transport parameters and give an indication about how well-connected the larger pore network is. A well-connected pore network results in a faster flow, hence a higher hydraulic conductivity. The relationship between the gas diffusivity and the saturated hydraulic conductivity (Figure 18 (a)) was originally derived for sandy soils with a mixture of clay and silt (Poulsen et al. 1999). This relation also fits for the denser and looser limestone samples as can be seen on Figure 18(a). The fragile limestone sample does not comply with this relation. There is an analogy between this fragile sample and soils that consist of gravel. Preferential flow paths arise when drainage takes place because of the larger radius of the pores that drain during the first steps of the gas diffusion experiment.

Figure 18(b) presents the same information as Figure 18(a), yet the diffusivity values are transformed to hydraulic conductivity values by using the Poulsen (1999) relationship. This allows a direct comparison of both values derived from direct and indirect measurement for the saturated hydraulic conductivity.
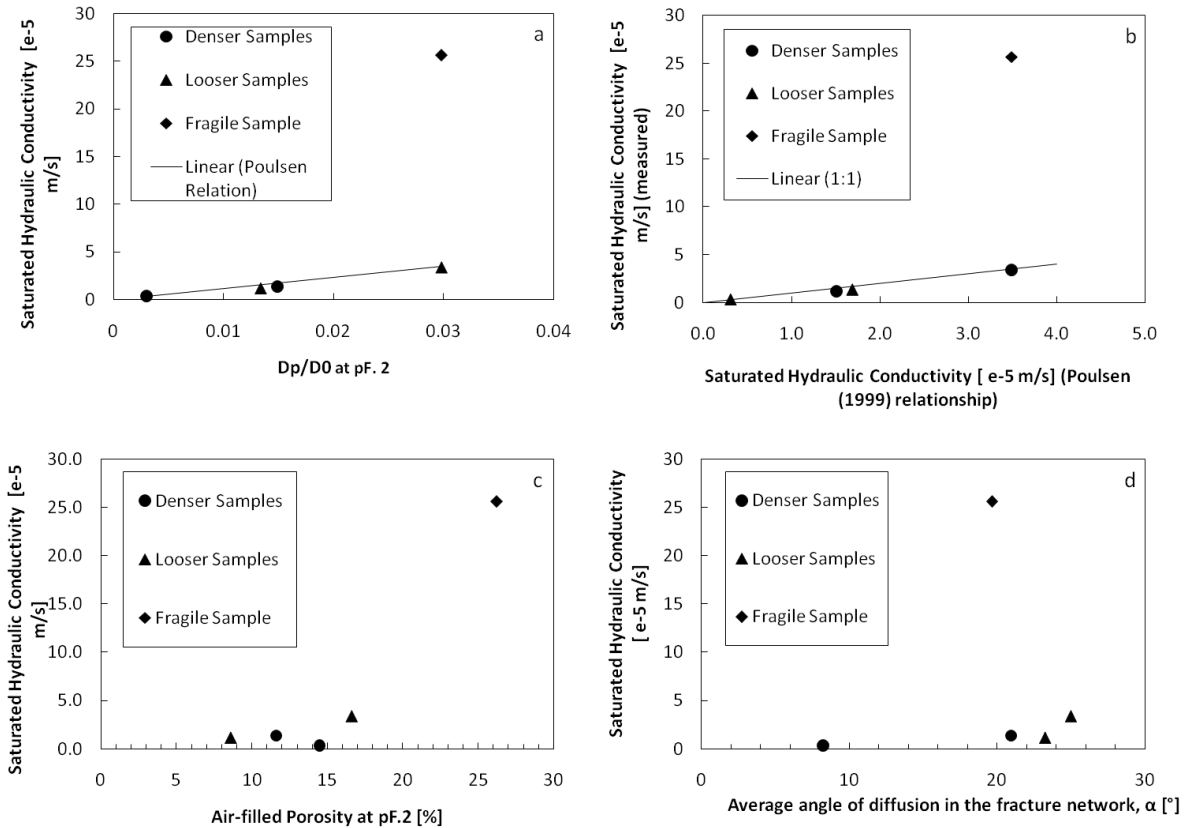
Figure 18: Overview of the relationship between the different limestone characteristics and the saturated hydraulic conductivity: (a) Dp/D0 at pF.2 vs. Ks (direct measured); (b) Calculated Ks from gas diffusivity (indirect measured) vs. Measured Ks (direct measured); (c) ε100 vs. Ks (direct measured); (d) α vs. Ks (direct measured)

Figure 18(c) compares the saturated hydraulic conductivity with the air-filled pore space at pF.2. Whereas the saturated hydraulic conductivity is a parameter that characterizes directly the transport properties of the limestone, the air-filled pore space does not. The air-filled pore space indicates the potential of a network that facilitates flow to occur. If the pore system is not good connected, the network is not suited for flow and a lower hydraulic conductivity is the result. An example of this are the two samples with both an air filled pore space of around 15% (vol.%) but with a different value for saturated hydraulic conductivity (Figure 18 (c)).

A last parameter that is compared with the saturated hydraulic conductivity is the average angle of diffusion, α. This parameter combines both the air-filled pore space at pF.2 with the diffusivity at the same drainage level. The potential of the network to facilitate flow and a transport parameter that actually defines this flow are combined in this angle of diffusion. Figure 18(c) and (d) demonstrates that one of the looser samples has the lowest air-filled pore space at pF.2 but still has a higher average angle of diffusion. The drained pore network of this sample is better connected and facilitates the flow better than the denser samples with a higher air-filled pore space.

3.3 Conclusion

The effective porosity and hydraulic conductivity, two parameters that are important for the transport of water and solutes through the limestone aquifer have been determined for small scale samples in this chapter. The effective porosity and has been determined through direct measurement of the samples, while the hydraulic conductivity of small scale samples has been established through both direct and indirect measurements. These measurements can be linked to the architecture of the fracture network that runs through the limestone matrix. The corresponding values for the hydraulic conductivity determined by indirect measurements through gas diffusion experiments and by direct measurement, demonstrate that this system of larger fractures is the most important part of the limestone architecture that facilitates the flow of water and solutes through the limestone.

4 Visualisation of the limestone structure

4.1 X-ray Computed Tomography

The dual-porosity structure in limestone can be divided in two parts. The larger macro-pores or small fractures are situated on one side. These will facilitate the flow of the water through the structure. On the other side are the smaller micro-pores in the limestone matrix situated. Their contribution to the overall water flow through the limestone is not significant; however, the interaction between the macro-pores and micro-pores with regards to the dynamics concerning the pollutant-exchange is critical. Several techniques to get a better understanding or overview of this structure inside the limestone comprise of diffusion of gasses through the sample at different matrix potentials (change in air-filled porosity). Other techniques measure the overall hydraulic properties of the samples when they are fully saturated. All these techniques risk to influence the structure of the samples and to deform their inner architecture in some way. A non-invasive technique to explore the pore geometry of the limestone sample on small scale is image analysis. Images that are generated by X-ray Computed Tomography (CT) can be used to get a picture of the structure inside a sample without disturbing it. The scale or resolution is dependent on the type of scanner that is used and the materials that are surrounding the sample.

The objective is to explore this technique and place it within the context of all the techniques that are available to investigate the limestone structure on small scale. This technique is used to analyse the macro-pore structure within this thesis.

4.1.1 Materials and methods

A sample, ET.1.V.C (see Appendix C), was scanned with a medical scanner at a resolution of 400 µm. This resolution is the smallest one that is possible to reach with medical scanners. The effective resolution of the scan is a little higher than 400 µm because of the stainless steel casing around the samples, which was not removed for stability reasons. The noise that is induced by this metal casing results in a disturbed image of the sample, which makes it more difficult to derive precise material properties from the images.

The program ImageJ was used to process and analyse the images from the X-ray Computed Tomography. All the images consist of pixels that have been given a value, determined by the computed tomography (Figure 19). This value is based on the measured linear attenuation coefficient, which is a function of the density and the ionic strength of the scanned sample. The scale that is used is the Hounsfield scale (HU), which varies from -1000 for air to 3000. Some examples of materials and their HU value (Duchesne et al. 2009):

- Air: -1000
- Water: 0
- Calcite: 1652
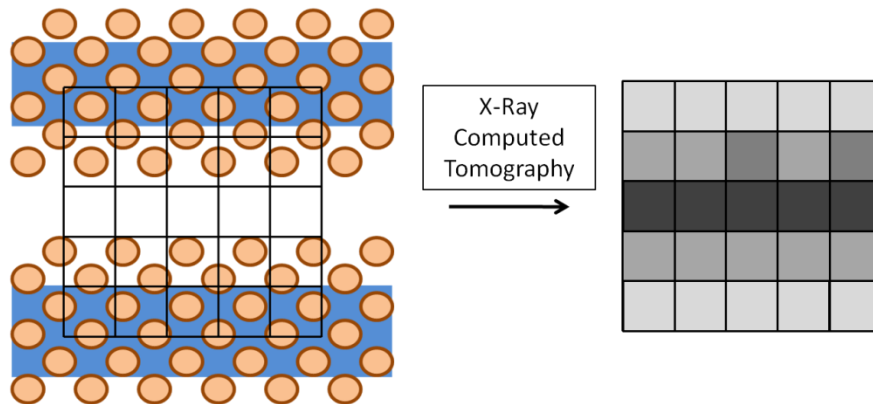
Figure 19: CT-scan principle: (left) Sample slice (white = air; blue = water; brown = limestone particles); (right) CT generated image (black = air; lighter colours mean a higher density)

The histogram of all the images from the CT-scan is used to determine the macro-porosity (pores >400 μm). This value is close to the effective porosity of the sample, since the macropores are the major flow paths through the sample. All the pixels with a HU value lower than 500 are considered to be part of the macropore-structure. The choice of 500 HU is an estimation, based on values from (Duchesne et al. 2009). The pixels with a value which is higher than this threshold value are denser and considered to be part of the micropore-structure and still filled with water or they are solid.

The macro-porosity that is determined this way can be considered as the effective porosity of the limestone sample. These large pores are the pores that are responsible for water and solute transport through the sample.

A 3D view of the total volume is generated to visualise the (macro)pore-structure of the sample and retrieve more information about the tortuosity of this structure. The average angle of diffusion for the macropores is used to characterize this tortuosity. This average angle of diffusion is observed from slices that are generated in the XZ and YZ plane (parallel with the principal axis of the sample).

4.1.2 Results

Macro-porosity

The macro-porosity of the sample is derived from the histogram that is generated from the computed tomography images (Figure 20). The macro-porosity equals 0.015 if a threshold of 500 HU is applied. A peak around the value of 1600 can be observed in the histogram (Figure 20). This value lies in the range in which calcite ($CaCO_3$) is situated on the HU scale (Duchesne et al. 2009). Calcite is one of the main components of limestone.
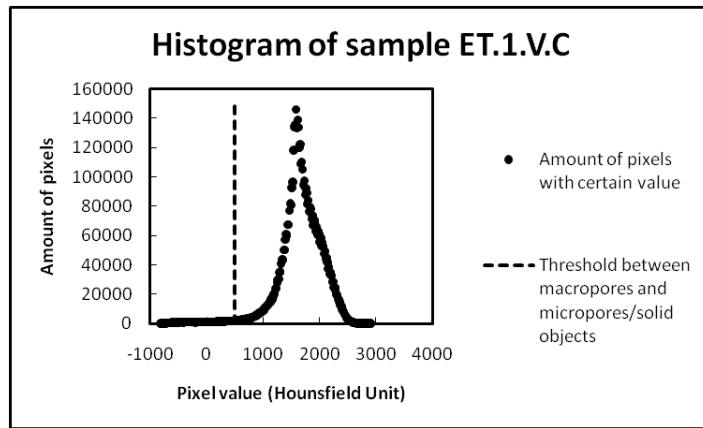
Figure 20: Histogram of sample ET.1.V.C (Hounsfield Units)

Visualisation of the macro-pore structure

The images of slices that are recovered from the 3D view of the sample suggest that there are 2 fracture or macro-pore systems (Figure 21). The first group of macro-pores has an average angle of diffusion, α, with an average value of 60°. The second group of macro-pores has an average angle of diffusion, β, with a value of 40°.
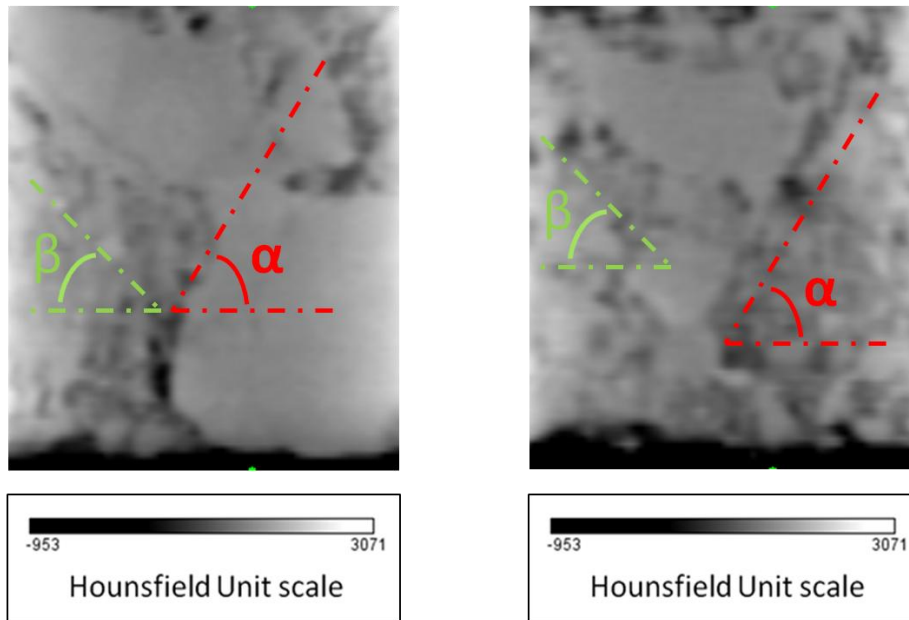
Figure 21: Sample ET.1.V.C.: Slice of resp. the XZ and YZ plane with average angles of diffusion: α and β

The two pore systems get more emphasized when a transformation from the grayscale image to an image with a Fire LUT is made (Figure 22). It can be observed that the pore system with an average angle of diffusion of 60° is less dense. The pores are wider and more pronounced. The pore system with an average angle of diffusion of 40° is denser, more compressed. This can be

related to the smaller angle of diffusion, which indicates a more tortuous system that is induced by higher stresses.
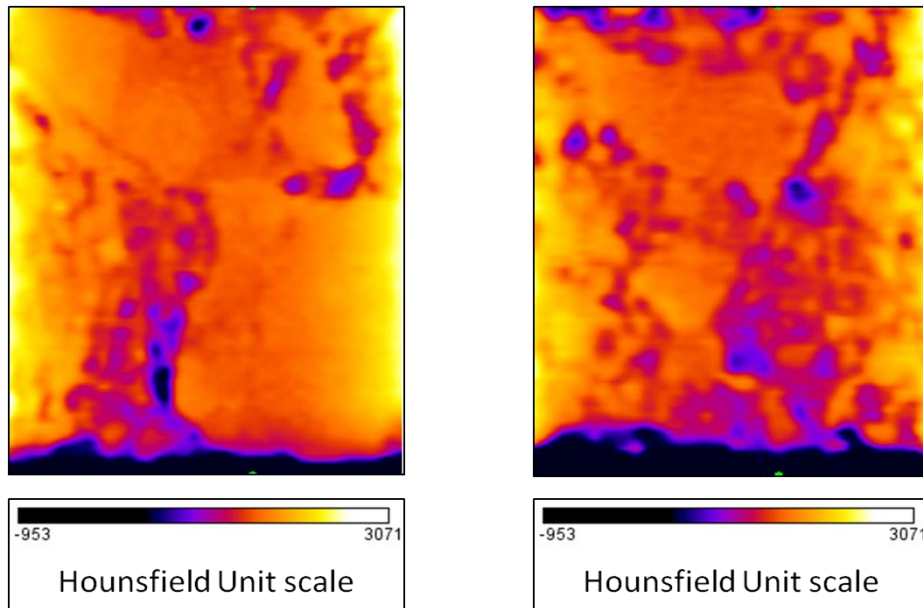
Figure 22: Sample ET.1.V.C.: Slice of resp. the XZ and YZ plane after transformation to a Fire LUT

4.1.3 Discussion

Macro-porosity
The analysis of the macro-porosity of the sample is depending on the threshold value that is chosen for the division between macro-pores on one side and micro-pores and solid structure on the other side. The choice of 500 HU is an estimation, based on values from (Duchesne et al. 2009). When another value is chosen as threshold value, the macro-porosity of the sample will change. The value of 0.015 that is obtained for the macro-porosity for sample ET.1.V.C is one that can be expected for this type of limestone (Downing, Price & Jones 1993).

Visualisation of the macro-pore structure
The stainless steel casing holding the sample causes noise that decreases the resolution of the images from the X-ray computed tomography. A better resolution would be obtained when the casing is made out of plastic.
As shown on Figure 22, the sides of the sample will suffer from more stress during the sampling, which results in a denser structure on the sides of the samples. The top and bottom of the sample are more disturbed due to the sampling. The sudden decrease of stresses that are exerted on these places just after the sampling will result in a relaxation of the materials in this area and can cause small piece to loosen.

4.2 IR image analysis

Next to X-ray computed tomography visualisation of the pore network in limestone can be done by letting a wetting front pass through a drained sample. The liquid that is used can contain a colouring agent which will cause the pore network to colour. Another method, as will be discussed in this section, is to use the temperature difference between the sample and the water as contrast middle.

4.2.1 Developed materials and method

Method

The developed method which is used to take the IR images is based upon the setup that is described by (Loll & Moldrup 2000) for horizontal infiltration experiments. Flow of water with a higher temperature than a cooled sample is realized by establishing a pressure gradient between the sample and the constant head burette. The velocity of the water flow through the sample will be higher in the bigger pores and fractures. This will result after a certain time period in water filled larger pores at the top surface of the sample, while the smaller pores are still filled with air. The IR camera registers the temperatures by assigning to each pixel of the generated image a value that corresponds to the emitted heath by the depicted material. This way an image can be produced that gives a rough estimate about the ratio between larger pores that are filled with warmer water and smaller, cooler pores or dense material.

Experimental setup

The setup consists of the cooled sample that is placed in a vertical position and connected to a constant head burette (Figure 23) by a flexible tube. The constant head burette is filled with water that has a temperature of 20 degrees Celsius. This temperature ensures a temperature difference between the cooled sample and the wetting front that is large enough to be registered by the IR camera.

The pressure level in the burette is set 2 cm higher than the middle of the sample (ΔH= 2 cm $H2O$). This will cause a hydraulic gradient over both ends of the sample and will cause water to flow through the sample. This level difference of 2 cm ensures a hydraulic gradient that is low enough to allow enough time to generate an image without flooding the surface of the sample.

The water is applied evenly over the surface of the sample through a moist GFC filter which is in direct contact with the Millex-FG 50 filter, mounted in the connecting PVC piece (Figure 23).
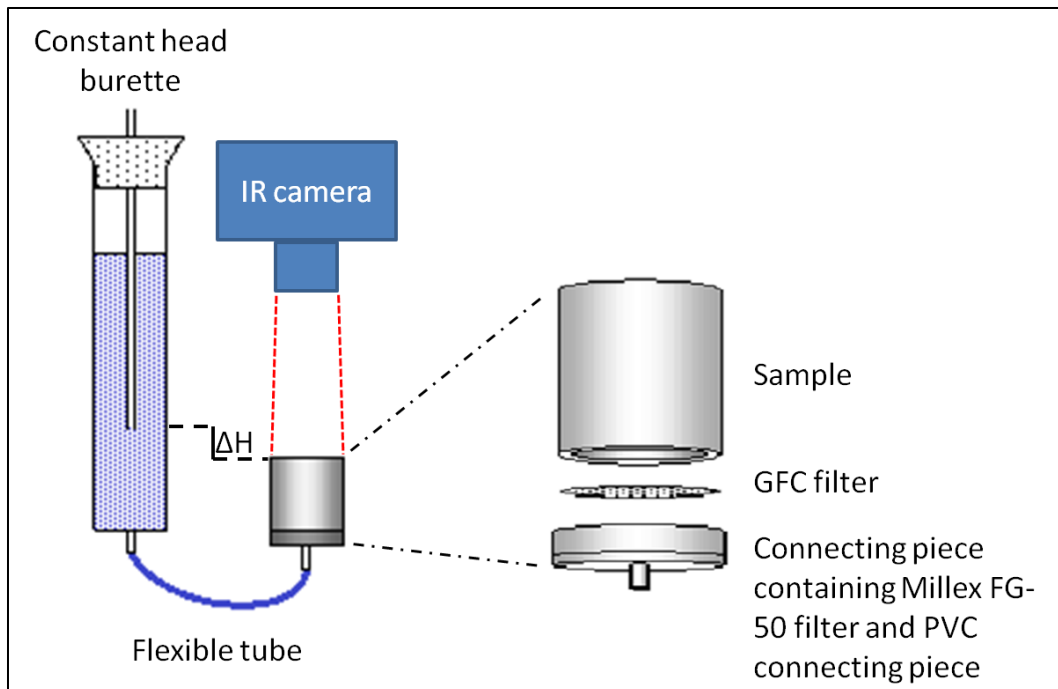
Figure 23: IR analysis setup

Experimental procedure

A. The air dried samples are cooled by placing them 2 days in a cooling facility at a temperature of 10 degrees.
B. After cooling of the sample, it is attached to the PVC connecting piece. The sample and PVC piece are sealed with connecting tape to make sure no water flows along the sides of the sample, instead of through the sample.
C. The flow of water with a temperature of 20 degrees Celsius is now established through the sample and the IR camera is activated.
D. The camera takes now continuously pictures until the wetting front has passed the top surface of the sample and the flooding of the sample surface occurs.

4.2.2 Discussion of the method

A critical parameter while performing this test is the time it takes for the water to reach the top surface of the sample. This parameter can be modified by changing the head in the constant head burette. If the water moves too fast through the sample, this results in a fast flooding of the sample surface. It might be not possible to take a clear picture of the sample surface with the IR camera. When the water moves to slow through the sample, a cooling of the water and heating of the sample may occur through heath exchange. This will result in a smaller difference between temperatures when the water has reached the top of the limestone surface and the contrast on the generated picture might be not clear.

The higher temperature of the water that is moving through the sample may cause a higher degree of erosion to occur in the larger pores which either can block the pores or enlarge them and increase the flow through them.

5 Characterization through a single-well tracer test

One of the hydrogeological parameters that determines the effective groundwater velocity in an aquifer is the effective porosity of the aquifer. This parameter is therefore important when it comes to estimation of travel time of solutes in aquifers.

The effective porosity of the limestone aquifer on a larger scale (5 – 50 m) can be estimated by a tracer test. The general idea in this test is to inject a tracer liquid in the aquifer and let it drift under a natural gradient. The time it takes until the centre of the injected tracer-plume is observed over a distance downstream of this injection point is determining for the effective velocity of the ground water and the effective porosity of the aquifer. At least two wells are needed for most tracer tests: an injection well and at least one observation well. Next to these logistic requirements, an estimation of the transmissivity, hydraulic gradient and aquifer thickness are necessary to analyse this test.

Another method to determine this effective porosity, which has less logistic requirements, is to perform a single-well tracer test. This test consists of only one well that functions both as the well where the tracer is injected and as the well where the tracer is observed after a certain time. The tracer is first injected in the aquifer, after which it will drift under a natural gradient (Figure 24). Water will be pumped from this injection well after a certain time. This will impose a gradient upon the natural gradient which causes the tracer to drift. The sum of both gradients will draw the plume of tracer liquid back to the well. The effective porosity is calculated based on the time it takes for the centre of the plume to arrive in the well and the applied pumping rate.

All the processes and methods that are discussed in this chapter take place in a confined saturated limestone aquifer.
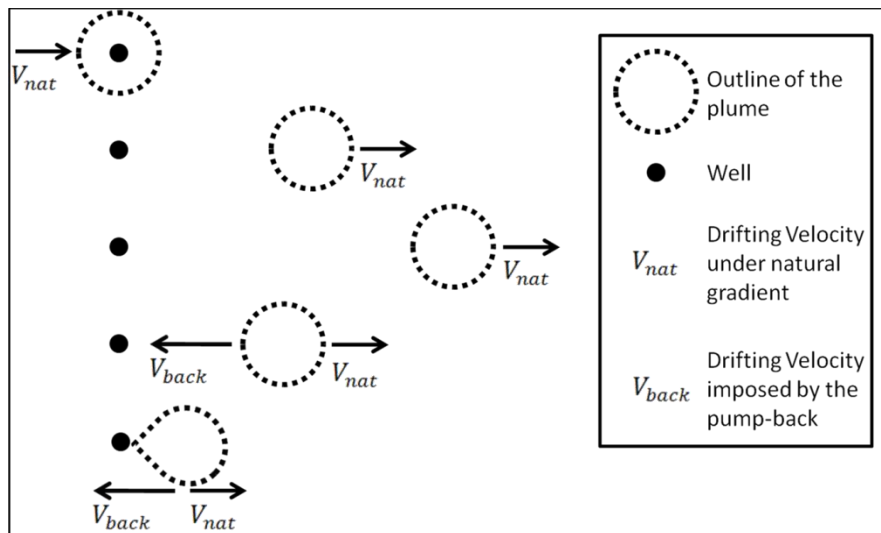

Figure 24: Single-well tracer test principle

5.1 Materials and methods

The effective porosity and hydraulic conductivity of a limestone aquifer is determined in this chapter by a single-well tracer test. The procedure that is followed throughout this chapter is an iterative process between a modelled tracer test and the implementation of an in situ tracer test (Figure 25). Each step in the process gets closer to the final idea and understanding of the hydrogeological situation around the test site.

5.1.1 Iterative process

The single-well tracer test is first modelled numerically in GMS7.1. This has two purposes. It allows setting up a conceptual model that can be evaluated after the execution of the tracer test in situ and it gives the possibility to design and perform this in situ test in a smart and economical way.

The numerical model provides a setting in which different scenarios can be modelled. In what way the tracer test is conducted in the field is decided based on the outcome of these different scenarios. The results of the in situ tracer test are analyzed by application of an analytical solution which couples the time it takes to recover the centre of the plume of the injected tracer to the effective porosity. The result of the in-situ test is afterwards coupled back to the numerical model to adjust our setup and understanding of the field conditions. The combination of the analytical solution and the numerical model results in a clear understanding of the hydrogeological situation in the vicinity of the well. This process is iterative, where each step leads towards a more precise idea about the in situ conditions (Figure 25).

1st numerical conceptual model: conceptual understanding of the situation

Pilot tracer test: validation of the conceptual model

n_{eff} : 0.01-0.06
K_{Sat}: 1e-3 – 1e-5 m/s

2nd numerical model: corrected and refined model

2nd tracer test: validation of the model and leading towards a detailed understanding

n_{eff} : 0.01-0.06
K_{Sat}: 9e-4 m/s

3rd numerical model: design of the final test

Final tracer test: filling the last gaps

n_{eff} : 0.01-0.06
K_{Sat}: 9e-4 m/s

Final model: final understanding of the situation, including all the hydrogeological parameters

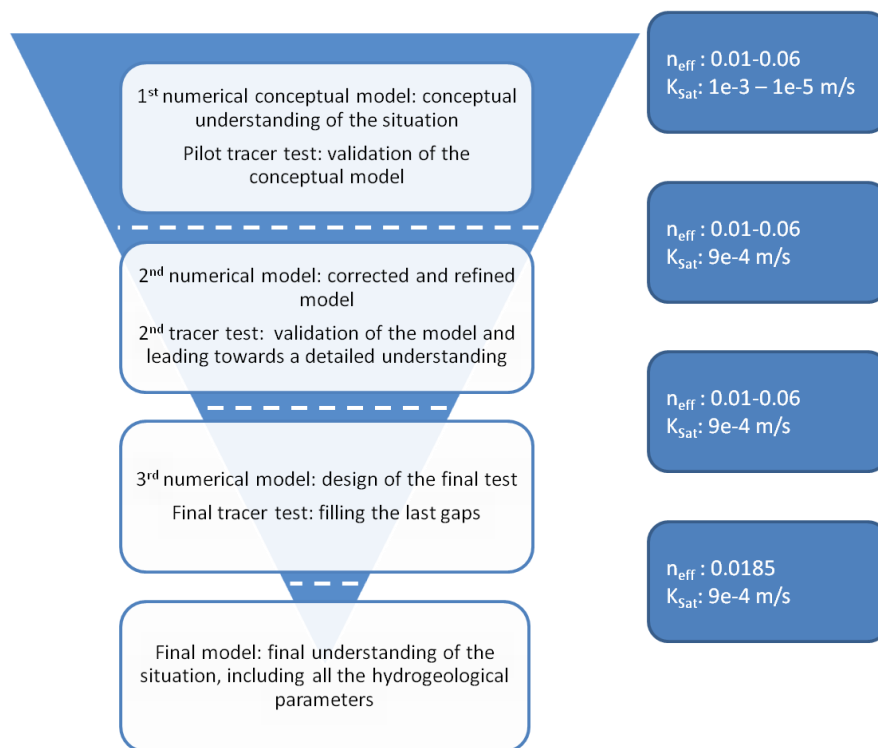n_{eff} : 0.0185
K_{Sat}: 9e-4 m/s

Figure 25: The iterative process that leads to a precise idea of the hydrogeological setting

Setting in which the modelling and in situ testing takes place

The limestone aquifer which is the subject of this test is located around 8 km South of Aalborg, near Skovstrup. The data about the hydrogeological properties around this location are rare. An overview of the geology, based on the borehole report of the testing well at the Skovstrup site, can be found in (Appendix M). Data from Volsted Plantage is used to fill the gaps in the available data for hydrogeological properties at the site in Skovstrup. Volsted Plantage is a drinking water abstraction site with a detailed description about the hydrogeological properties of the limestone aquifer, located 10 km Southwest of Skovstrup (Figure 26).
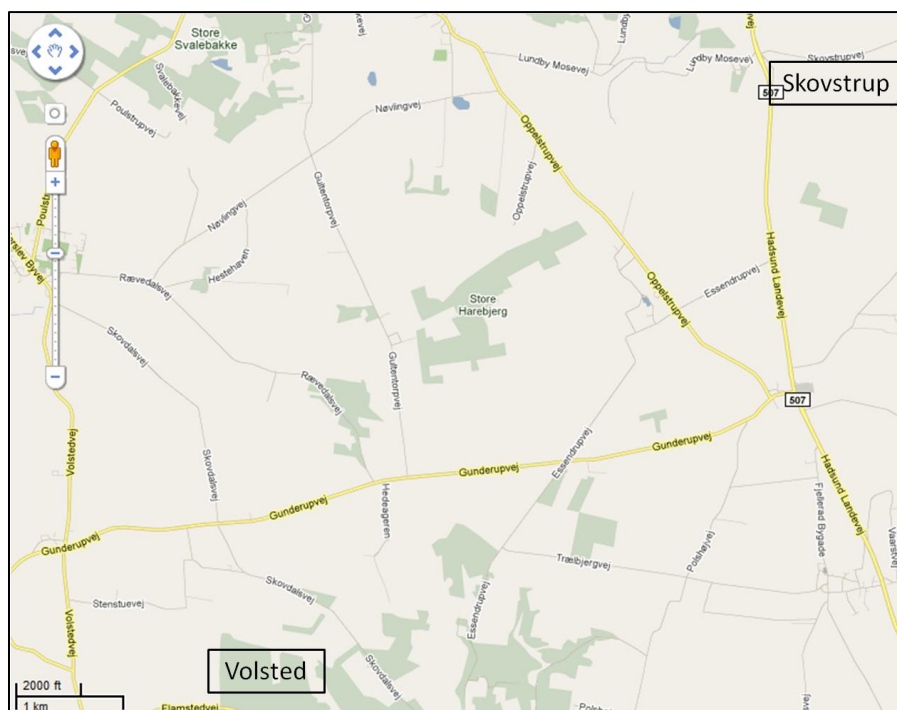
Figure 26: Location of the Skovstrup site in relation to the Volsted site (edited from Google Earth)

1ˢᵗ numerical conceptual model and pilot in situ tracer test

This first numerical model is constructed through the use of parameters that are derived from measured parameters at Volsted Plantage (Figure 26) and values typical for limestone aquifers found in litreature. The setup and a detailed overview of the parameters that are used to construct this model can be found in (Appendix H). Different scenarios are modelled in this first model to estimate the timeframe for the execution of the pilot tracer test.

After this rough model has been constructed, it is tested by a pilot in situ tracer test. The setup and the execution of this test are described in (Appendix I). The tracer test consists of 4 different stages. First a solution that contains chloride as tracer liquid is injected in the aquifer. The second step is to flush this plume with tracer liquid out of the vicinity of the well by use of clean water as a chaser. During the third stage, the plume is allowed to drift under a natural gradient, after which it will be pumped back to the test-well during the last stage. This tracer test demonstrates if the parameters that have been used in the model match with the

hydrogeological situation around the test-well and provides data that can be used to change or optimize these parameters. The measurements of the drawdown of the water table in the well during the in situ test are used to adjust the saturated hydraulic conductivity of the limestone layers through following relation (eq.7) (Bear 1979):

$$s \sim 1/T \tag{7.}$$

with:

$$T = bK \tag{8.}$$

where s is the drawdown (m) and T is the transmissivity (m^2/s) of the aquifer. The thickness, b (m), of the limestone is assumed to be correct, which makes it possible to substitute the transmissivity with the saturated hydraulic conductivity, K (m/s), in (eq.7).

2nd numerical model and tracer test

The second model is an updated version of the first model. The values for hydraulic conductivity are adjusted after the results of the pilot tracer test have been analyzed. The main objective of this second model is to estimate the timeframe for the second in situ tracer test. More detailed information about the setup of this model is provided in (Appendix J).

Details about the execution and a more thorough description of the second tracer test can be found in (Appendix K). This second tracer test is analyzed to get a better overview about the effective velocity of the groundwater just outside the testing well. The effective groundwater velocity is determined based on the assumption that the injected tracer is forced into the aquifer with the same velocity, but in the opposite direction as the local pore water velocity (eq.9). This assumption has been made after analysis of the first and second in situ tracer test and only applies to the area directly upstream from the well:

$$v = \frac{Q}{2\pi r l n} \tag{9.}$$

Where v (m/s) is the effective groundwater velocity, Q (m^3/s) is the applied input rate and n is the effective porosity. The two other parameters, r (m) and l (m) are respectively the radius of the well and the length of the well screen. The well screen is assumed to be fully situated in the aquifer.

3rd numerical model and tracer test

The goal of this 3rd tracer test is to recover at least half of the injected tracer mass, whereas this was not possible in previous two tests. The time it takes to recover half of the tracer mass, or the centre of the injected plume, leads to an analytical solution for the effective porosity. The parameters that are used to set up this model are the same as the parameters used in the second model (Appendix J).

A steady state model is constructed together with a transient model to obtain the catchment area of the testing well. The outcome of the analysis and comparison of both models is the distance over which the plume can travel and can still be recovered by pumping in the test well.

This distance is connected to an analytical estimation of the local pore water velocity just outside the well (eq.9), derived from the second tracer test. An estimation about the time that the tracer is allowed to drift during the third in situ experiment is made based on this comparison.

Analysis of the data that is retrieved from the third tracer test gives the time it takes to recover half of the injected tracer mass, or the centre of the injected tracer plume. The local effective porosity can be derived from this recovery time. Leap and Kaplan (1988) developed a formula for the description of the average linear groundwater velocity, v, during a single-well tracer test based on this recovery time, t (s):

$$v = \frac{\sqrt{(\frac{Qt}{\pi n b})}}{d} \tag{10.}$$

where Q (m^3/s) is the pumping rate during the pumping back period, t (s) is the time it takes to pump half of the mass of the tracer back and d (s) is the time that has passed after the injection of the tracer until half of the mass of the tracer is recovered. The two other parameters: n and b, are respectively the effective porosity and the aquifer thickness. This expression can be modified to obtain the effective porosity (eq.11) when it is combined with Darcy's law.

$$n = \frac{\pi b K^2 d^2 I^2}{Qt} \tag{11.}$$

where K is the horizontal hydraulic conductivity of the aquifer and I is the local horizontal hydraulic gradient. This expression for the effective porosity is only valid under the following assumptions that include the assumptions used to set up the numerical model for the tracer test (see Appendix H):

- The aquifer is homogeneous;
- There is a steady-state horizontal advective transport;
- There is a local constant gradient around the testing well;
- There is no mass stored in the system during the test period.

Final model
The final model leads to a final understanding of the hydrogeological situation around the testing well. The same hydrogeological parameters as in previous model are used to construct this model (Appendix J). Not only are the natural hydrogeological characteristics taken into account in this model, but also the disturbance of the natural system that might have occurred during installation of the well are considered. The aquifer might have been disturbed during drilling and constructing of the well and this might result in a local change of the hydrogeological properties (e.g. higher local porosity due to introduction of small fractures). The characteristics of the well casing and borehole filter are also an important factor in the model when the test is only modelled over a short time period and covers only a limited area around the well. For this reason, the cells around the well screen, where the gravel pack is located, are given a higher

effective porosity (0.30) and higher horizontal hydraulic conductivity (0.01). These values correspond to properties of gravel (Spitz & Moreno 1996).

A final comparison is made between the final model and the outcome of the third in situ tracer test, based on the modelled and observed concentrations of the injected tracer.

5.2 Results

The most important observations and recovered data from the numerical models and the in situ tracer test are presented in this section. An overview of all the results and can be found in the Appendixes that cover the according model or test. Referrals to the relevant appendixes are made when necessary or appropriate.

5.2.1 1st and 2nd numerical model in combination with the pilot and 2nd tracer test

A complete overview of the recovered data from both models and the pilot tracer test are presented in (Appendix H, I, J and K). The measured pressure drop of 0.21 meters, when the pumping back of the tracer starts, is presented on Figure 27. This drop of 0.21 meters is not expected based on the pressure drop of 4.5 meters that occurs in the first model (Figure 28 left).
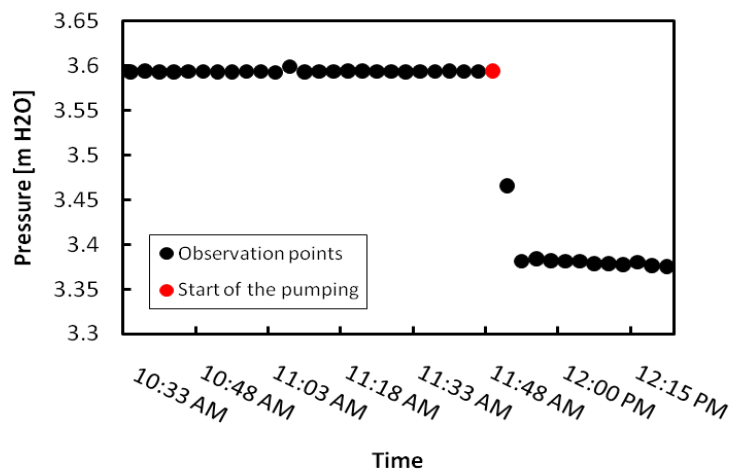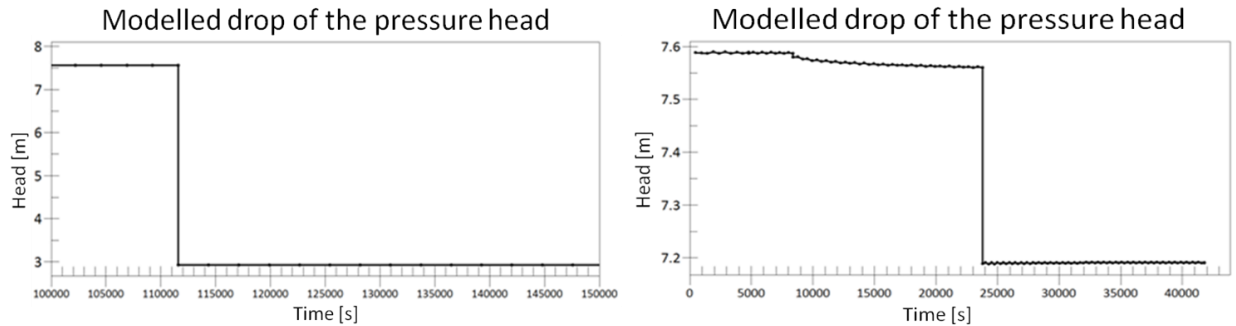
Figure 27: Observed drop of the pressure head at the start of the pump back period

The hydraulic conductivity of the limestone aquifer in the model is modified in the second model based on this observed drawdown at the start of the pump back period in the pilot tracer test with a factor 12. This change of the hydraulic conductivity results in a hydraulic conductivity for the limestone aquifer that equals: 9.6 e-4 m/s. The result of this higher hydraulic conductivity is a drawdown of the pressure head that changes from 4.5 meters in the first model to 0.38 meters in the second model (Figure 28). The difference in time at what the pumping back starts in both models (Figure 28) has no influence on the result.

Figure 28: Modelled drop of the pressure head is noticed at the start of the pump-back period: (left) first model; (right) second model

A probe that is located down in the well measures next to the height of the water table, relative to its position, also the specific conductivity (Appendix I). This measured specific conductivity can directly be related to the concentration of chloride (the tracer liquid) which is shown on Figure 29 . The difference in the concentration trend during the input of the tracer liquid can be explained by the used method: the second test ensured a better mixing of the tracer liquid before it was pumped into the aquifer.

The actual introduction of the tracer solution in the pilot test started at 8:12 am, yet the rise in concentration occurs only 25 minutes after the solution is introduced in the well. Figure 29 suggests that the chloride and chaser introduction can be modelled as a plug-flow with a lag of 25 minutes. These 25 minutes can be seen as the time it takes for the liquid to travel from the ground surface to the bottom of the well.

An analytical solution to obtain the effective porosity and effective velocity of the groundwater could not be used in the first two tracer tests since it was not possible to recover half of the injected tracer mass during the pump back period. However, the registered concentration of the tracer in the groundwater during the drift period (Figure 29) gives information about the effective velocity in the vicinity of the well; more precisely upstream of the well.

The groundwater transports the injected tracer when the injection of the chaser liquid is stopped. This means that the part of the tracer liquid that has been injected in the upstream direction passes again through the well at some point and will be registered by the probe down in the well. Figure 29 shows that this part of the tracer liquid passes the well immediately after the termination of the input of chaser liquid. This means that the tracer is not transported outside the vicinity of the well in upstream direction.

43
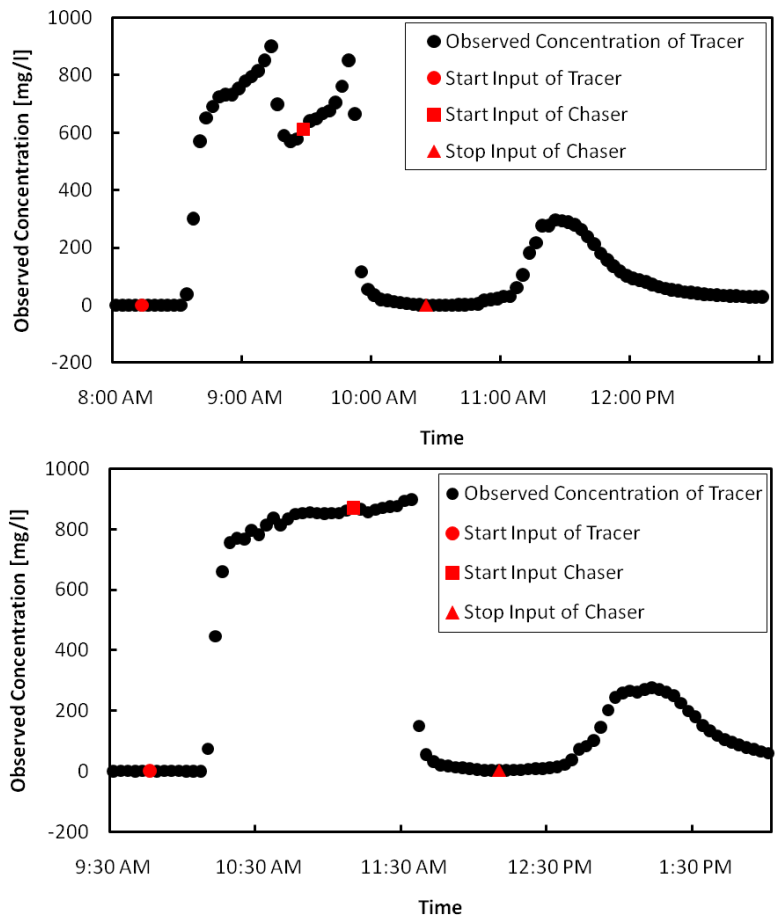
Figure 29: Observed specific conductivity down in the well: (up) during the pilot tracer test; (down) during the second tracer test

An explanation for the fact that the tracer is not transported outside the vicinity of the well in upstream direction, is that the local pore water velocity has an equally high velocity, but in opposite direction as the injected tracer liquid. The local pore water velocity, v, of the introduced water just outside the well can be expressed as:

$$v = \frac{Q}{2r\pi nb}$$

(12.)

where r and b are well parameters, r is the well radius (0.1 m) and b is the length of the screen (16 m). Q (1.5 m^3/hour) represents the injection rate and n is the effective porosity. The expected effective porosity lies in the range from 0.01 to 0.06, which results in a local pore water velocity in the range of 2.5-15 m/hour.

5.2.2 3rd numerical model and 3rd tracer test

The estimated local pore water velocity that has been retrieved after analysis of the second tracer test, is now compared with the catchment area of the well. From (Figure 30) can be

observed that the catchment area of the well, when a pumping rate of 18 m^3 /hour is applied, only extends 5.5 meters downstream of the well. It is important that the tracer does not travel outside the catchment area of the well during the drift period of the test (Figure 24) to be able to recover this tracer again. A drift time of 30 minutes is therefore initially chosen for this reason (Appendix L).

As calculated from (eq.12), an effective porosity of 0.01 would cause the plume to travel 7.5 meters. Yet, the actual travelling distance is assumed to be lower than the predicted by this pore water velocity due to the effect of the gravel pack. The gravel pack, which is in contact with the well screen, has a higher effective porosity and results therefore in a lower velocity. The gravel pack has therefore a braking effect on the effective velocity of the groundwater.
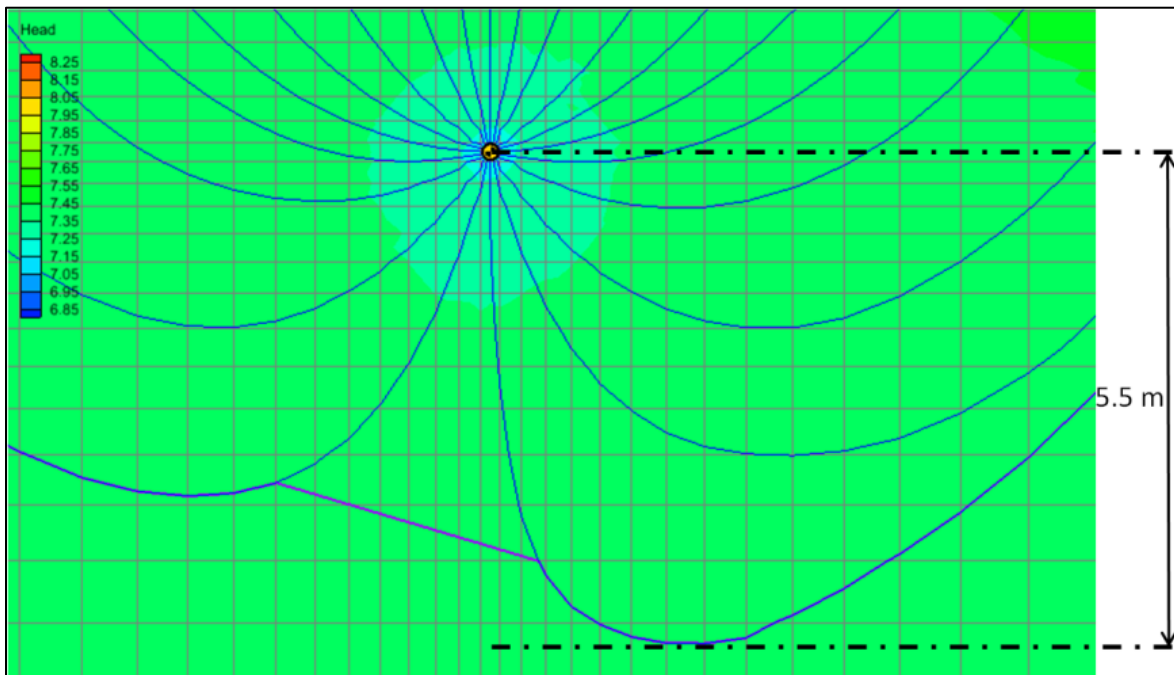

Figure 30: Catchment area downstream of the well

The observed concentrations during the third tracer test can be seen on (Figure 31). The lag time between the actual input of tracer at the start of the test and the increase in concentration down in the well is again 25 minutes. This lag time is not occurring during the pump back period of the test. The probe down in the well is located close to the pump and the well screen, which causes this probe to detect changes in concentration down in the well during pumping back immediately.
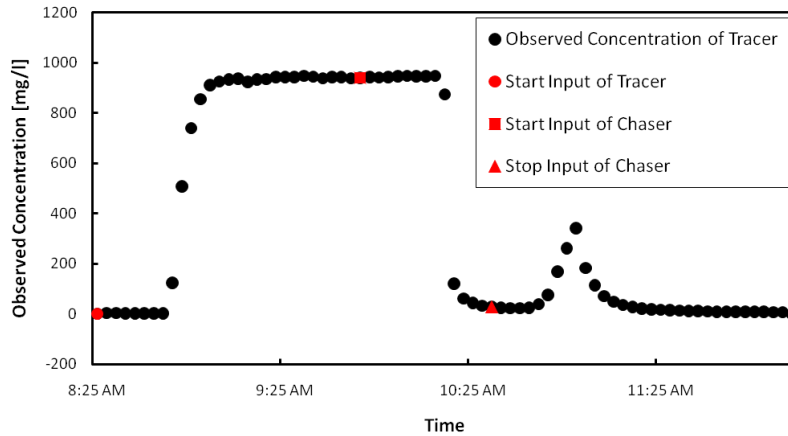
Figure 31: Observed concentration of the tracer down in the well during the 3rd tracer test

The time it takes to recover half of total injected mass or the centre of the plume of the tracer liquid can be determined from the measured concentrations of tracer in the groundwater during the pumping back of the tracer (Figure 32). This recovery time for the centre of the plume equals 54 minutes.
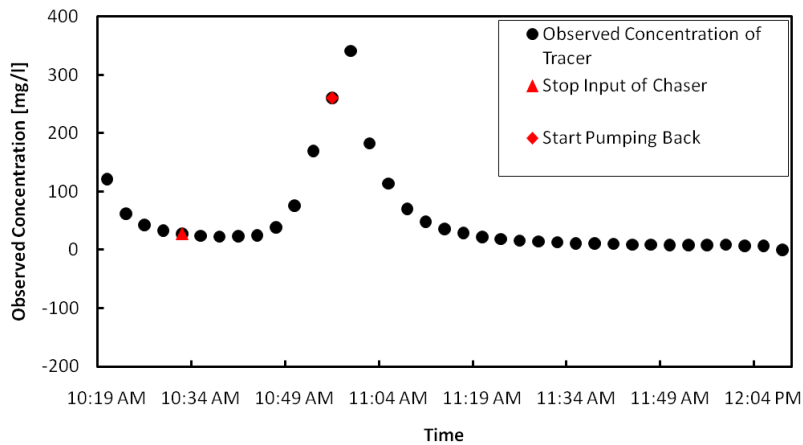
Figure 32: Observed specific conductivity down in the well during pumping back of the tracer

The effective porosity of the limestone aquifer in the vicinity of the well can now be calculated from the modified Darcy equation (eq.11) with the following parameter values:

- The aquifer thickness is estimated to be 52 meter (see also Appendix H)
- A horizontal hydraulic conductivity of 0.00096 m/s is found near the abstraction well
- The horizontal hydraulic gradient around the well is 0.008
- The applied abstraction rate is 18 m^3/hour
- The time, t, it takes to retrieve half of the injected chloride mass after pumping back has started is 3240 seconds

46

- The time, *d*, that elapses for the centre of the tracer plume to drift under natural gradient and to be retrieved equals 5580 seconds (based on Figure 31)

This results in an effective porosity, *n*, of 0.0185.

5.2.3 Final model

Throughout the iterative process, a precise idea about the hydrogeological settings in the vicinity of the testing well has been formed. A more precise value for the effective porosity and hydraulic conductivity has been determined. The final model that is constructed is based on the first model, with a change in values for the hydraulic conductivity and the effective porosity as they were determined during this process of modelling and field tests. The parameters that are used can be found in (Appendix J), modified with the values for hydraulic conductivity and effective porosity (*n*=0.0185 and *K*=9.6e-4 m/s). The modelled concentrations of tracer down in the well can be found on Figure 33.
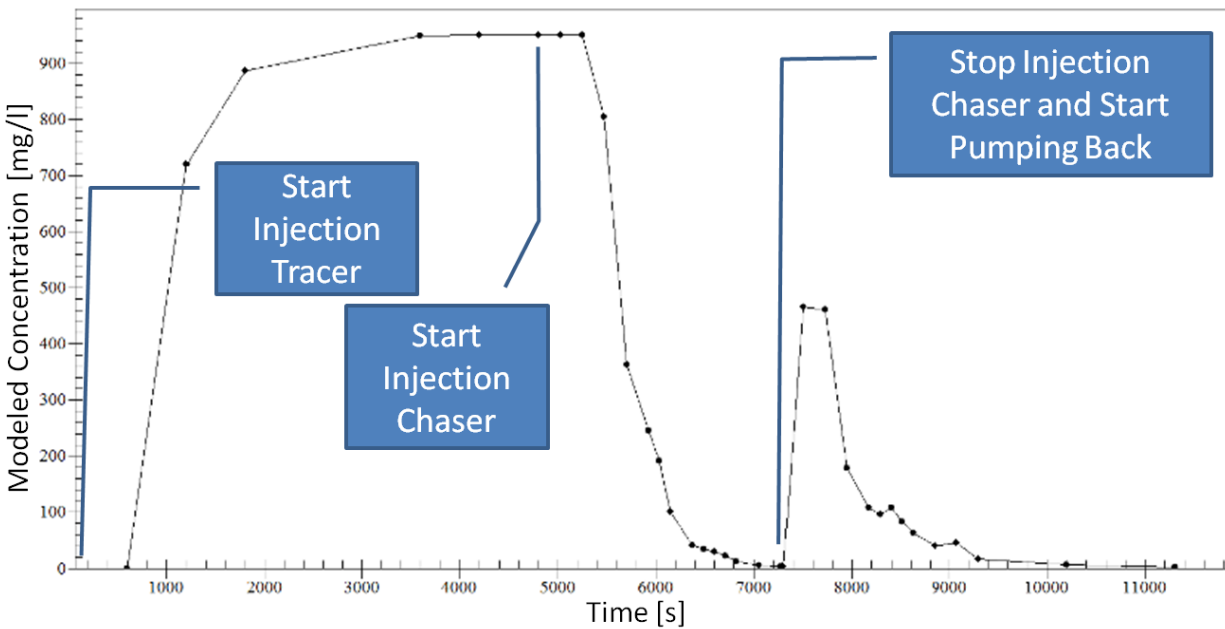
Figure 33: Modelled concentration of tracer liquid

These modelled concentrations (Figure 33) can now be compared with the observed concentrations in the field (Figure 34). The lag in time (25 min.) has been made up in this figure for convenience of this comparison.
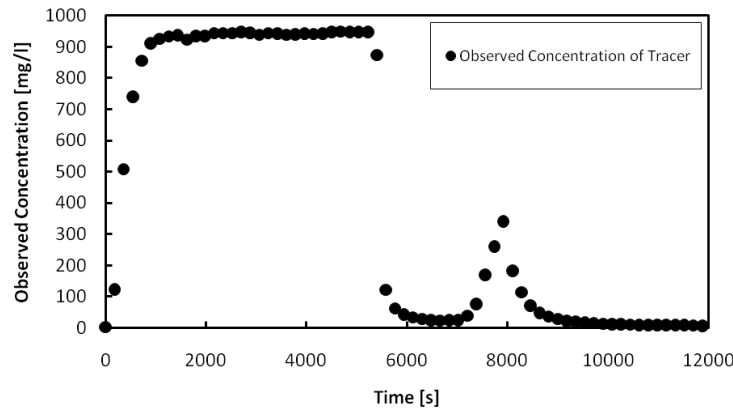
Figure 34: Observed concentrations [mg/l], taking the lag-time into account

The observed concentrations (Figure 34) and the modelled concentrations (Figure 33) differ from each other when the upper part of the tracer plume passes the well, just when the pumping back is started (peak just before t=8000s). There is a difference in concentration of 80 mg/l. This lower concentration in the observations in the field can be attributed to losses due to tracer that escapes out of the catchment area of the well through larger fractures.

5.3 Discussion

The drawdown of the pressure head changes from 4.5 meters to 0.38 meters (Figure 28) after the change of the initial hydraulic conductivity with a factor 12 (from 7.97 m/s to 9.6 e-4 m/s). This drawdown is still 1.8 times higher than the observed 0.21 meters during the in situ test (Figure 27). The value of 9.6 e-4 m/s for the hydraulic conductivity is supported by values provided by literature sources (Spitz & Moreno 1996), while values higher tend to sandy characteristics.

The method that is used in this analysis of the hydrogeological parameters is only truly valid for the assumptions that were stated before (Appendix H). The more the field conditions are diverging from these assumptions, the bigger the difference between the in situ obtained results and the model will be (Figure 33 & Figure 34). One will have to adjust the model then manually to get matching results or change the test procedure. An example of this is the manually changing of the cell parameters in the vicinity of the well to mimic the gravel pack around the well as has been explained in the setup of the final model. Another option could have been to increase the drifting time and the time over which the test would be carried out. This would then flatten out the effect of the well screen because of the much longer travel time in the aquifer out of the vicinity of the well. This option would have required pumps with a higher capacity and was not feasible within this project.

Another important point is the heterogeneity of limestone in itself. There is always the possibility of the presence of a large crack or fracture in the aquifer. This larger fracture will act as a pollution highway and is difficult to notice with tests that only investigate the vicinity of the testing well. The difference in concentration between the modelled and the observed

concentration at the start of the pumping back period (Figure 33) and (Figure 34) can be explained by this assumption of heterogeneity in the model. When there is a suspicion of larger fractures in the aquifer, single-well tracer tests are not the best option to obtain more information about the aquifer. A tracer test with more wells, strategically placed over the investigated area, is more recommended for this setting.

The method for analyzing the single well tracer test observes the drifting time of the tracer plume and the time it takes for the centre of the mass of the plume to be recovered. The definition of this time is important. Since from the moment of injection of the first mass of the tracer, the tracer plume is already subject to the advection by the groundwater, one can choose the starting time of injection as the starting time of the drift period. This can lead to an overestimation of the drifting time. Another possible starting point, which is used in this thesis, is the moment after the complete injection of the tracer.

A last remark concerns the tracer that has been used and the diffusion into the limestone matrix. The application of the analytical formula (eq.5.) is only valid when no tracer mass is stored in the system. Because of the very short time period of the tracer test, this condition is assumed to be met.

5.4 Conclusion

Hydrogeological parameters have been determined for a limestone aquifer through a single-well tracer test. An iterative process between modelling and measuring in the field leads to a detailed understanding of both parameters: the effective porosity and the hydraulic conductivity. Each step in this process leads to a more detailed overview of the effective porosity and hydraulic conductivity. The merging of the information obtained through both modelling and measuring, leads to a final picture of the hydrogeological setting around the testing well.

From an idea about the hydrological settings around the test well, based on litreature values and information about the wide area (10 km) around the well, a more detailed understanding of the hydrogeological setting has been built up:

- The effective porosity has been precisely determined to be 0.0185, whereas the initial model started with values in the range of 0.01-0.06.
- The hydraulic conductivity is 9.6 e-4 m/s, 12 times higher than the initial value of 7.97 e-5 m/s

6   Connecting the different scales

The hydraulic conductivity and effective porosity have been determined in this thesis through different experiments at different scales (Table 3). These parameters were determined on small scale through three different types of measurements and on large scale by an iterative process of in situ tests and model fitting.

Table 3: Different values for hydraulic conductivity and effective porosity determined in this thesis

	Hydraulic Conductivity Ks [m/s]	Effective Porosity n [cm^3/cm^3]
Small scale		
Direct measurements: liquid phase experiments	(0.34 - 25.64) e-5	0.086 -0.26
Indirect measurements: gas phase experiments	(0.31 - 3.49) e-5	-
Indirect through visualisation	-	0.015
Large scale		
Iterative process between modelling and measuring	9 e-4	0.0185

Two important differences can be observed in Table 3. One is the difference of values within the same scale, as can be noticed for the small scale effective porosity. The second difference is between the parameters that are determined on a different scale. This is clear for the hydraulic conductivity. The first difference, within the same scale, is caused by the heterogeneity in soils and aquifers. The difference between the small and large scale is caused by scaling of the investigated sample volume. Both phenomena, heterogeneity in soils and aquifers as well as scaling are further discussed in this chapter.

6.1   Heterogeneity in soils and aquifers

Uniformity and heterogeneity of the hydrogeological properties of a limestone aquifer are defined with respect to the volume of the sample that is measured upon. The heterogeneity is therefore dependent on the size of the element that is measured upon. The larger the size is of the sample that is measured upon, the more this heterogeneity is averaged within the volume. This results in more homogeneous hydrogeological properties of the aquifer if larger sample sizes are used to determine the aquifer properties. If smaller sample sizes are measured upon, this might result in a more heterogeneous result for the hydrogeological parameters of the aquifer, as can be seen for the effective porosity values, determined by direct measurements and visualisation. Figure 35 demonstrates the reason for the large variation of the effective porosity within the small scale samples (Table 3). A volume of a limestone aquifer with small volumes of incorporated sand is shown. A different value for the hydraulic conductivity and the effective porosity of this limestone aquifer is found depending on the size of the different elements that is measured upon. Elements with size 1 risk to only consisting of limestone or only of sand. This will result in either a low value for the effective porosity, in the range of 0.01-

0.08, or when there is a lot of sand a very high value, in the range 0.20-0.26. The result will be in both cases not representative for the complete limestone aquifer. Measurements that are done on a volume with size 3 result in values that are more representative for the complete limestone aquifer and can be used in risk assessment. The scale of the sample that is measured upon is large enough to average the hydrogeological properties within each sample. This results in properties that do not vary much from each other for different samples with the same size.
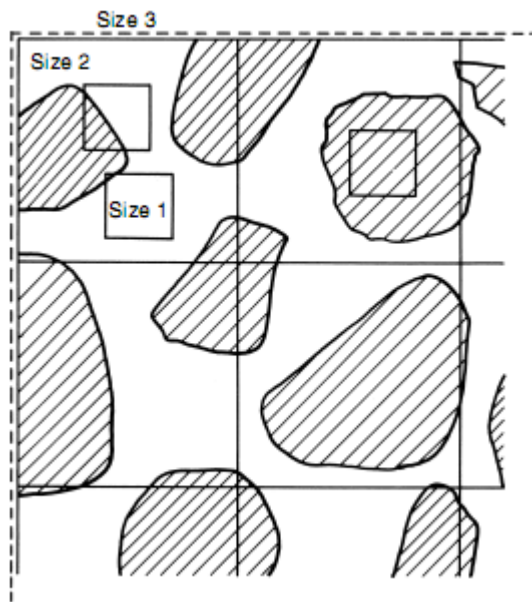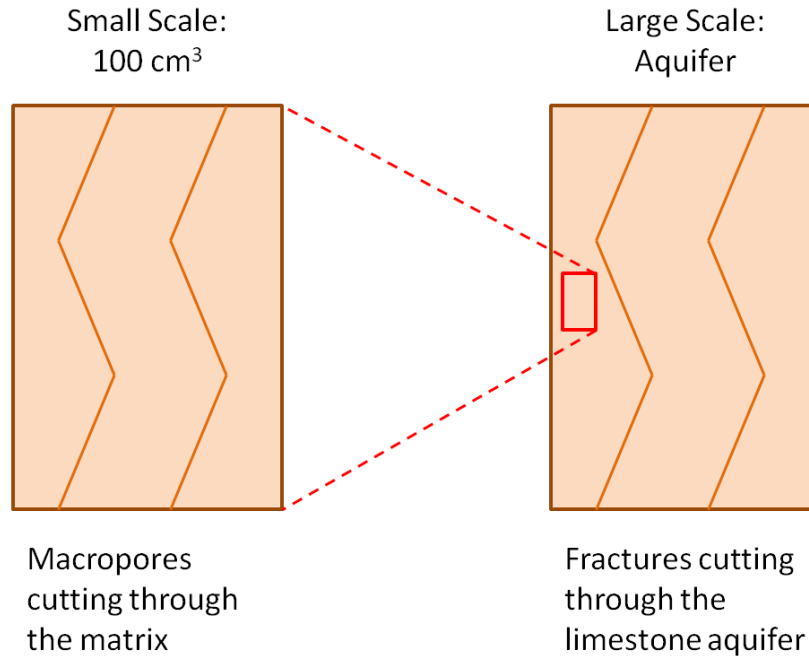

Figure 35: Different sample sizes within the same field (striped = sandstone; white = limestone) (taken from (Miyasaki 2006))

The concept of the representative elementary volume has been introduced to address this problem. The representative elementary volume (REV) describes the relationship between the variability of a parameter and the sample volume that is measured upon (Lauren et al. 1988). This REV consists of the smallest volume of limestone that contains a representation of microscopic variations inside the limestone structure. Another characteristic of this REV, which is added for the convenience of the experiments, is that the REV must result in a convenient method for measuring.

Another example of this REV with regards to the saturated hydraulic conductivity is given by (Lauren et al. 1988). They investigated the REV for hydraulic conductivity of a silty loam with macropores by applying different sample sizes (Figure 72) and measured the hydraulic conductivity in situ. An overview about this investigation and the results can be found in (Appendix N). The relevance of this example towards the limestone architecture is the similarity in flow mechanism in this silt loam. Whereas transport occurs in the macropores in the samples investigated by (Lauren et al. 1988), water and solutes are transported by fractures or macropores in limestone.

6.2 Scaling from sample to aquifer

The hydrogeological system of a limestone aquifer can be considered as a fractured system. From the point of view of an aquifer scale (10-100m), the small fractures in the 100 cm³ that are measured upon, are merely pores (Figure 36). This analogy in pore-system on both scales (Figure 36) explains the similar results for effective porosity on both scales.

Small Scale:
100 cm³

Large Scale:
Aquifer

Macropores cutting through the matrix

Fractures cutting through the limestone aquifer

**Figure 36: Upscaling from small scale macropores to large scale fractures**

While these small fractures or macropores are important for the flow of water through the small samples, they do not contribute much to the flow through the aquifer on large scale. The larger fractures (with radii that can measure up to centimetres), which are not captured within the small sampled volumes, are the fractures that are determining the flow properties of the aquifer on a large scale.

The difference of a factor 100 the hydraulic conductivity of the small scale samples and the in situ tracer test can be explained by this difference in size of the fractures that are governing the flow in both systems. The hydraulic conductivity, K_s, is related to the size of the fractures or pores that facilitate the flow:

$$K_S = \frac{\rho g r^2}{8\mu}$$

(13.)

Where ρ is the density of water, g is the gravitational constant, r is the diameter of the fractures or pores and μ is the viscosity. An increase in the size of the governing fractures in the flow system with factor 10, results in an increase in hydraulic conductivity with factor 100 if all the other conditions are identical.

This increase of hydraulic conductivity with the size of the pores or fractures can be found in other properties that are describing flow characteristics of aquifers, such as dispersivity. Figure 37 shows the increase of dispersivity with an increase in scale. As earlier explained, the small samples can be seen as porous or dual-porous samples from the point of view of the aquifer and can therefore be situated at the start of the curve (Figure 37). The performed single-well tracer test covers an area with a radius between 5 and 10 meters. Smaller fractures are incorporated in the investigated volume. This test is therefore considered as characterising the fractured system of the limestone aquifer.
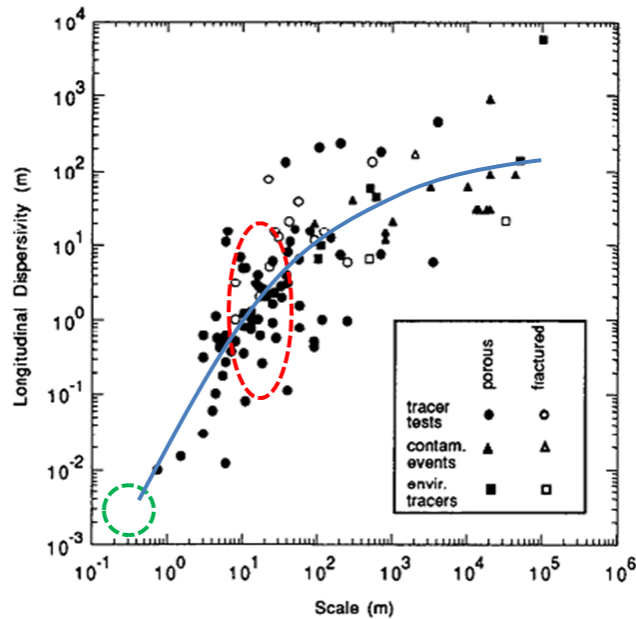
Figure 37: Overview of the longitudinal dispersivity depending on the scale with the average relation shown in blue (green: estimated region of own small scale samples; red: estimated region of own in situ test) (modified from (Gelhar, Welty & Rehfeldt 1992))

A remark that has to be made to this difference with scales is that an increase in scale not necessarily results in an increase in flow properties. Values that are lying under the blue line (Figure 37), which depicts the average increase with scale, are characterising a system where the maximum fracture size has been reached or a system with a less well-connected fracture network. Values for dispersivity that lie above the blue line indicate a system that has an increase in fracture connectivity when the scale is increased.

6.3 Conclusion

The difference and similarities between the hydrogeological parameters on both scales and how they relate to each other are important information in the process of risk assessment. This allows to make sound estimations based on measurements that are collected through small and large scale experiments.

The difference between measurements at the same scale for hydrogeological parameters such as hydraulic conductivity and effective porosity is caused by the heterogeneity in the limestone aquifer. This difference can be taken into account by changing the sample volume that is measured upon, as suggested by the relevant elementary volume theory.

The phenomenon of scaling causes the difference in values of hydraulic conductivity at different scales. This scaling is not affecting all the hydrogeological properties in the same way, as can be seen for the effective porosity. The similarity of the structure of the limestone on different scales, as is demonstrated in this chapter, is the likely reason for the same values for the effective porosity for small and large scale.

7   General conclusion

The first part of this thesis focused on small scale limestone samples (100 cm^3). An effective way of characterising the dual porosity system, typical for the limestone architecture, has been set up through gas phase experiments. Fingerprints which describe the tortuosity and pore connectivity of the limestone architecture have been developed and analysed based on measurements of gas diffusivity during different steps in the drainage process of the limestone samples. The fracture system that runs between the limestone matrix has been characterised by the average angle of diffusion and the pore-connectivity factor, while the matrix system characterisation happened through the matrix connectivity factor and the internal Buckingham (1904) pore-connectivity factor as describing parameters.

A link has been established between these gas-phase experiments and the liquid phase transport properties through the indirect estimation of the saturated hydraulic conductivity. This resulted in values for the hydraulic conductivity in the range of (0.31-3.49) e-5 m/s. Next to these indirect measurements, direct measurements have been performed to determine the hydraulic conductivity. This direct measured hydraulic conductivity was found to lie in the same range as the one determined through indirect measurements, except for one outlier of 25.64 e-5 m/s. This direct measured hydraulic conductivity has been connected to the limestone fracture network and its architecture, described by the three presented fingerprints.

The effective porosity of the small samples has been measured through direct measurements and image analysis of the samples. The range in which this effective porosity is situated for the direct measurements lies between 0.086 and 0.26. This wide range is caused by the heterogeneity of the limestone. The value for the effective porosity of 0.015 that has been obtained through image analysis is differing from this range for the same reason. A visual description of the tortuosity of the limestone fracture network has been obtained through image analysis next to this effective porosity.

An iterative process between modelling and in situ experiments has been setup to determine the hydrogeological properties of a limestone aquifer. Single-well tracer experiments provided data that were used to refine or readjust the constructed model in GMS7.1. Each step in this iterative process led to a more accurate estimation of the hydrogeological parameters around the testing well. This resulted in precise values for the hydraulic conductivity and effective porosity for this aquifer of respectively 9.6 e-4 m/s and 0.0185.

The hydraulic conductivity and effective porosity that were determined at both scales were connected to each other as a final part of this thesis. The phenomenon of scaling causes the difference in values of hydraulic conductivity at different scales, yet the effective porosity is in the same range for both scales. This is most likely due to the similar structure of the limestone on both scales. The knowledge about what is happening inside the limestone architecture and how the different scales relate to each other is important. It allows to make sound estimations in the process of risk assessment and the exploitation of aquifers.

8 Further perspectives

During the development of this thesis other ideas for further research came across. They were not carried out at the time due to restrictions in time and equipment. These ideas are enlisted below and can be used as a basis for further research or inspiration.

8.1 Characterisation through gas diffusion

8.1.1 Angle of diffusion

The average angle of diffusion that describes the tortuosity and pore connectivity in the limestone fractures characterises the complete fracture system. This parameter is based on the gas diffusivity after the matrix is fully drained (Appendix B). This does not take into account what happens inside the matrix during the different steps in the process of drying and draining. To characterise what happens during this process, a local angle of diffusion can be calculated (Figure 38). This parameter uses the change in gas diffusivity between each step ($\Delta\varepsilon, \Delta D_p/D_o$) in the drainage process and therefore gives an image of the extra tortuosity or the loss in tortuosity that is induced by draining the sample more.
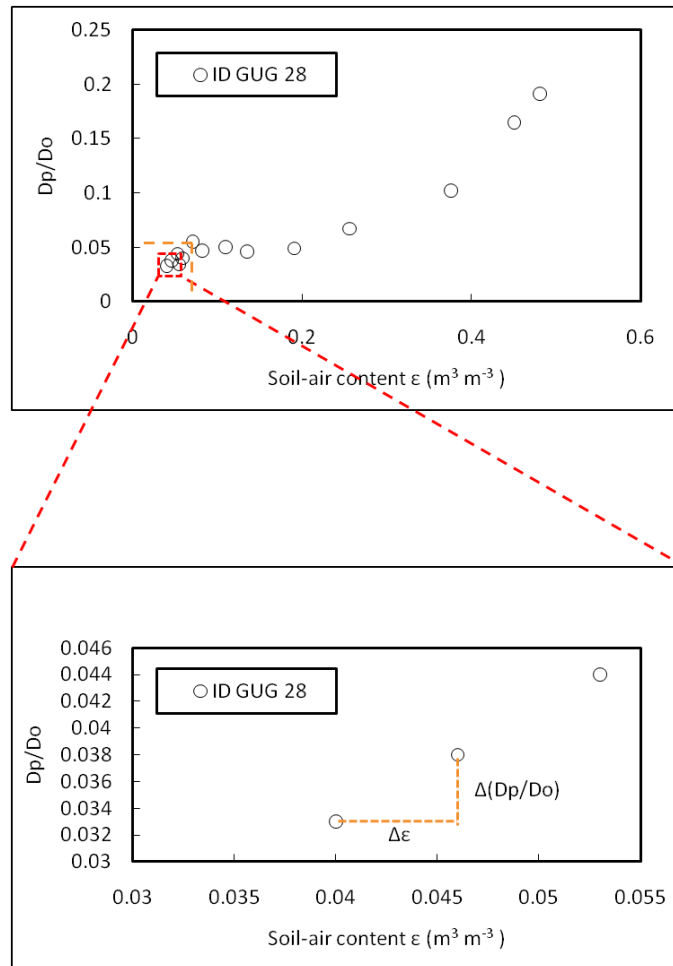
Figure 38: Example of gas diffusivity measurements of a limestone sample with orange colours demonstrating the used values for calculating the average angle of diffusion (up) and local angle of diffusion (down)

8.1.2 Modified Buckingham (1904) pore-connectivity factor

The modified Buckingham pore-connectivity factor, X*M, that is used in this thesis to describe the pore-connectivity and tortuosity inside the limestone matrix (Figure 39) is calculated based on the values that characterise the fully drained matrix (Appendix B). Yet to characterize the changes in tortuosity and transport properties during the drainage of the limestone matrix, an average of the Buckingham (1940) pore-connectivity factor can be used instead of value that is based on the upper limit.
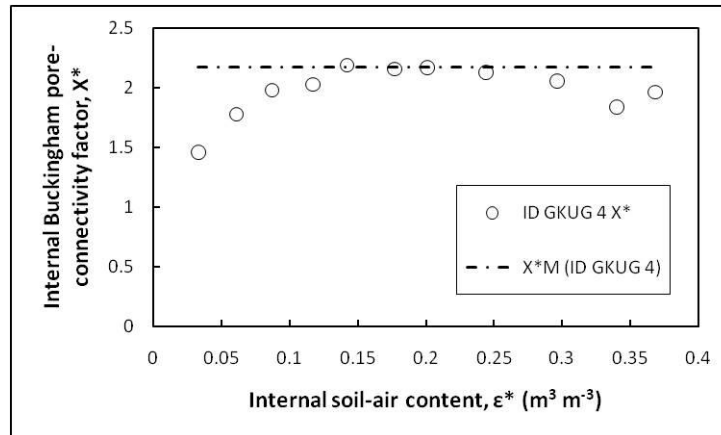

Figure 39: Example of the internal Buckingham (1904) pore-connectivity factor and X*M, calculated as mean of the 3 highest values for X*

8.2 Visualisation of the limestone structure

A better resolution for the X-ray Computed Tomography images would be obtained when the casing of the sample is made out of plastic instead of stainless steel. For this reason a new sampling device is suggested (Figure 40). Only during the sampling of the limestone sample, the casing has to withstand high stresses. After the sampling, the casing is only required for structural purpose and is not suffering from high stresses. The new sampling device consists of an outer ring that is made of stainless steel and can be removed after sampling. The inner sample casing is made of plastic and will preserve the structure after sampling and result in images that are less influenced by noise.
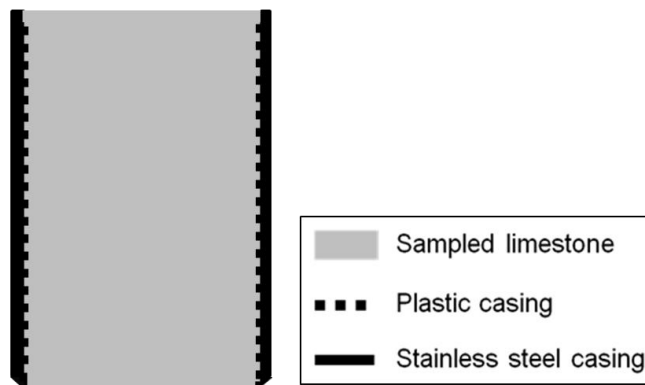

Figure 40: Limestone sampler

X-Ray Computed Tomography images which are generated by a scanner with a higher resolution, such as benchtop scanners with a resolution up to smaller than 1 µm allow to make a more precise estimation about the macro-porosity in the limestone sample and can be used to even characterise the porosity inside the limestone matrix to a certain degree.

IR image analysis can be used to give an image of the interconnected macropores which are located at the surface of the limestone sample, as discussed earlier in this thesis. The IR technique is used to generate images of a liquid with a different temperature than the surrounding architecture. Another possibility to use the IR technique to visualise or characterise the macro-porosity system is to apply this visualisation technique during the process of drainage of the limestone. Analysis of the recovered images can provide extra information about the processes that are happening during the drainage of the macropores, the matrix and what is happening when the draining process enters the area on the border between these two systems.

8.3 Characterisation through a single-well tracer test

8.3.1 Development of the method

Due to constrictions on the pumps that are used to perform the single-well tracer test, only a small area around the testing well could be investigated in this thesis. Larger pumps make it possible to cover a larger area around the testing well. When the tracer plume is allowed to drift further away from the well, the influence of local hydrogeological conditions around the testing well, will be small in comparison with the contributions of the characteristics of the whole aquifer. This allows building up an understanding of the hydrogeological conditions that is valid for the complete aquifer and not only characterises the area in the vicinity of the testing well.

The measured concentrations of tracer liquid in the well during the pumping back period can be used to calibrate the effective porosity of the aquifer in the model. An idea is to use the maximum concentration and the shape of the peak during the pumping back period (Figure 41) to calibrate the effective porosity in the model.
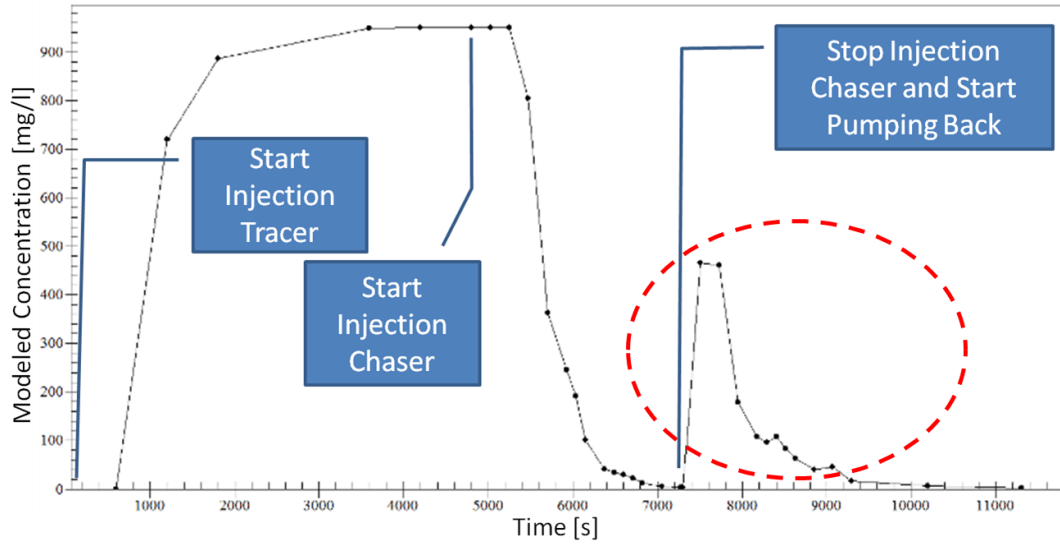
Figure 41: Modelled concentration peak (area circled in red)

8.3.2 Risk Assessment

Further application of this method to investigate the hydrogeological parameters of the limestone aquifer within the process of risk assessment and exploitation of aquifers is planned in the near future. Plans for the implementation of this method in the investigation of limestone aquifers on the island of Funen and the Copenhagen area lie now on the table and are planned to be carried out soon.

9 Bibliography

Ball, BC 1981, 'Modelling of soil pores as tubes using gas permeabilities, gas diffusivities and water release', *Journal of Soil Science*, vol 32, no. 4, pp. 465-481.

Bear, J 1979, *Hydraulics of Groundwater*, McGraw-Hill, New York.

Bear, J 1979, 'Undsteady flow to a well in a confined aquifer', in *Hydraulics of Groundwater*, McGraw-Hill, New York.

Buckingham, E 1904, 'Contribution to our knowledge of the aeration of soils', *Bur. Soil Bull.*, no. 25.

Claes, N, Chamindu, TD, Jensen, JB & Moldrup, P 2010, 'Soil-gas diffusivity fingerprints of the dual porosity system in fractured limestone', *1st International Conference and Exploratory Workshop on Soil Architecture and Physico-Chemical Functions "CESAR"*, Research Centre Foulum, Tjele, Denmark.

Downing, RA, Price, M & Jones, GP 1993, *The Hydrogeology of the Chalk of North-West Europe*, Clarendon Press, Oxford.

Duchesne, MJ, Moore, F, Long, BF & Jacques, L 2009, 'A rapid method for converting medical Computed Tomography scanner topogram attenuation scale to Hounsfield Unit scale and obtain relative density values', *Engineering Geology*, no. 103, pp. 100-105.

Gelhar, LW, Welty, C & Rehfeldt, KR 1992, 'A Critical Review of Data on Field-Scale Dispersion in Aquifers', *Water Resources Research*, vol 28, no. 7, pp. 1955-1974.

GEUS 2010, 'Jupiter', WebArchive, De Nationale Geologiske Undersøgelser for Danmark og Grønland.

GEUS 2011, 'Borereport: DGU arkivnr: 34.1887', Borereport, De Nationale Geologiske Undersøgelser for Danmark og Grønland.

Haggerty, R, Fleming, SW, Meigs, LC & McKenna, SA 2001, 'Tracer tests in fractured dolomite', *Water Resources Research*, vol 37, no. 5, pp. 1129-1142.

Haggerty, R, Schroth, MH & Istok, JD 1998, 'Simplified Method of "Push-Pull" Test Data Analysis for Determining In Situ Reaction Rate Coefficients', *Ground Water*, vol 36, no. 2.

Hall, SH, Luttrell, SP & Cronin, WE 1991, 'A Method for Estimating Effictive Porosity and Ground-Water Velocity', *Ground Water*, vol 29, no. 2.

Hamamoto, S, Perera, MSA, Resurreccion, A, Kawamoto, K, Hasegawa, S, Komatsu, T & Moldrup, P 2009, 'The Solute Diffusion Cofficient in Variably Compacted, Unsaturated Volcanic Ash Soils', *Vadose Zone Journal*, vol 8, no. 4, pp. 942-952.

Hunt, AG, Skinner, TE, Ewing, RP & Ghanbarian-Alavijeh, B 2011, 'Dispersion of solutes in porous media', *The European Physical Journal B*, vol 80, pp. 411-432.

Jacobsen, OH, Poulsen, TG, Moldrup, P & Schjonning, P 1997, 'Relating Saturated and Unsaturated Hydraulic Conductivity to Gas Diffusivity and the Campbell Water Retention Model', *Characterization and Measurement of the Hydraulic Properties of Unsaturated Porous Media*, University of California, Riverside, California.

Janniche, GS, Mouvet, C & Allbrechtsen, H-J 2010, 'Acetochlor sorption and degradation in limestone subsurface and aquifers', *Pest Management Science*, vol 66, no. 12, pp. 1287-1297.

Kristensen, AH, Thorbjørn, A, Jensen, MP, Pedersen, M & Moldrup, P 2010, 'Gas-phase diffusivity and tortuosity of structured soils', *Journal of Contaminant Hydrology*, vol 115, no. 1-4, pp. 26-33.

Lauren, JG, Wagenet, RJ, Bouma, J & Wosten, JHM 1988, 'Variability of Saturated Hydraulic Conductivity in a Glossaquic Hapludalf with Macropores', *Soil Science*, vol 145, no. 1, pp. 20-28.

Leap, DI & Kaplan, PG 1988, 'A Single-Well Tracer Tracing Method for Estimating Advective Velocity in a Confined Aquifer: Theory and Preliminary Laboratory Verification', *Water Resources Research*, vol 24, no. 7, pp. 993-998.

Loll, P & Moldrup, P 2000, *Soil Characterization and Polluted Soil Assessment*, Aalborg University, Aalborg.

Meigs, LC & Beauheim, RL 2001, 'Tracer tests in fractured dolomite', *Water Resources Research*, vol 37, no. 5, pp. 1113-1128.

Miyasaki, T 2006, 'Heterogeneity of Soils in Fields', in *Water Flow in Soils*, 2nd edn.

Moldrup, P, Hamamoto, S, Kawamoto, K, Komatsu, T, de Jonge, LW, Schjønning, P, Jacobsen, OH & Rolston, DE 2010, 'Taking Soil-Air Measurements Towards Soil-Architectural Fingerprints', *1st International Conference and Exploratory Workshop on Soil Architecture and Physico-Chemical Functions "CESAR"*, DJF, Faculty of Agricultural Sciences, Aarhus University, Tjele.

Neville, CJ 2006, 'Solute Transport in Fractured-Porous Media', S.S. Papadopulos & Associates, Inc.

Nielsen, S 2001, 'FRACFLOW', European Commission: Environment and Climate, European Commission: Environment and Climate.

Nielsen, KA 2007, *Fractured Aquifers: Fromation Evaluation by Well Testing*, Trafford Publishing, Copenhagen.

NIRAS 2009, 'Ressourceundersøgelse, Volsted Plantage fase 3: Grundvandsmodellering', Ressourceundersøgelse, NIRAS, NIRAS.

NIRAS 2009, 'Ressourceundersøgelse, Volsted Plantage fase 3: Nye boringer, moniteringsrunder og prøvepumpningsforsøg', Ressourceundersøgelse, NIRAS, NIRAS.

Poulsen, TG, Moldrup, P, Yamaguchi, T, Schjonning, P, Massmann, JW & Hansen, JA 1999, 'Predicting soil-water and soil-air properties and their effects on soil vapor extraction efficiency', *Ground Water Monitoring & Remediation*, vol 19, no. August, pp. 61-70.

Resurreccion, AC, Moldrup, P, Kawamoto, K, Yoshikawa, S, Rolston, DE & Komatsu, T 2008, 'Variable Pore Connectivity Factor Model for Gas Diffusivity in Unsaturated, Aggregated Soil', *Vadose Zone Journal*, vol 7, no. 2, pp. 397-405.

Schjønning, P, Munkholm, LJ, Moldrup, P & Jacobsen, OH 2002, 'Modelling soil pore characteristics from measurements or air exchange: the long-term effects of fertilization and crop rotation', *European Journal of Soil Science*, vol 53, no. 2, pp. 331-339.

Shahraeeni, E & Or, D 2010, 'Thermo-evaporative fluxes from heterogeneous porous surfaces resolved by infrared thermography', *Water Resources Research*, vol 46.

Shook, MG, Ansley, SL & Wylie, A 2004, 'Tracers and Tracer Testing: Design, Implementation, and Interpretation Methods', Idaho National Engineering and Environmental Laboratory, U.S. Department of Energy , Idaho Falls.

Spitz, K & Moreno, J 1996, *a Practical Guide to Guide to Groundwater and Solute Transport Modeling*, John Wiley & Sons, Inc., New York.

SSSA 2002, *Methods of Soil Analysis, Part 4: Physical Methods*, Soil Science Society of America, Inc., Madison.

10 Appendixes

Appendix A: Gas-diffusion: physical explanation of the behaviour

Appendix B: Three fingerprints describing the limestone architecture

Appendix C: Sampling

Appendix D: Gas diffusion experiments

Appendix E: Total porosity

Appendix F: Saturated hydraulic conductivity and effective porosity measurements

Appendix G: Overview of the Eternitten samples

Appendix H: Design and setup of the first numerical conceptual model

Appendix I: Pilot single-well tracer test

Appendix J: Design and modelling of the second single-well tracer test

Appendix K: Second single-well tracer test

Appendix L: Third single-well tracer test

Appendix M: Borehole report

Appendix N: Example of the REV theory

Appendix O: Abstract and presented poster from the CESAR conference (30.11-02.12.2010)

Appendix A: Gas-diffusion: physical explanation of the behaviour

Gas diffusion and diffusion in more general, is the movement of particles. In these gas-diffusion experiments, a closer look is been taken to the behaviour of gas-particles that are diffusing trough the limestone sample as function of the air-filled pore-space: starting with a saturated sample and drying or draining it gradually. These experiments result in the curves that can be observed in Figure 42. Figure 42 shows the results of gas diffusivity (Dp/Do, where Dp and Do are, respectively, the gas diffusion coefficient in soil and in free air) against air content (ε). The obtained curve for the gas-diffusivity can be split in 4 different stages, each corresponding to a phase in the drainage process (Figure 42).
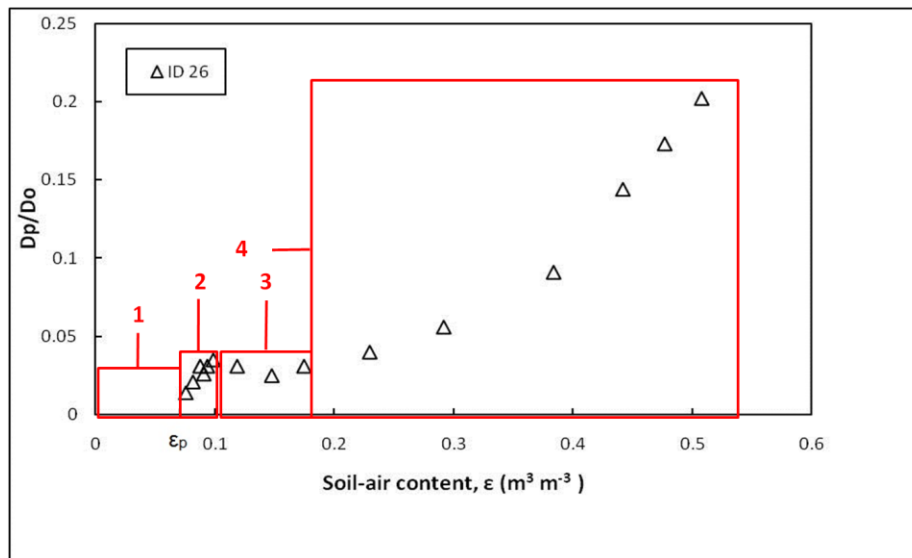
Figure 42: 4 stages in the gas-diffusivity measurement

The first stage (Figure 42) is corresponding to the period in the drainage process where the percolation threshold in the fractures between the limestone matrix has not been reached yet. This means that the gas is not able to travel through the whole sample, but some pore space has already been drained. There is not yet a free pathway from one side to the other side of the sample (Figure 43). During this period in the drainage process, the unconnected pores or dead ends in the fracture structure are draining.
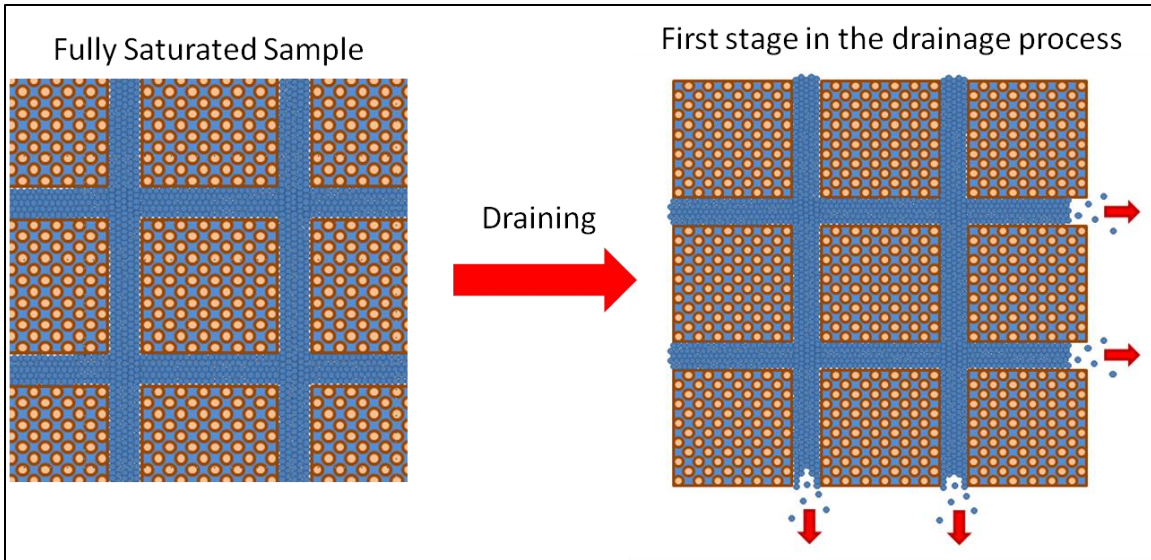
Figure 43: Fractures surrounding the limestone matrix during the first stage of the draining process (blue: water particles; brown: limestone particles)

The fractures in the limestone continue to drain in the second stage. The gas is now able to move from one side to the other side of the sample (Figure 44) and while the fractures get more drained, this movement of the gas through the sample gets facilitated as can be noticed by the increased gas-diffusion through the sample (Figure 42). This stage continues until the fractures are fully drained.
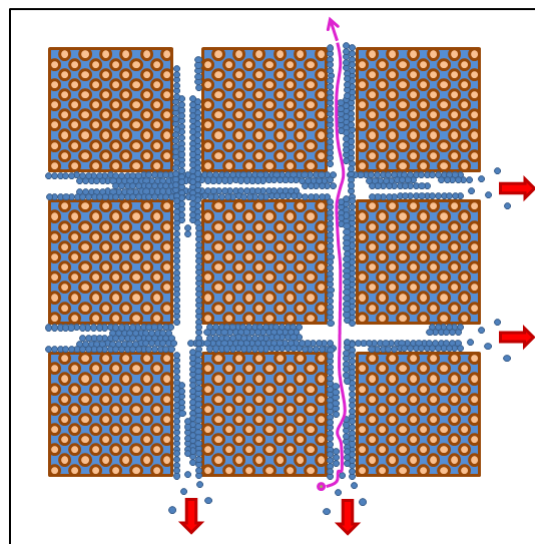
Figure 44: Second stage of the draining process: drying of the fractures, with gas particles (pink) moving through the sample

The drainage of the limestone matrix starts after the fractures in between the limestone are completely drained. Two mechanisms start working simultaneously when the drainage of the matrix starts (Figure 45):

The first mechanism is the drainage of the matrix until the percolation threshold has been reached. The second mechanism causes the gas-diffusivity curve to drop a little (Figure 42). One theory to explain this behaviour is the occurrence of a reconfiguration in the liquid phase, which will not only affect the gas-diffusion in the limestone matrix. It will also hinder the gas-diffusion trough the bigger fractures. Particles that were located on the boundary region of the limestone matrix, such as biofilm, will erode while the draining process in the matrix starts.
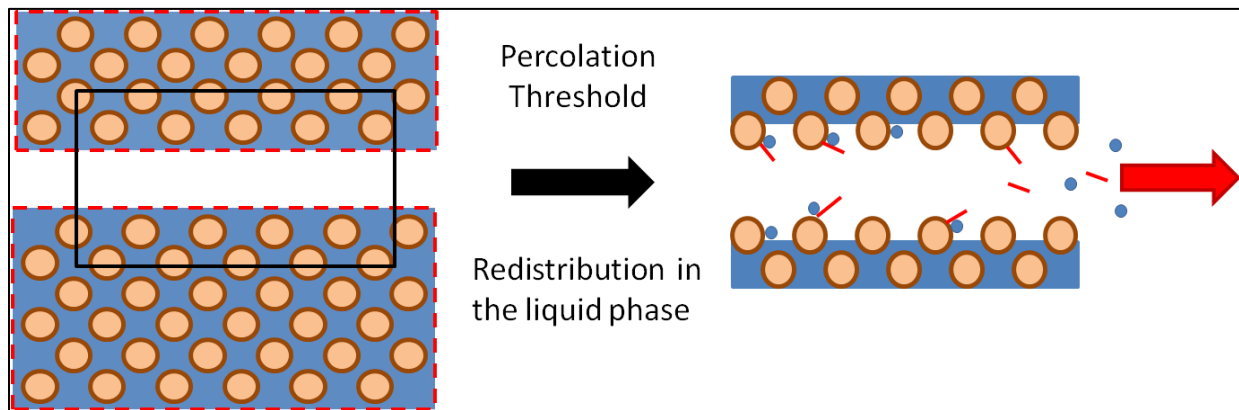
Figure 45: Third stage in the drainage process (Red stripes: biofilm; blue: water; brown: limestone particles)

The last stage in the drainage process is the further draining of the limestone matrix (Figure 46). During this stage the gas-diffusion through the sample increases not linearly as when the fractures where draining, but exponentially (Figure 42).
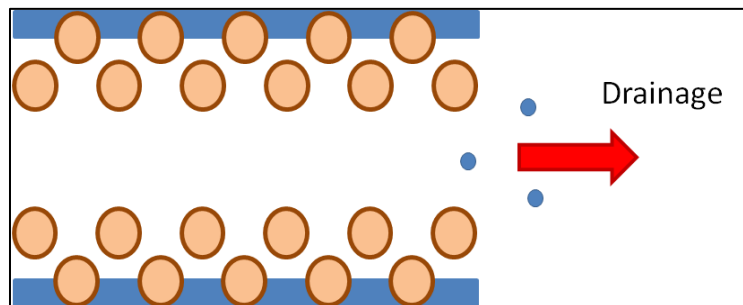

Figure 46: Fourth and last stage in the drainage process

Appendix B: Three fingerprints describing the limestone architecture

A more detailed explanation regarding the three suggested fingerprints for describing the tortuosity and connectivity of the pore network within the dual-porosity system of limestone follows.

The average angle of diffusion, α

This fingerprint was developed by (Moldrup et al. 2010). It is depending on the behaviour in the fractures. Only the second stage (Figure 42) of the gas diffusivity measurements is considered for this analysis. The average angle of diffusion can be calculated as:

$$\alpha = \sin^{-1}(\sqrt{(D_p/(D_0\varepsilon_0))}) \tag{14.}$$
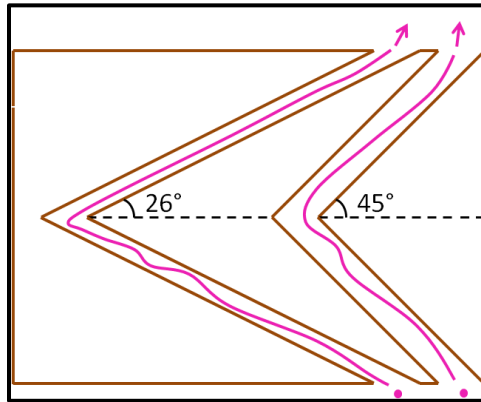
Figure 47: Average angle of diffusion in the fractures (pink: gas particles)

A lower value for the average angle of diffusion results in a longer or more tortuous pathway through the sample (Figure 47).

The modified Buckingham (1904) pore connectivity factor, X*

For the second fingerprint of the fractured limestone, a modified Buckingham (1904) model for matrix diffusivity is adopted. Buckingham (1904) suggested:

$$D_p/D_0 = \varepsilon^X \tag{15.}$$

With X typically equal to 2 in the Buckingham's model. This pore connectivity factor is a measure for the connectivity and tortuosity of a pore network. A higher pore connectivity factor characterizes a system with a more tortuous pore network. A modified version of this model is suggested to describe the gas diffusivity in the matrix:

$$(D_p/D_0)^* = (\varepsilon)^{*X^*} \tag{16.}$$

or

$$(D_p - D_{p0})/D_0 = (\varepsilon - \varepsilon_0)^{X^*} \quad ; \varepsilon \geq \varepsilon_0 \tag{17.}$$

where D_{po} and ε_0 are, respectively, the gas diffusivity and air-filled porosity at the condition of fully drained fractures, and X^* is the modified Buckingham pore-connectivity factor. This procedure corresponds to performing the Buckingham pore connectivity analysis after moving

the origin of the data to the point where the fractures are fully drained and the matrix starts to drain (Figure 48). Only the last stage of the diffusivity measurements, while the limestone matrix is draining, is considered for this analysis (Figure 42 (stage 4)).
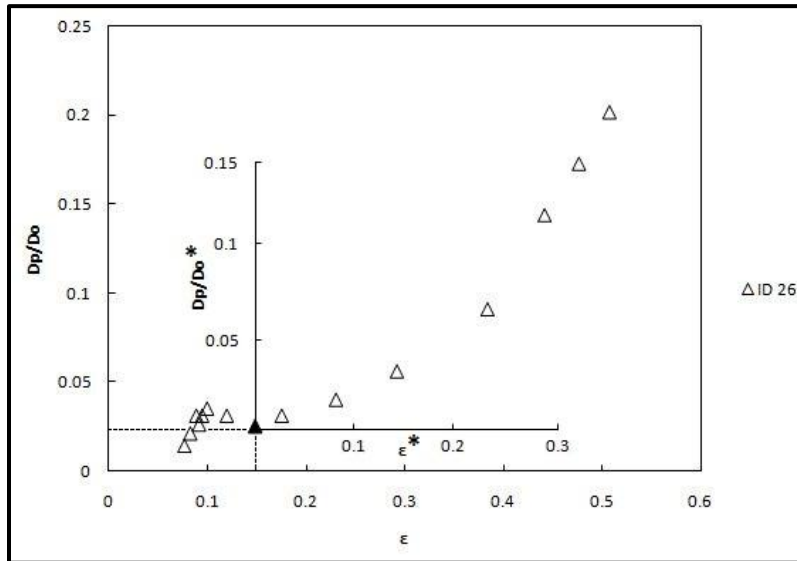

Figure 48: Example of data used for determination of the modified Buckingham (1904) pore-connectivity factor

Figure 49 shows an example of the variation of X* against the internal air-content, ε^* (=ε- ε_0) for a Gug limestone. Also shown is the upper Buckingham pore-connectivity factor, X*M, which is the average value of the three highest X* factors for each sample (in dotted and dashed lines). This value is used later for comparison between the soil-groups to filter out any outliers.
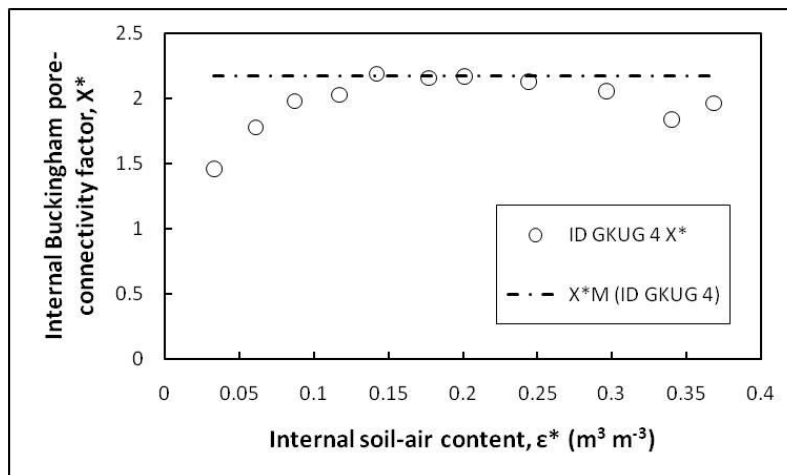

Figure 49: Example of the modified Buckingham pore-connectivity factor, X*

The two-parameter (A,B) exponential model

The non-linear increase in D_p/D_0 within the matrix (Figure 42) can be described by a two-parameter exponential model by taking into account both the fracture connectivity and the matrix pore-connectivity as follows:

$$D_p/D_0 = Ae^{B\varepsilon} \quad ; \varepsilon \geq \varepsilon_0 \tag{18.}$$

where A is the fracture connectivity factor, B is the matrix pore-connectivity factor, and ε_0 is the soil-air content at which all the factures are fully drained. Figure 50 illustrates the observed D_p/D_0 vs. ε in the matrix region for two selected samples together with the model predictions.
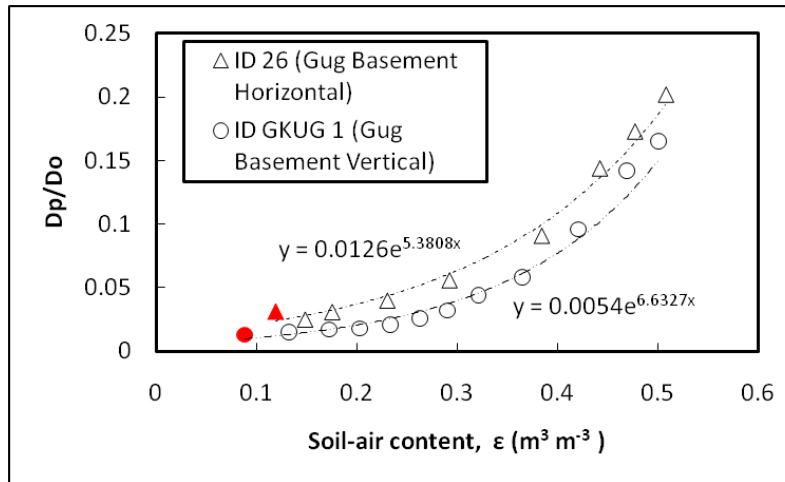

Figure 50: Example of the two-parameter (A,B) exponential model

Appendix C: Sampling

Materials and methods

The samples that were used in the second part of this thesis were sampled at the Eternitten site, located in the South-East of Aalborg (Figure 51). Three sets of samples with a volume of 100 cm^3 (h:5.1 cm; A: 19.61 cm^2) were taken just under the ground surface. Each set is consisting of three horizontal and three vertical samples. Each set was taken at distance of 13 meters from each other in a triangular grid. The sampling had to be done by manually applying a force by a hammer at the back of the stainless steel sampling cores.
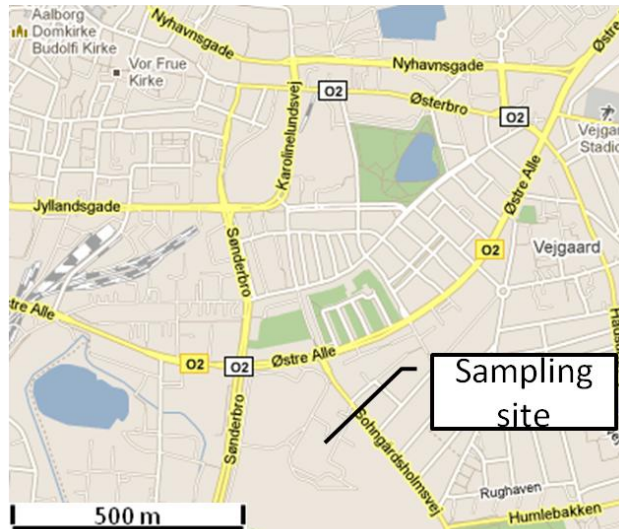

Figure 51: Eternitten sampling site

The naming of the samples is been done as follows:

- The first number represents the sample number within the set: 1, 2 or 3
- The first two letters represent the sampling site: ET
- The third letter indicates if the sample is taken horizontally or vertically: H or V
- The fourth letter represents the set to which the sample belongs: A, B or C

Results and discussion

Each set consists of three horizontally and three vertically taken samples. Due to a lack of time during this project period, only a total of six samples have been analyzed for gas diffusion. The following samples have been analyzed for gas diffusion:
1 ETVA, 1ETVC, 1ETHB, 1ETHC, 2 ETVC and 2ETHB

It appeared during the sampling that the samples that were taken within the first sampling set seemed to consist of clean limestone. The samples taken within the second set of samples appeared to be more contaminated or disturbed with a sandy material, positioned within the larger fractures or pores.

Due to the sampling method, fully undisturbed samples were not obtained. The hammering of the sample core into the limestone induces fractures in the limestone in the vicinity of the sampling core.

Appendix D: Gas diffusion experiments

Gas diffusivity is measured on the following 5 samples: 1 ETVA, 1ETHB, 1ETHC, 2ETVC and 2ETHB (see Appendix C). The gas diffusivity is measured during 2 stages of the drainage process. The first measurement is done at a drainage stage of pF. 2, when the pores with a diameter of 30 µm or more have been drained. The second stage is after air drying of the sample. No water is assumed to be left at this stage.

Method of the gas diffusion experiment

The principle behind this experiment is the measurement of air diffusivity by a non-steady method with oxygen as a diffusing gas. The change of oxygen concentration over time gives the diffusivity through the sample. An overview of the theory behind this principle and the used lab equipment is provided in further section. More information about the used technique can be found in (Schjønning et al. 2002).

Materials and theory

Fick's Law for gas diffusion can be rewritten as suggested by Taylor (1949)(SSSA 2002):

$$\frac{dM_g}{dt} = -D_p A \left(\frac{dC_g}{dx}\right) \tag{19.}$$

With:

- M_g: the mass of the gas that is diffusing (g)
- A: the cross-sectional area of the limestone sample and chamber (m^2)
- t: the time (s)
- C_g: the concentration in the gaseous phase (g gas m^{-3} limestone air)
- x: the distance or height of the sample (m limestone)
- D_p: the soil or limestone gas diffusion coefficient (m^3 limestone air m^{-1} limestone s^{-1})

where the concentration of the gas in the chamber with volume V is given by:

$$M_g = C_g V \tag{20.}$$

Substituting (20) in (19) results in:

$$\frac{dC_g}{dt} = -D_p \frac{A}{V} \left(\frac{dC_g}{dx}\right) \tag{21.}$$

The concentration gradient in the limestone can (dC_g/dx) be approximated by the difference in the concentration at both ends of the sample, divided over the length (x) of the sample:

$$\frac{dC_g}{dx} = \frac{\Delta C_g}{x} \tag{22.}$$

Application of this substitution on the used setup (Figure 52) results in:

$$D_p dt = -h_s h_c \frac{d(\Delta C_g)}{\Delta C_g}$$ (23.)

Integration of (eq.23) results (for $\Delta C_g = \Delta C_0$ for t = 0, $\Delta C_g = \Delta C_g$ for t = t):

$$\ln\left(\frac{\Delta C_g}{\Delta C_0}\right) = -\frac{D_p}{h_s h_c} t$$ (24.)

The diffusion coefficient in limestone, D_p, can now be calculated from the linear relation that is expressed in a logarithmic plot.
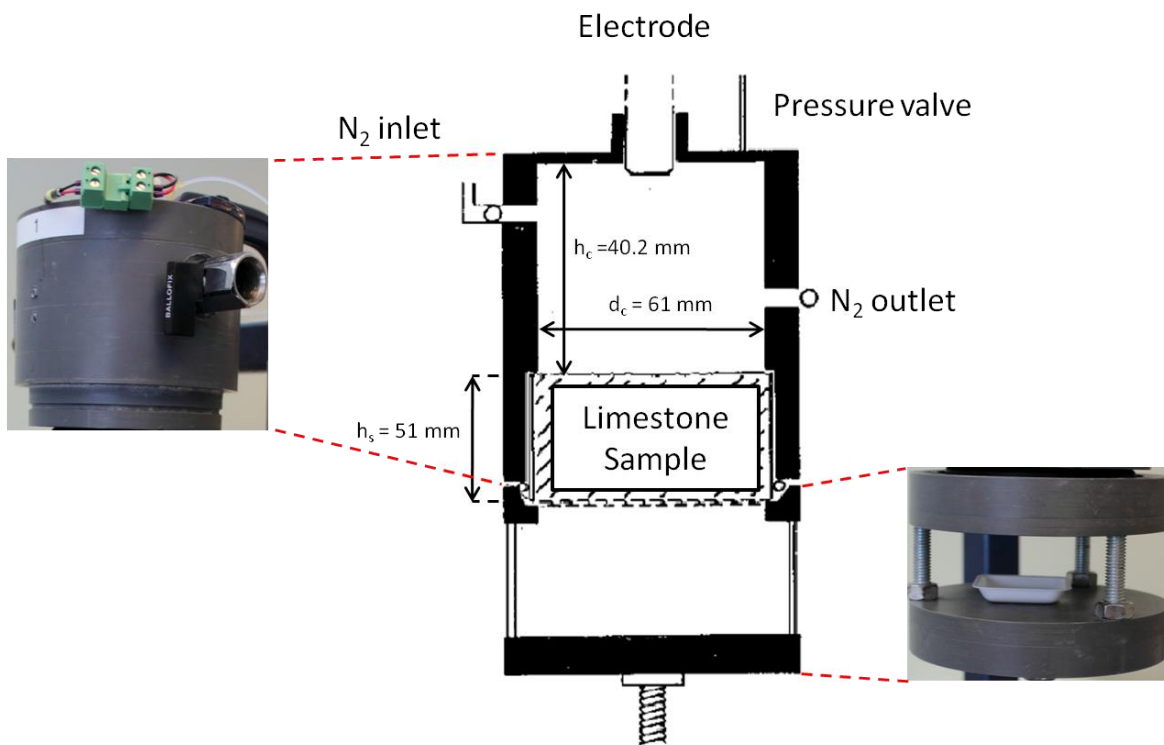

Figure 52: Gas diffusion chamber, used in the experiments

Results and discussion

The results of the gas diffusion experiment can be found in Table 4.

Table 4: Gas diffusivity measurement results

Sample	Dp/D0 at pF2	Dp/D0 after air-drying
1ETVA	0.029770904	0.163739973
1ETHC	0.029770904	0.208396329
1ETHB	0.013396907	0.193510877
2ETVC	0.00297709	
2ETHB	0.014885452	0.148854521

Only 4 of the samples could be measured after air-drying due to problems with the adapter that has been used in these measurements. This adapter was constructed to fit the samples that were taken by sample cores which were not initially destined for the used gas-diffusion chambers.

Appendix E: Total porosity

Method and results

The total porosity is calculated from the dry weight of the samples that is subtracted from weight from the saturated samples. The dry weight is measured after air-drying of the samples for 12 days at 30° Celcius. All the samples are considered to have the same volume of 100 cm^3 and the particle density of limestone is considered to be 2.7 g/cm^3.

Results and discussion

The results for the total porosity of the five measured samples are enlisted below in Table 5.

Table 5: Total porosity for measured samples

Sample	Total Porosity [vol.%]
1ETVA	52.12
1ETHC	55.14
1ETHB	50.67
2ETVC	39.60
2ETHB	43.52

The difference in total porosity between the five samples allows to make a classification of the different samples: denser samples (2ETVC and 2ETHB), looser samples (1ETVA and 1 ETHB) and a fragile sample (1ETHC).

The results for the fragile sample and looser samples are higher than what was expected to be found before the experiment took place. The fragile sample consists of a more gravel-like structure inside the sample as can be seen on (Figure 53).

Figure 53: Sample 1ETHC after cutting through

Since all the samples were sampled just above ground surface, a possible cause for this higher porosity or more fragile behaviour is that this limestone has been exposed to the weather elements over a considerate long time interval.

Appendix F: Saturated hydraulic conductivity and effective porosity measurements

Materials and methods

Method

The method which is used to perform the hydraulic conductivity measurements is analogue to the method that is described by (Loll & Moldrup 2000) for horizontal infiltration experiments. The saturated hydraulic conductivity is calculated from the basic Darcy equation, presented further in the experimental procedure.

The effective porosity is calculated from difference in weight between the fully saturated samples and the samples that are drained until pF. 2. Only the larger pores that are drained at this stage are contributing to the transport of water and solutes in the aquifer.

Experimental setup for hydraulic conductivity measurements

The setup consists of the sample that is placed in a horizontal position and connected to a constant head burette (Figure 54) by a flexible tube.

The pressure level in the burette is set 15 cm higher than the middle of the sample ($\Delta H = 0.15$ m). This will cause a hydraulic gradient over both ends of the sample and will cause water to flow through the sample. This level difference of 15 cm ensures a hydraulic gradient that is high enough to exclude the influence of the gravity during this experiment.
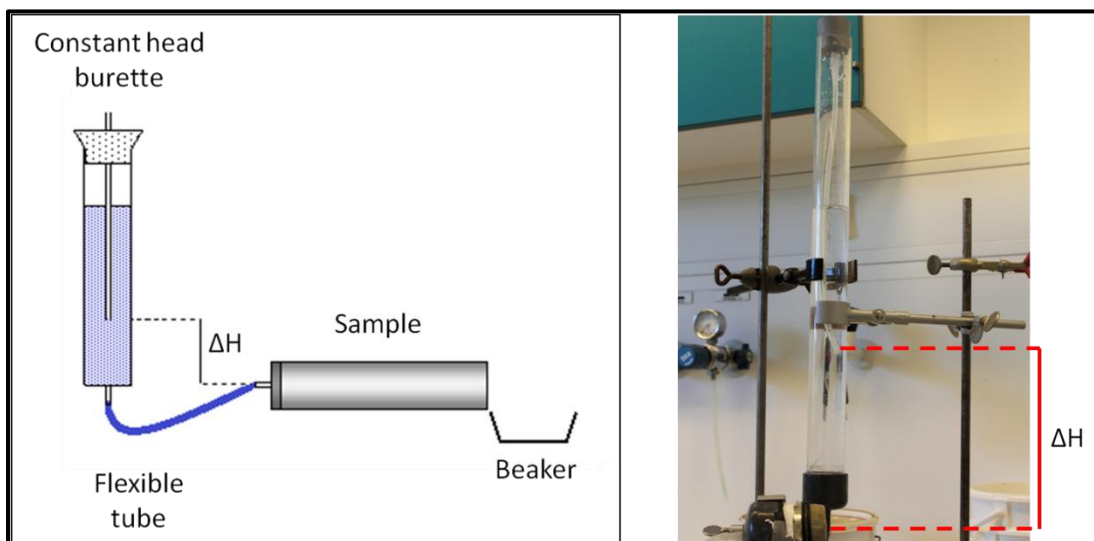

Figure 54: Setup for saturated hydraulic conductivity measurements (edited from (Loll & Moldrup, 2000))

The water is applied evenly over the surface of the sample through a moist GFC filter which is in direct contact with the Millex-FG 50 filter, mounted in the connecting PVC piece (Figure 55)
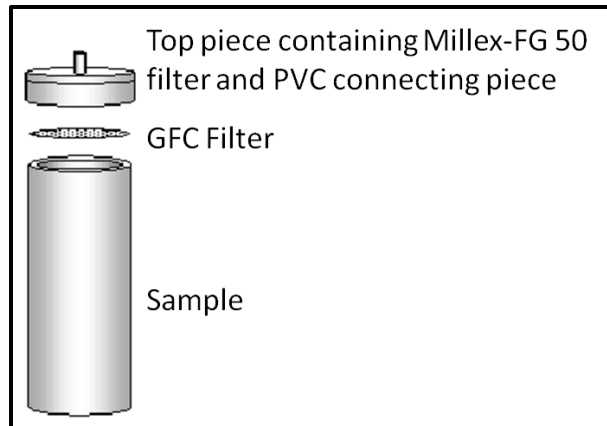
Figure 55: Connecting PVC piece with filter (edited from (Loll & Moldrup, 2000))

Experimental procedure for hydraulic conductivity measurements

1. The samples are saturated by placing them in a bucket that is filled with water until a height that equals the height of the limestone sample, minus 1 mm. This will cause the sample to saturate until 1 mm under the top of the sample. This last millimetre will be saturated by gently applying water on top of the sample, without causing the top of the sample to be disturbed.
2. After saturating the sample, it is weighted and the saturated weight is registered, before conducting the saturated hydraulic conductivity experiment.
3. The sample is attached to the PVC connecting piece (Figure 55). The sample and PVC piece are sealed with connecting tape to make sure no water flows along the sides of the sample, instead of through the sample.
4. Water flow is established through the sample for 2 minutes to make sure that the water which drained while mounting the sample is replaced.
5. The weight of the water which flows through the sample during one minute is noted for three consecutive time periods.
6. An average of the weights is taken and the conversion to flux is made.
7. Darcy's law now gives us the saturated hydraulic conductivity:

$$v = AK\frac{\Delta H}{L}$$ (25.)

with v the flux through the sample, A, the cross-section of the sample (20 cm^2) and $\Delta H/L$ equal to 3.

Experimental procedure for effective porosity measurements

The saturated samples that are used in the hydraulic conductivity measurement experiment are weighed. The mass of the samples is then compared with the weighed mass of the samples during the gas diffusion experiment at pF.2. The difference in mass for the same volume of sample gives the total porosity.

Results and discussion

Table 6 shows the weight of the saturated samples. The direct measurements of the saturated hydraulic conductivity can be found in (Appendix G).

Table 6: Saturated weight of the samples

Sample	Saturated weight [g]
1ETVA	182.506
1ETHC	182.706
1ETHB	183.556
2ETVC	210.206
2ETHB	198.826

The saturation of sample 2ETVC took more time than the other samples: it took 2 days until sample 2ETVC was completely saturated, while the other samples only needed 2-3 hours to be fully saturated by the presented method.

The effective porosity for each sample is listed in Table 7:

Table 7: Effective porosity for each sample

Sample	Effective porosity, n [cm^3 air/cm^3 sample]
1ETVA	0.17
1ETHC	0.26
1ETHB	0.09
2ETVC	0.14
2ETHB	0.12

Appendix G: Overview of the samples

A brief overview of the different parameters of the 5 samples that were measured upon for hydraulic conductivity is provided in following table:

Table 8: Overview of the different measured parameters for measured samples

Sample	Total porosity [%]	Air-filled porosity at pF. 2 [vol.%]	Dp/D0 at pF2	Dp/D0 after airdrying
1ETVA	52.116	16.590	0.030	0.164
1ETHC	55.142	26.210	0.030	0.208
1ETHB	50.668	8.580	0.013	0.194
2ETVC	39.601	14.490	0.003	
2ETHB	43.516	11.610	0.015	0.149

Sample	T at pF. 2	α at pF.2	Ks (Poulsen relationship) [e-5 m/s]	Ks direct measured [e-5 m/s]
1ETVA	2.36	25.00	3.49	3.39
1ETHC	2.97	19.68	3.49	25.64
1ETHB	2.53	23.23	1.51	1.18
2ETVC	6.98	8.24	0.31	0.34
2ETHB	2.79	20.96	1.69	1.38

Appendix H: Design and setup of the first numerical conceptual model

A transient hydrogeological model is constructed in GMS7.1 to be able to make a reasonable estimation about the strategy that should be applied for the in situ pilot tracer test. A transient model allows the injection concentrations of the tracer liquid and abstraction rates to be varied during the running of the model. The comparison between the results of the model and the outcome of the in situ test will validate our understanding of the hydrogeological situation around the well.

Setup of the model

Geological setting

The dimensions of the model in the horizontal plane are 200m by 200m, with the test well located in the middle. The model consists of a 52 meter thick limestone aquifer with 6 meters of sand on top, divided in layers of 2 meters. This makes 3 layers of sand and 26 layers of Limestone. All the processes in this model are happening in the limestone layers. The sand layers are only used to cover the limestone layers. A report of the borehole can be found in (Appendix M). The estimation of the thickness of the limestone is based on the conceptual model that has been constructed by NIRAS for Volsted Plantage (NIRAS 2009). This is a drinking water abstraction site, located 10 km southwest of the test site (Figure 26). The aquifer in both places is assumed to be the same aquifer.

Hydrogeological parameters

The hydrogeological parameters are the parameters that will guide the groundwater flow in the model. These parameters that define the model are based on 3 assumptions (Leap & Kaplan 1988):

- The aquifer is homogeneous
- There is a steady-state horizontal advective transport
- There is a local constant gradient around the testing well

This results in the following hydrogeological parameters:

- 2 Constant Head Boundaries (North and South of the well) and 2 No-Flow Boundaries (West and East of the well) to direct the groundwater flow from North to South and impose a constant natural hydraulic gradient. Based on measurements (GEUS 2010) the constant on the northern boundary is 8.35 m and 6.75 meter on the southern boundary. This corresponds to a hydraulic gradient of 0.008.
- Hydraulic Conductivity parameters for both layers are calculated from the observed transmissivity values or literature values:
  - Sand: 5e-4 m/s (Spitz & Moreno 1996)
  - Limestone: 7.97 e-5 m/s (NIRAS 2009)
  The anisotropy between the hydraulic conductivity in horizontal and vertical direction is considered to be 10, based on (Spitz & Moreno 1996).
- The well-parameters (applied pumping rates and time periods) are changed according to the different scenarios explained further below. The well screen is located from layer 12 to layer 19, covering a depth of 16 meters.

Physico-Chemical parameters

These parameters are affecting only the limestone aquifer. The physico-chemical part is neglected in the sand layer, since this layer is only used to cover the limestone layer in the model, without any other significant function. The limestone layer is modelled as a dual-porosity system. The transport of the groundwater and tracer will occur mainly in the larger fractures. The tracer liquid that is used in the modelled and in situ tests is Chloride. The effective porosity in the limestone layer is the determining parameter for this transport velocity. Three different scenarios are modelled, with in every one of them another value for the effective porosity: 0.01, 0.04 and 0.06. In the same time when this advective transport happens, diffusion of the tracer will occur into the matrix or back from the matrix into the fractures, depending on the concentration gradient. A 'dual domain mass transfer' model is used in the MT3D package to describe this diffusion process. The parameters that are used for this package are:

- The immobile porosity (matrix porosity): 0.42 (Nielsen 2001)
- 2nd sorption constant for Chloride, the tracer liquid: 1e-10 /s (Spitz & Moreno 1996)

These parameters are considered constant for every layer.

Overview of the different scenarios

The different scenarios that are modelled are 2 sets of 3 scenarios (Figure 56). The first set consists of 3 scenarios where the drift time is 27 hours, while in the second set the drift time is extended to 47 hours and 23 minutes. The three scenarios differ from each other in effective porosity: 0.01, 0.04 and 0.06. The pumping rates are the same for both sets (Figure 56).

Short drift time	Long drift time
• Injection of 1200 mg/L of Chloride during 2 hours at a rate of 1000 L/hour	• Injection of 1200 mg/L of Chloride during 2 hours at a rate of 1000 L/hour
• Chaser of 1000 L/hour for 2 hours	• Chaser of 1000 L/hour for 2 hours
• Drift of 27 hours	• Drift of 47 hours
• Pump-back at a rate of 15000 L/hour	• Pump-back at a rate of 15000 L/hour

Figure 56: Different drift time scenarios
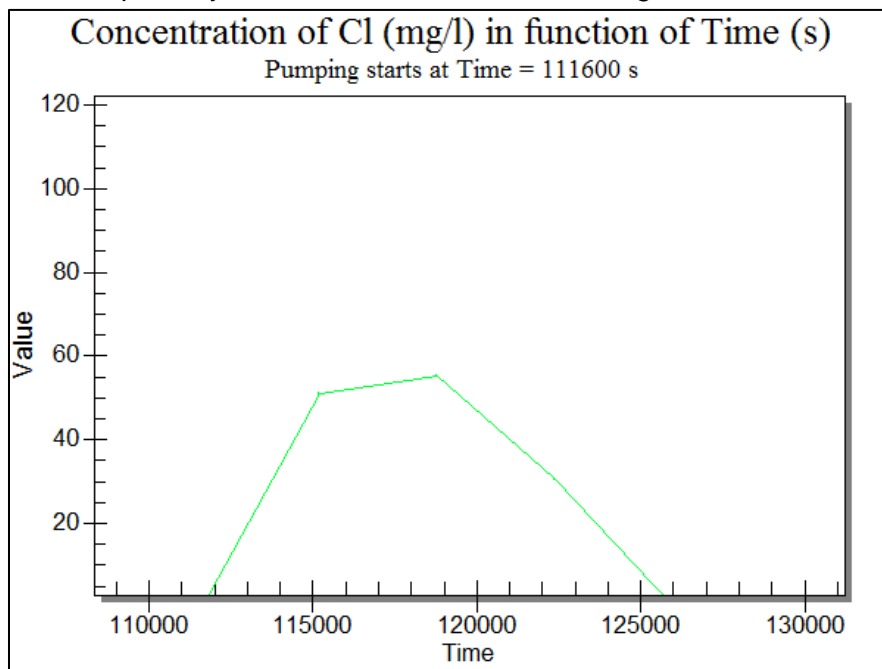
Short drift time

The time until the centre of the chloride plume will be recovered is depending on the effective porosity (Table 9). The recovery of the centre of the plume is considered the moment when half of the total injected mass of the tracer is recovered.

Table 9: Recovery times for a short drift period

| N	Short drift time (hours)	
	Time until recovery of 50%	Time until recovery of 90%
0.01	2	3.44
0.04	0.65	1.17
0.06	0.53	0.94

The modelled concentrations in the test-well will also differ, depending on what the effective porosity of the aquifer is. An overview of these modelled concentrations in the well during the pump back period follows for each scenario. The noise or fluctuations in the modelled concentrations can be attributed to the numerical dispersion in the program. The concentration curve in reality is expected to be a smooth curve.

- A low porosity of 0.01 will result in the following concentrations:

Figure 57: Concentration of the tracer: Cl (mg/l)

- A medium porosity of 0.04 will result in following concentrations:
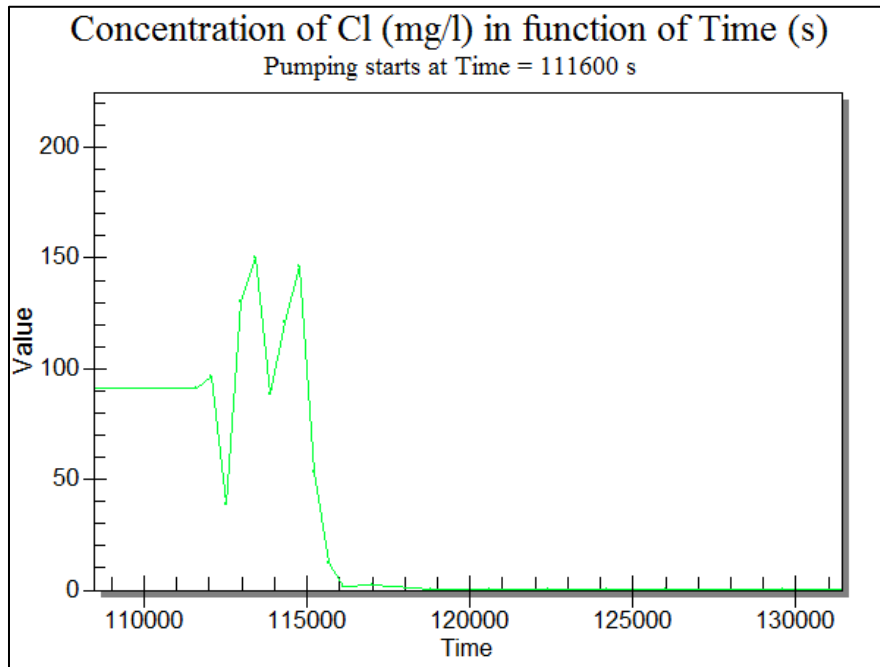
Figure 58: Concentration of the tracer: Cl (mg/l)

- A high porosity of 0.06 will result in following concentrations:
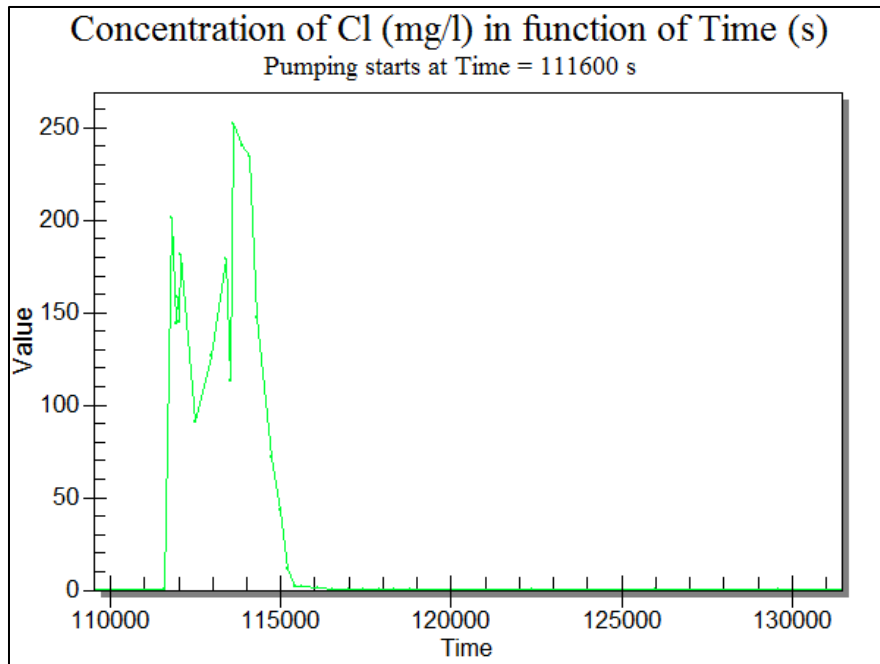
Figure 59: Concentration of the tracer: Cl (mg/l)

Long drift time

The chloride plume is now allowed to travel over a period of 47 hours. The time until the centre of plume will be recovered is depending on the effective porosity. The recovery of the centre of the plume is considered just as before to be the moment when half of the total injected mass of the tracer is recovered. The modelled recovery times are shown in (Table 10).

Table 10: Recovery times for a long drift period

N	Long drift time (hours)	
	Time until recovery of 50%	Time until recovery of 90%
0.01	5.55	9.72
0.04	3.2	6.2
0.06	2.3	4.37

The concentrations in the test-well will again differ, depending on what the effective porosity of the aquifer is. An overview of these concentrations follows for each scenario:

- A low porosity of 0.01 will result in the following concentrations:
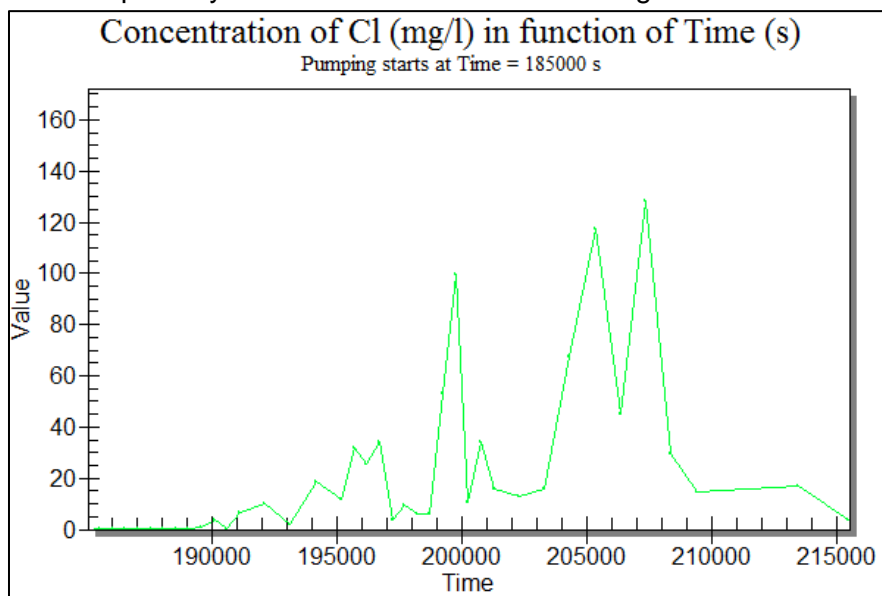
Figure 60: Concentration of Cl (mg/l) with a porosity of 0.01

- A medium porosity of 0.04 will result in the following observed concentrations:
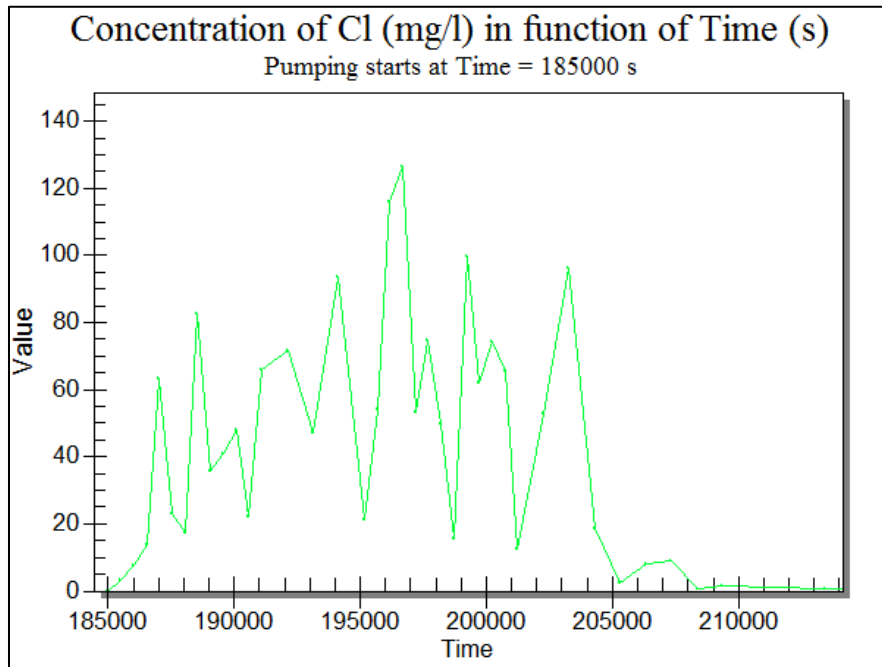
Figure 61: Concentration of Cl (mg/l) with a porosity of 0.04

- A high effective porosity of 0.06 will result in the following concentrations:
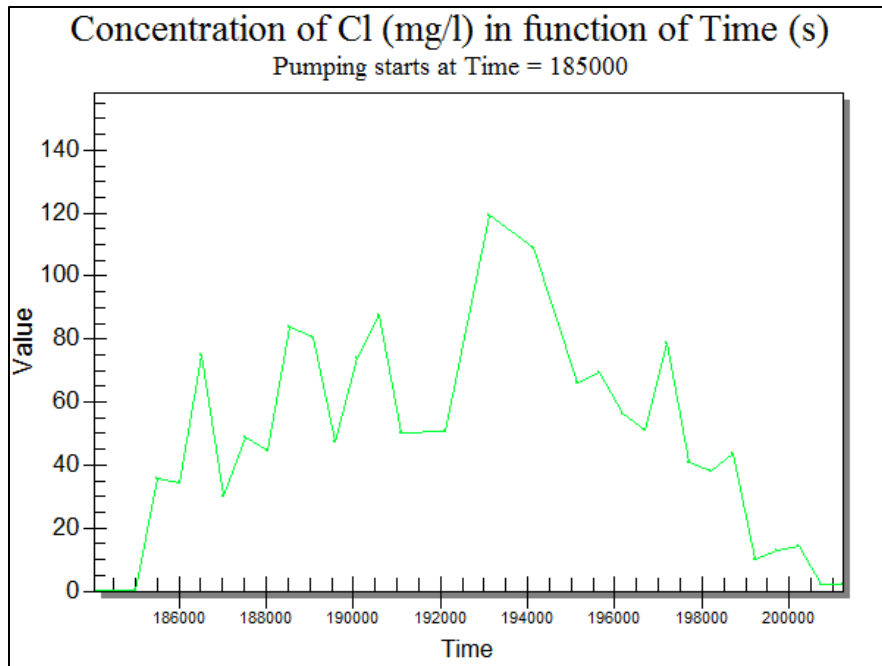
Figure 62: Concentration of Cl (mg/l) with a porosity of 0.06

The pumping back of the tracer at a rate of 15 m³/hour results in all the scenarios in a drop of 4.5 meters of the pressure head (Figure 63). This drop is influenced by the hydraulic conductivity or transmissivity of the aquifer and a change in drift time or effective porosity does not change this drop.
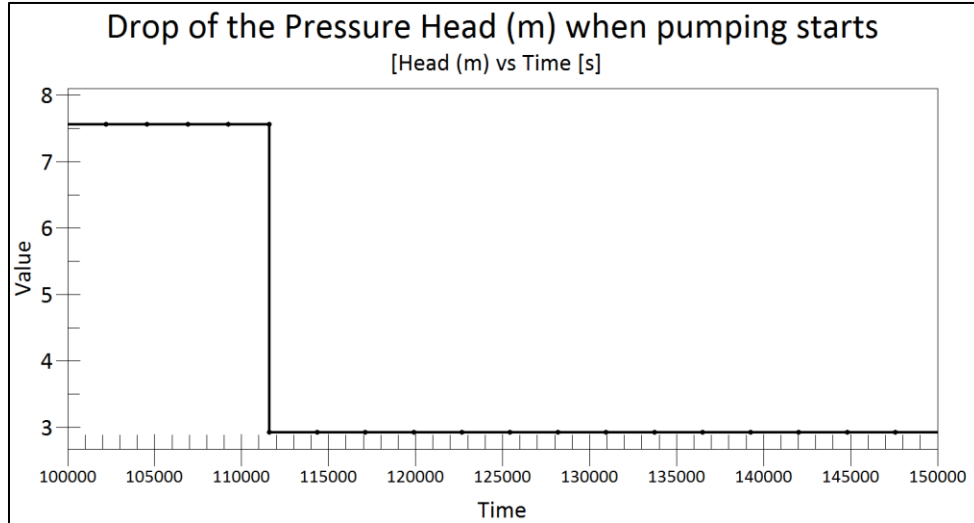
Figure 63: Modelled Drop of the pressure head during pumping back

Appendix I: Pilot single-well tracer test

The objective of this pilot test is to verify that this method can be used to determine the hydrogeological parameters that are searched for. This means that the changes of chloride concentrations (the tracer) and the changes in hydraulic head that are caused by this test should be observed. A second objective is to couple the outcome of this test back to the results from constructed model. The model and our understanding of the hydrogeological setting are adjusted based on this comparison.

The period of time for each step of this test is decided based on the GMS model (Appendix H). A short and rather conservative time period and pumping rate is chosen since the objective is not to get a final result, but to evaluate the test procedure. The parameters that are close to the scenario with a short drift time and a low effective porosity (Figure 56) are chosen to make sure that the injected doughnut-shape plume can be pumped back within a reasonable period of time.

Method of the test

The first step of the test is the introduction of a volume of 2000 litres of a tracer solution that contains chloride as a tracer. The initial objective was to introduce a total mass of 2400 g. of chloride. Due to problems with the dissolving of NaCl in the water-tanks, which was noticed after the injection of the 2000 litres of tracer solution, only a total mass of 1348 g of chloride was introduced in the aquifer. The total time over which the injection happened was 75 minutes.

The second step of the test is the introduction of a 'clean' volume of 1500 litres of a chaser at the same rate as the tracer is injected. This is to make sure that the plume has left the immediate area around the well and drifts in the actual aquifer. The plume is allowed to drift 25.5 hours after the introduction of this chaser volume.

The last step of the test is the pumping back of the plume. The rate of pumping back is 17.8 m^3/hour. The centre of the mass of the plume is expected to be recovered after 2 hours of pumping at this rate (Appendix H: Table 9).

The change of concentration in the groundwater is measured by 2 probes that register the specific conductivity of the groundwater. One of them is a handheld probe, which is used to measure the conductivity of the water that is pumped back each minute. This probe provides us with up to date information about the concentrations in the groundwater while the test is running. Adjustments or a termination of the test are based on the measurements of this probe. The second probe is based inside the well, between the well-screen and the pump. This probe is used to measure the change in concentration of chloride in the groundwater through the change in the conductivity of the groundwater. The calibration of this probe is done in the lab before the test starts and results in following relationship between the measured specific conductivity and the chloride concentration in the water:

$$y = 0.0043\,x \hspace{6cm} (26.)$$

with y the measured specific conductivity (mS/cm) and x the chloride concentration in the water (mg/l). This probe measures also the change of pressure and temperature. The data that is stored in this prober are only recovered after the test is carried out. The actual analysis of the test is performed based on the data from this second probe.

Results

After the retrieval of the data from the diver in the bottom of the well an unexpected outcome of this test is observed. Instead of an increase in the concentration of tracer or the specific conductivity in the groundwater, due to a rise in chloride concentration, a decrease is observed (Figure 64) when the plume is pumped back. The value of 572 µS/cm that is observed while pumping back is even lower than the initial background value of 587 µS/cm. During the pump-back stage only slightly cleaner groundwater is attracted and the introduced chloride plume is lost in the aquifer. This suggests that at least in the vicinity of the well, the local effective porosity is lower than 0.01 or a large crack with different hydraulic properties than the surrounding limestone aquifer might be present.
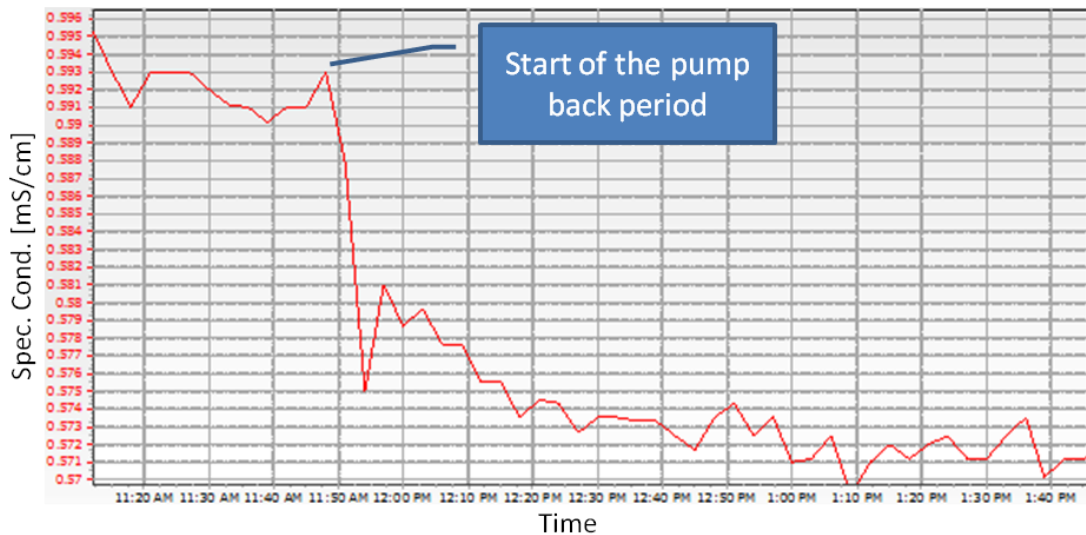
Figure 64: Observed drop in specific conductivity when pumping back in function of time

When looking at the used scenario in GMS, a drop of approximately 4.5 meters was expected to occur (Figure 63). However, a decrease of the pressure head of only 21 cm occurs together with the drop of the observed specific conductivity (Figure 65). This drop with 21 cm is due to the pumping back with a rate of 17.8 m^3/hour.
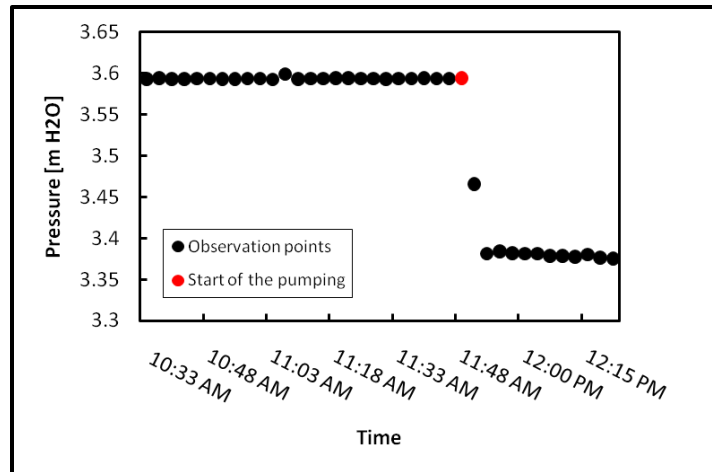
Figure 65: Observed drop of the head when the pumping starts in function of time

The actual introduction of the tracer solution in the pilot test started at 8:12 am, yet the rise in concentration occurs only 25 minutes after this solution is introduced in the well. Figure 66 suggests that the chloride and chaser introduction can be modelled as a plug-flow with a lag of 25 minutes. These 25 minutes can be seen as the time it takes for the liquid to travel from the ground surface to the bottom of the well.
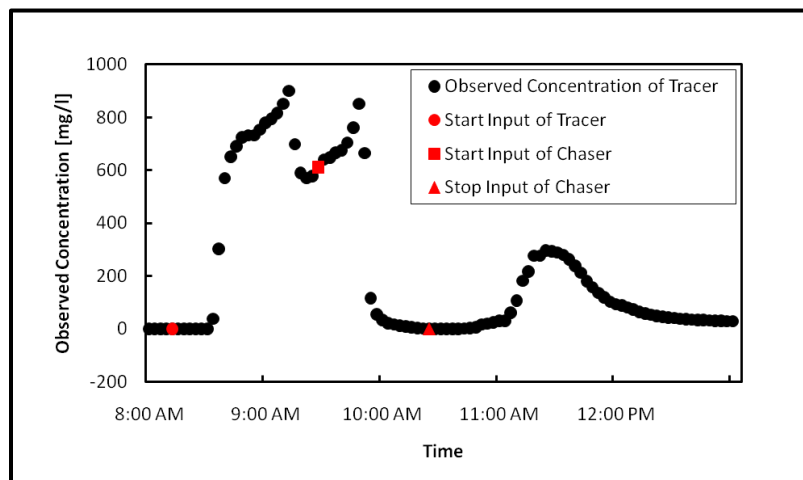
Figure 66: Observed upper part of the tracer plume passing the well after the chaser introduction in function of time

After the second step of the test, after the tracer is injected and pushed into the aquifer by the chaser, an increase in conductivity can be observed in the ground water (Figure 66). There are 2 explanations possible for the immediate increase in chloride concentration. One explanation is that the chloride is not leaving the vicinity of the well, even after applying the chaser solution. This behaviour can be contributed to a higher effective porosity of around 0.06 or more. This higher effective porosity can be caused when the well was constructed and the volume of the

aquifer that is in direct contact with the well got disturbed. This doesn't mean that the entire aquifer has this property.

Another explanation is that this is the chloride that has been left in the filter. This is less likely since it would imply that the flushing clean water had no effect and that the natural groundwater flow would carry this chloride after we stop flushing without any problem into the well.

Appendix J: Design and modelling of the second single-well tracer test

The pilot test in the field demonstrated through the observed drawdown data a mistake in the idea about the hydraulic conductivity. The hydraulic conductivity of the limestone aquifer is adjusted in this second model, based on the drawdown that occurs during the pumping back period in this test (Figure 65). The value is raised with a factor 12, resulting in a horizontal hydraulic conductivity for the limestone of 9.6 e-4 m/s. This is a value what also in literature can be found for limestone aquifers (Spitz & Moreno 1996). This change of hydraulic conductivity in the model results in the observed drop of 0.38 m, which can be seen in (Figure 67). All the other parameters in this model are kept the same as in the first constructed model (Appendix H).
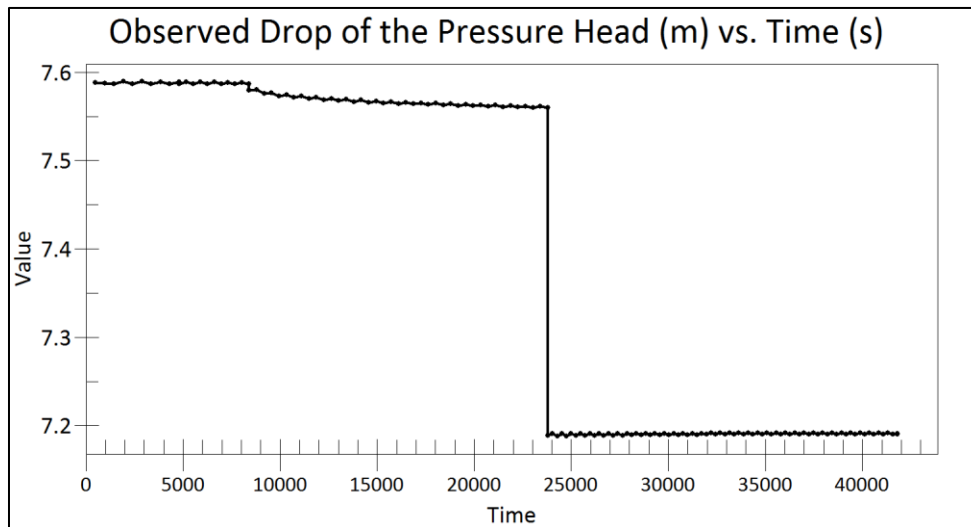
Figure 67: Drop of the pressure head in the second model

Appendix K: Second single-well tracer test

Method of the test

The first step of the test is the same as for the pilot tracer test. A volume of 2000 litres of a tracer solution that contains chloride as a tracer is injected during 80 minutes. A total mass of 2044 g of Chloride is injected in the aquifer this time.

The second step of the test is the introduction of a 'clean' volume of 1500 litres of a chaser at the same rate as the injection of the tracer. This is again to make sure that the plume has left the immediate area around the well and drifts in the actual aquifer. The plume is now only allowed to drift 2.5 hours after the introduction of this chaser volume. This restriction in drift time is based on the results of the pilot test and the second model in GMS.

The last step of the test is the pumping back of the plume. The rate of pumping back is 18 m^3/hour. The centre of the mass of the plume is expected to be recovered within 2 hours of pumping at this rate. This expectation is based on the model of the recovery of the chaser in the first model. The rise of the hydraulic conductivity in the second model and the reduction of the drift time should reduce the time it takes for the plume to return to the well. This should result in a recovery time that is less than in the first model. The change of concentration in the groundwater is again measured by 2 conductivity measuring probes.

Results

The observed concentration during the injection and drift period (Figure 68) shows that the total injected chloride mass is more than the injected mass in the pilot test. The upper part of the doughnut passes again the well after the application of the chaser end. The maximum concentration in this part of the doughnut is the same as in the pilot test, yet the total injected mass in the pilot test was less.
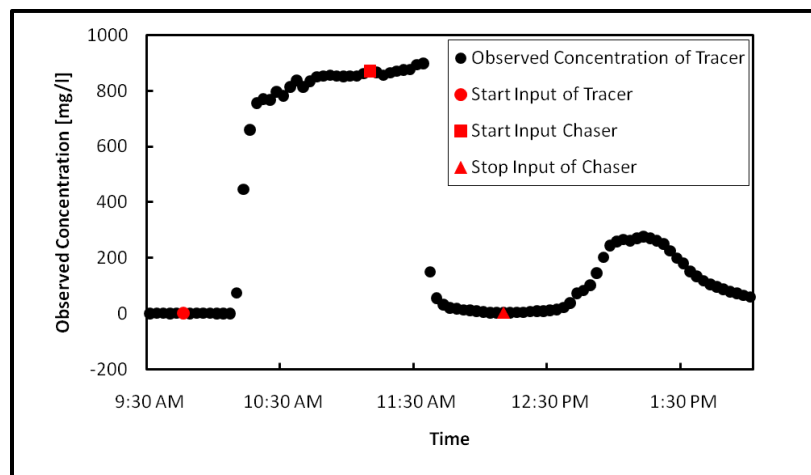

Figure 68: Observed upper part of the tracer plume passing the well after application of the chaser in function of time

The upper part of the tracer plume, which passes the well immediately after the chaser stops (taking the lag time into account), suggests that the generated flow velocity of chaser is equal or

nearly equal to the natural flow velocity in the aquifer. This might explain why the upper part of the plume is not pushed away from the well.

A small increase in the specific conductivity, and hereby the chloride concentration, can be observed when the pumping back of the tracer starts (Figure 69). After this short increase (Figure 69, at time 2.45 pm), a decrease until the background concentration occurs.

Only 339 g of Chloride is recovered during this second single-well tracer test. This is approximately 17 percent of the injected chloride mass. This amount of recovered tracer solution is not enough to be able to make any conclusions about the hydrogeological situation in the vicinity of the test-well or to apply an analytical method to analyze these results.
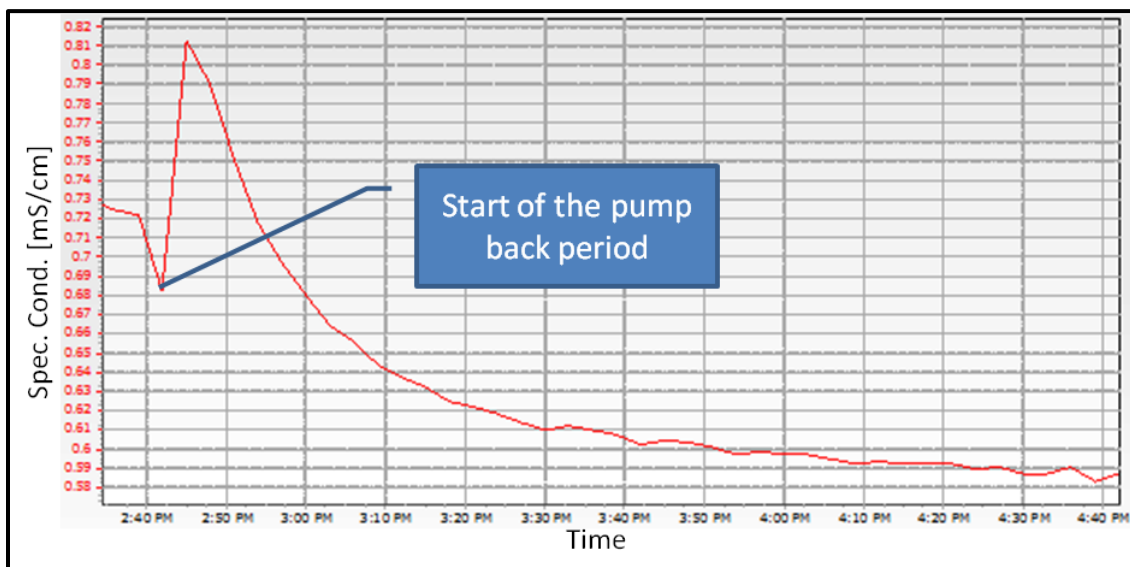
Figure 69: Measured specific conductivity during the pumping back period of the tracer in function of time

Appendix L: Third single-well tracer test

The results that are obtained from this test are used to finalize our idea about the hydrogeological properties of the limestone aquifer around the testing well. The obtained results of this test are used to calculate the effective porosity and ground water velocity from an analytical formula (eq.5), derived by (Hall, Luttrell & Cronin 1991). The method of the in situ test is presented in the following paragraph, while the results and analysis can be found in the thesis under chapter 'Characterization through a single-well tracer test'.

Method of the test

The first step of the test is the introduction of a volume of 1880 litres of a tracer solution that contains chloride as a tracer during 85 minutes. A total mass of 1922 g of chloride was introduced in the aquifer during this period. The second step of the test is the introduction of a volume of 1000 litres of clean water as a chaser during 40 minutes. This is to make sure that the plume has left the immediate area around the well and drifts in the actual aquifer. The plume is now only allowed to drift 30 minutes. This restriction in drift time is based on the results of the modelling of the catchment area downstream of the well in GMS.

The last step of the test is the pumping back of the plume. The rate of pumping back is 18 m^3/hour. The change of concentration in the groundwater is again measured by 2 conductivity measuring probes.

Appendix M: Borehole report

The report that is provided by (GEUS 2011) gives a detailed overview of the geology at the place of the testing well and the height of the water table (Figure 70 & Figure 71) at the moment of the in situ tests. This report however was only obtained after the performing of these in situ tests.

Figure 70: Borehole report of well 34.1887 (top section)

35 KALK/KRIDT, blød, slammet, flint-holdig, lys gulgrå, "coccolithkalk/slamkalk". Prøve udtaget ved 39 m.

40 KALK/KRIDT, blød, slammet, flint-holdig, lys grå, "coccolithkalk/slamkalk". Prøve udtaget ved 43 m.

45 KALK/KRIDT, blød, slammet, flint-holdig, lys grå, "coccolithkalk/slamkalk". Prøve udtaget ved 48 m.

50 KALK/KRIDT, blød, slammet, flint-holdig, lys grå, "coccolithkalk/slamkalk". Prøve udtaget ved 53 m.

55 KALK/KRIDT, blød, slammet, flint-holdig, lys grå, "coccolithkalk/slamkalk". Prøve udtaget ved 58 m.

60 KALK/KRIDT, blød, slammet, flint-holdig, lys grå, "coccolithkalk/slamkalk". Prøve udtaget ved 64 m.

Gruskastning 8-16mm Filter (i1)

Aflejringsmiljø - Alder (klima-, krono-, litho-, biostratigrafi)

meter u.t.

0	-	0,5	terrigen- postglacial
0,5	-	35	glacigen- glacial
35	-	65	marin- maastrichtien

Figure 71: Borehole report of well 34.1887 (bottom section)

Appendix N: Example of the REV theory

An example of this REV with regards to the saturated hydraulic conductivity is given by (Lauren et al. 1988). They investigated the REV for hydraulic conductivity of a silty loam with macropores by applying different sample sizes (Figure 72) and measured the hydraulic conductivity in situ.
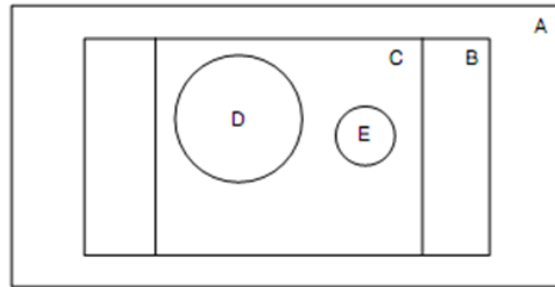
Column	Dimensions (cm)	Volume (cm³)
A	160 × 75 × 20	240,000
B	120 × 75 × 20	120,000
C	50 × 50 × 20	50,000
D	20 (diam.) × 20	6,283
E	7 (diam.) × 6	884

Figure 72: Different sample sizes used by Lauren et al. (modified from (Lauren et al. 1988))

An overview of the results of these hydraulic conductivity measurements and their statistical parameters can be found in Table 11. The size of the standard deviation gives an idea about the suited REV. The higher standard deviation for samples with volume D and E is caused by the larger size heterogeneities in the soil, which are not averaged out over the complete volume of the sample. The measurements on these volumes are not acceptable as representative for the whole in situ soil volume. The small standard deviation for samples with volume B and C means that the hydraulic conductivity of this heterogeneous soil is averaged over the complete volume of these samples.

Table 11: Overview of the results of in situ hydraulic conductivity measurements for the sample sizes stated in Figure 72 (taken from (Lauren et al. 1988))

Size	cm day^{-1}			Standard deviation	Coefficient of variation (%)	Number of samples
	Mean	Mode	Median			
A	21.3	10.3	16.6	16.9	79	37
B	13.7	6.4	10.7	11.0	81	36
C	14.4	6.3	10.9	12.5	96	37
D	36.6	6.3	20.3	54.9	150	37
E	34.5	4.8	16.3	64.0	186	35

Water transport through a limestone aquifer is governed by the transport through the cracks and larger fractures and not so much by the matrix or smaller fractures. Larger volumes to measure the hydrogeological properties on are therefore required. The volumes that are appropriate to determine these hydrogeological properties are dependent on the distribution of these larger cracks. Table 12 lists different sizes for REV that were empirically determined.

Table 12: Empirical determined REV size (taken from (Miyasaki 2006))

	REV size	Subject
Large	REV > 1000 (m)	Hydrological modeling of a river basin
	REV > 5 (m)	Water balance in field with cracks
	REV > 0.5 (m)	Saturated hydraulic conductivity of soil with macropores
	REV > 0.05 (m)	Bulk density, water content, and solute concentration
Small	REV > 0.01 (m)	Microstructures

Appendix O: Abstract and presented poster from CESAR conference (30.11-02.12.2010)

The following pages contain the poster and abstract that both were presented at the 1st International Conference and Exploratory Workshop on Soil Archicture and Physico-Chemical Functions "CESAR". This conference took place from November 30th-December 2nd 2010 at Research Centre Foulum, Tjele, Denmark

Soil-gas diffusivity fingerprints of the dual porosity system in fractured limestone

Niels Claes, Deepagoda TKK Chamindu, Jacob Birk Jensen, and Per Moldrup

Aalborg University, Sohngaardsholmsvej 57, DK-9000 Aalborg, Denmark
nclaes09@student.aau.dk

Summary

The presence of fractured vadose zones (e.g., limestone or clay tills) may potentially pose significant environmental concerns due to the rapid, preferential migration of gaseous plumes through interconnected pore networks. However, recent modelling studies related to fractured vadose zone processes are mostly limited to hydrogeological (water and solute) transport studies with very poor attention to the gaseous phase transport studies (Kristensen et al. 2010).

This study characterizes fractured limestone soils for gas diffusion based on three different gas diffusivity fingerprints. The first fingerprint is a two-parameter exponential model, which mainly describes the gas diffusivity in the limestone matrix while taking both fracture connectivity and matrix pore connectivity into account. With the second fingerprint, we make a close observation of the tortuous matrix pore network by means of a modified Buckingham (1904) pore connectivity factor (X^*). The third fingerprint of the fracture network involves the average angle of diffusion α (Moldrup et al. 2010), a parameter which characterizes the average angle at which the fractures are penetrating the sample.

Methods

In this study, we considered in total of 13 fractured limestone samples from literature which were sampled from two different vadose zone profiles in Denmark: Gug limestone and Storvorde limestone (data from (Kristensen et al. 2010)). From Gug limestone, we considered two samples (ID 37 and ID38) taken vertically just below the ground surface, six samples (ID 28 and ID GKUG 1 to 5) taken vertically under the basement of a house, and two samples (ID 25 and 26) taken horizontally under the basement of the same house. Three Storvorde limestone samples were retrieved vertically about 2 m below the ground surface. For details on the sampling, preparation and measurements, see (Kristensen et al. 2010).

Results

Figure 1 shows the results of gas diffusivity (D_p/D_o, where D_p and D_o are, respectively, the gas diffusion coefficient in soil and in free air) against air content (ε) for all the 13 soil samples. The soil gas diffusivity increases with increasing soil-air content for all samples. This increase in D_p/D_o occurs in 2 stages, which suggest that a dual-porosity model is more suited to describe this behaviour.

In the first stage, a linear increase occurs when the cracks within the limestone matrix start draining, and it continues until all the cracks are completely drained. The higher gradient of this increase in gas diffusivity for the Storvorde samples compared to Gug samples suggest a more pronounced fracture network. The higher values of gas-diffusivity in the horizontal Gug (basement) samples compared to those in the vertical samples taken at the same location reveals the anisotropy of the media. When the drainage of the matrix starts, a non-linear trend in gas diffusivity with increasing ε can be observed for all the samples.

114
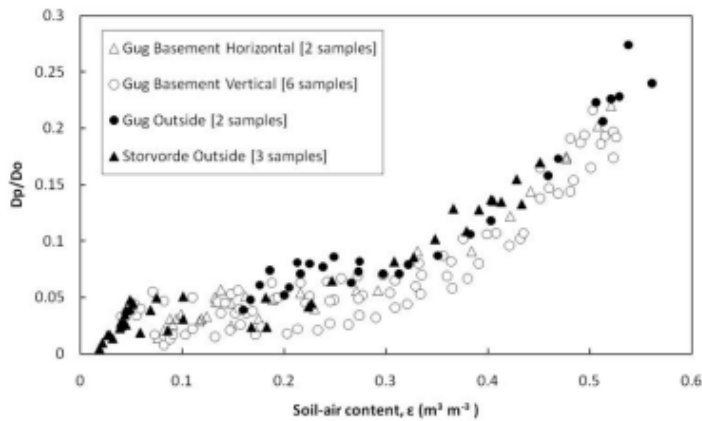
Fig. 1. Gas diffusivity (D_p/D_o) against air-content (ε) for the limestone samples.

The non-linear increase in D_p/D_o within the matrix can be described by a two-parameter exponential model by taking into account both the fracture connectivity and the matrix pore-connectivity as follows:

$$D_p/D_o = Ae^{B\varepsilon} \; ; \; \varepsilon \geq \varepsilon_0 \tag{1}$$

where A is the fracture connectivity factor, B is the matrix pore-connectivity factor, and ε_0 is the soil-air content at which all the factures are fully drained. Fig. 2a illustrates the observed D_p/D_o vs. ε in the matrix region for two selected samples together with the model predictions (Eq. (1)). The same data, when presented in a log-normal plot, yield a linear relation (Fig. 2b). We further observed an apparent overall linear relation between the parameters A and B (Fig. 2c), which can be adequately described by:

$$B = -117\,A + 6.94 \tag{2}$$

This linear relationship suggests that a higher diffusivity in the fracture network will also imply a higher diffusivity in the matrix and thereby reveals a useful geological feature of the location.
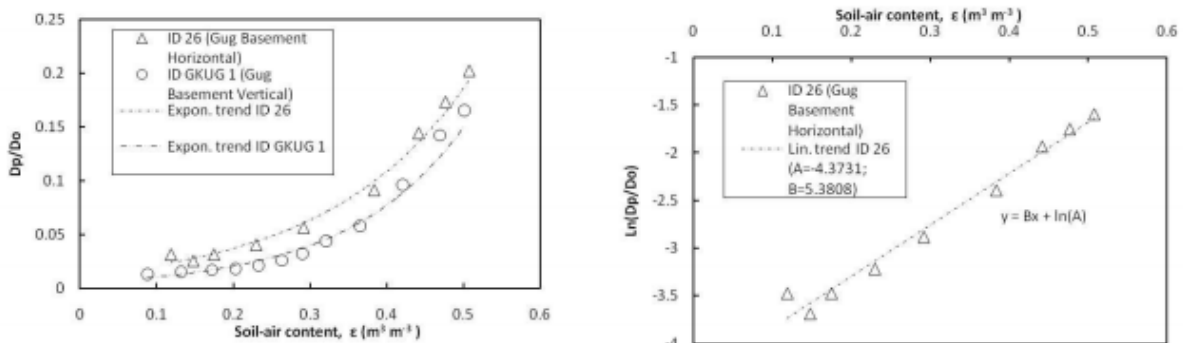
Fig. 2. Gas diffusivity in the limestone matrix: (a) D_p/D_o vs. ε and (b) $\ln(D_p/D_o)$ vs. ε

115
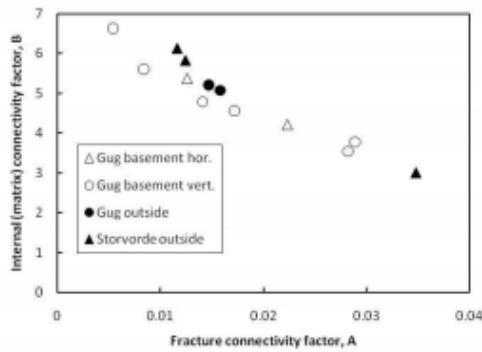
Fig. 2. (c) A-B relation for the exponential model (Eq.(1)).

For the second fingerprint of the fractured limestone, we adopt a modified Buckingham (1904) model for matrix diffusivity. Buckingham (1904) suggested:

$$D_p/D_o = \varepsilon^X \tag{3}$$

With X typically equal to 2 in the Buckingham's model. We suggest a modified version of this model to describe the gas diffusivity in the matrix:

$$(D_p - D_{po})/D_o = (\varepsilon - \varepsilon_0)^{X^*} \quad ; \varepsilon \geq \varepsilon_0 \tag{4}$$

where D_{po} and ε_0 are, respectively, the gas diffusivity and air-filled porosity at the condition of fully drained fractures, and X^* is the internal Buckingham pore-connectivity factor.

Fig. 3a shows the variation X^* against the internal air-content, ε^* ($=\varepsilon - \varepsilon_0$) for two Gug limestones. Also shown are the upper Buckingham pore-connectivity factor, X^*M, which is the average value of the three highest X^* factors for each sample (in dotted and dashed lines). Fig. 3b gives an overview of the maximum and minimum value for X^*M for each sample-group, together with the average value. The maximum value for X^*M is lower for the limestone in the surface layer in Gug due to a lower compaction of these samples, in comparison with the ones that were taken in Gug under the basement of the building. This absence of compaction will result in less tortuosity and a lower internal pore-connectivity factor.
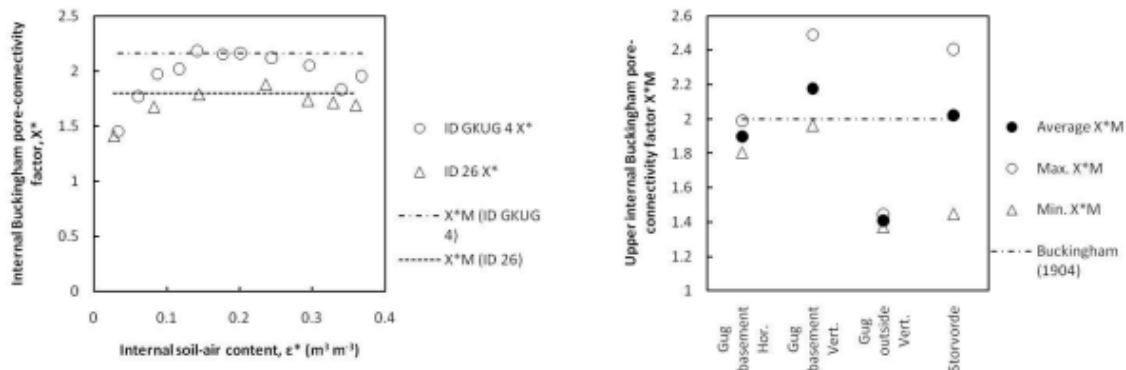
Fig. 3. Internal Buckingham pore-connectivity factor: (a) Examples of the upper internal pore-connectivity factor X^*M; (b) Overview of X^*M in comparison with the pore-connectivity factor suggested by Buckingham (1904).

Except for the uncompacted Gug limestone, other Gug and Storvorde limestones have an average X^*M factor close to 2, the value suggested by Buckingham (1904). Further, the slight anisotropy observed for the fractured region (Fig. 1) in Gug (under the basement) samples could also be noticed in the matrix region (Fig. 3b).

The orientation of fractures is an important characteristic governing most of the fractured media transport processes. In the third fingerprint, therefore, we observed the average angle of diffusion α (Moldrup et al. 2010) for the selected four soil groups. The, average angle of diffusion (Fig. 4a) can be calculated as:

$$\alpha = \sin^{-1}(\sqrt{(D_p/D_o\varepsilon_o)}) \tag{5}$$

The observed smaller angle of diffusivities for the samples taken below the basement compared to the samples taken from outside (Fig. 4b) can be attributed to the high soil compaction below the building foundation.
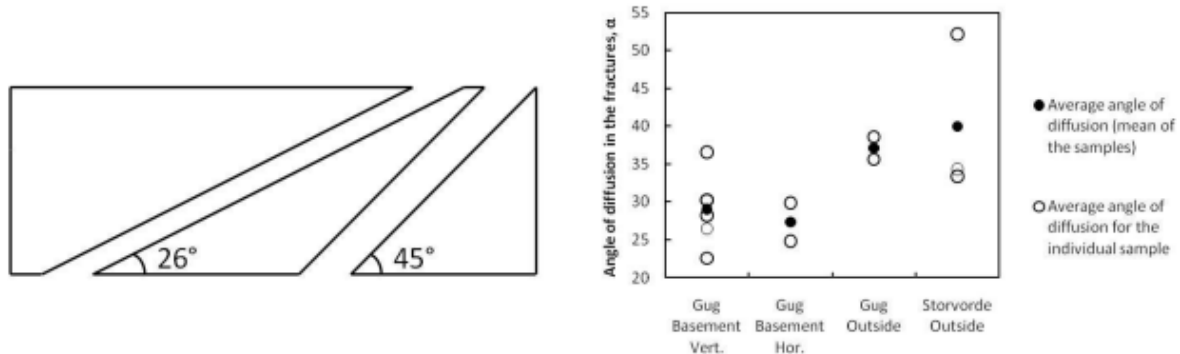
Fig. 4. Angle of diffusion, α, in the fracture network: (a) Examples of α; (b) for the considered samples.

Conclusions

- The three presented fingerprints provided us with valuable insights into both the fracture connectivity and matrix pore-connectivity.
- The two-parameter exponential model showed that the diffusivity in the fracture network is related to the diffusivity within the limestone matrix; a lower diffusivity in the fracture network will result in a low diffusivity in the limestone matrix.
- The modified Buckingham (1904) connectivity factor X^* gives a fingerprint of the limestone matrix. It shows that the tortuosity inside the limestone matrix is related to compaction. A higher tortuosity will cause a higher value for X^*.
- The average angle of diffusion, α, gives a fingerprint of the fracture network in the limestone. Less compaction results in higher values for this parameter.

Bibliography

Ball, BC 1981, 'Modelling of soil pores as tubes using gas permeabilities, gas diffusivities and water release', *Journal of Soil Science*, vol 32, no. 4, pp. 465-481.

Hamamoto, S, Perera, MSA, Resurreccion, A, Kawamoto, K, Hasegawa, S, Komatsu, T & Moldrup, P 2009, 'The Solute Diffusion Cofficient in Variably Compacted, Unsaturated Volcanic Ash Soils', *Vadose Zone Journal*, vol 8, no. 4, pp. 942-952.

Kristensen, AH, Thorbjørn, A, Jensen, MP, Pedersen, M & Moldrup, P 2010, 'Gas-phase diffusivity and tortuosity of structured soils', *Journal of Contaminant Hydrology*, vol 115, no. 1-4, pp. 26-33.

Moldrup, P, Hamamoto, S, Kawamoto, K, Komatsu, T, de Jonge, LW, Schjønning, P, Jacobsen, OH & Rolston, DE 2010, 'Taking Soil-Air Measurements Towards Soil-Architectural Fingerprints', these proceedings.

Resurreccion, AC, Moldrup, P, Kawamoto, K, Yoshikawa, S, Rolston, DE & Komatsu, T 2008, 'Variable Pore Connectivity Factor Model for Gas Diffusivity in Unsaturated, Aggregated Soil', *Vadose Zone Journal*, vol 7, no. 2, pp. 397-405.

Soil-Gas Diffusivity Fingerprints of the Dual Porosity System in Fractured Limestone

Niels Claes, Deepagoda TKK Chamindu, Jacob Birk Jensen, and Per Moldrup

Aalborg University, Sohngaardsholmsvej 57, DK-9000 Aalborg, Denmark
nclaes09@student.aau.dk

Summary

The presence of fractured vadose zones (e.g., limestone or clay tills) may potentially pose significant environmental concerns due to the rapid, preferential migration of gaseous plumes through interconnected pore networks. However, recent modelling studies related to fractured vadose zone processes are mostly limited to hydrogeological (water and solute) transport studies with very poor attention to the gaseous phase transport studies (Kristensen et al. 2010).

This study characterizes fractured limestone soils for gas diffusion based on three different gas diffusivity fingerprints:

The first fingerprint is a two-parameter exponential model, which mainly describes the gas diffusivity in the limestone matrix while taking both fracture connectivity and matrix pore connectivity into account.

With the second fingerprint, we make a close observation of the tortuous matrix pore network by means of a modified Buckingham (1904) pore connectivity factor (X*).

The third fingerprint of the fracture network involves the average angle of diffusion α (Moldrup et al. 2010), a parameter which characterizes the average angle at which the fractures are penetrating the sample.

Method

In this study, we considered a total of 13 fractured limestone samples from literature (fig.1-2) which were sampled from two different vadose zone profiles in Denmark: Gug limestone and Storvorde limestone (data from (Kristensen et al. 2010)). From Gug limestone, we considered two samples (ID 37 and ID38) taken vertically just below the ground surface, six samples (ID 28 and ID GKUG 1 to 5) taken vertically under the basement of a house, and two samples (ID 25 and 26) taken horizontally under the basement of the same house. Three Storvorde limestone samples were retrieved vertically about 2 m below the ground surface.
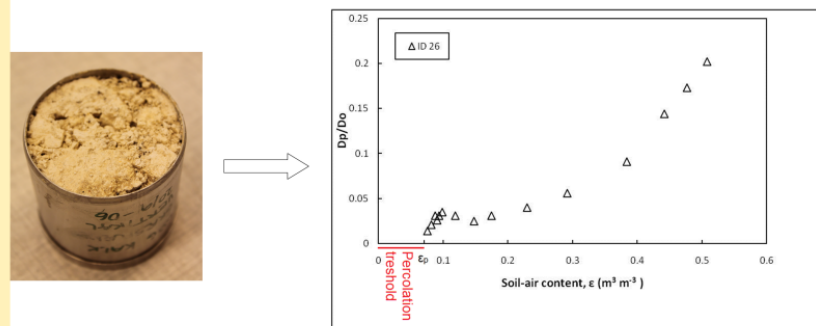
Fig.1 Example of a tested limestone sample and the result of the gas diffusivity experiment on the sample.

The results of gas diffusivity experiments (D_p/D_o, where D_p and D_o are, respectively, the gas diffusion coefficient in soil and in free air) against air content (ε) for all the 13 soil samples are analyzed in 2 different ways (fig.2).
The first analysis is an analysis of the three different fingerprints that are extracted from the measurements of the gas diffusivity experiment (D_p/D_o, ε). The second analysis takes the percolation threshold (ε_p) into account (D_p/D_o, ε-ε_p)(fig.1).This threshold is caused by inactive pore-space which results in a delay in increase in diffusivity with increasing soil-air content.
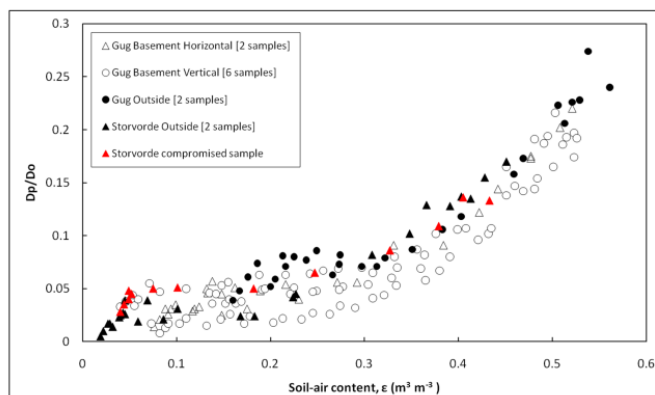
Fig.2 Overview of the gas diffusivity (Dp/Do) against air content (ε) of all the limestone samples

3 Fingerprints

The three different parameters are presented with an overview of the results for both analyzing methods (without and with taking the percolation threshold into account):

1. Two-parameter (A,B) Exponential Model

The non-linear increase in D_p/D_o within the matrix can be described by a two-parameter exponential model by taking into account both the fracture connectivity and the matrix pore-connectivity.

$$D_p/D_0 = Ae^{B\varepsilon} \; ; \; \varepsilon \geq \varepsilon_0$$

A: Fracture Connectivity Factor
B: Internal (Matrix)Connectivity Factor
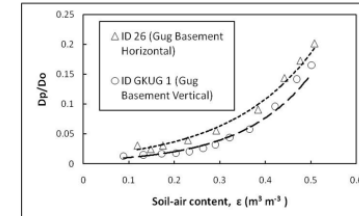ε_0: Soil air content at which all the fractures are fully drained
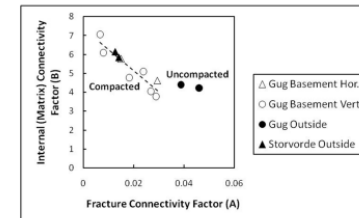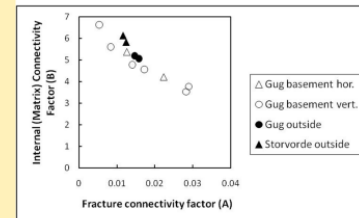
Fig.3 Example of two-parameter model.

Fig.4 Relation between fracture connectivity and internal connectivity: (left) Analyses without percolation threshold (right) Analyses with percolation threshold.

2. Internal Buckingham Pore-connectivity Factor (X*)

A Modified Buckingham (1904) model for the matrix diffusivity is applied. Buckingham (1904) suggested:

$$\frac{D_p}{D_0} = \varepsilon^X$$

With X typically equal to 2.

We suggest inside the limestone matrix:

$$\frac{D_p - D_{p0}}{D_0} = (\varepsilon - \varepsilon_0)^X$$

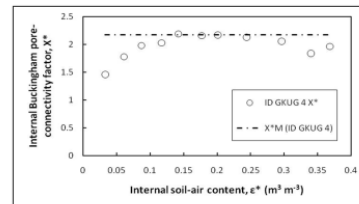Where D_{p0} and ε_0 are gas diffusivity and air-filled porosity at the condition of fully drained fractures.

*Fig.5 Example of the upper Buckingham pore-connectivity factor, X*M*

The upper Buckingham pore-connectivity factor, X*M (fig.5), which is the average value of the three highest X* factors for each sample, are compared as a characterization of the tortuosity inside the limestone matrix.
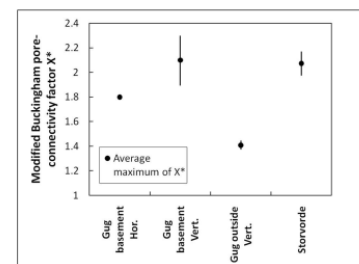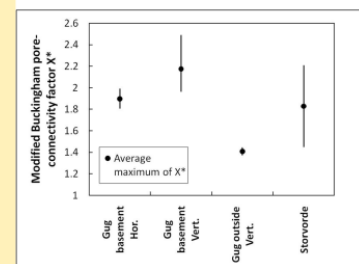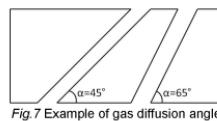
Fig.6 The interval and average of the maximum values for X: (left) Analyses without percolation threshold (right) Analyses with percolation*

3. Average Angle of Diffusion, α

The orientation of fractures is an important characteristic governing most of the fractured media transport processes. In the third fingerprint, therefore, we observed the average angle of diffusion α (Moldrup et al. 2010) for the selected four soil groups.
The, average angle of diffusion (fig.7) can be calculated as:

$$\alpha = \sin^{-1}(\sqrt{D_p/(D_0\varepsilon_0)})$$

Fig.7 Example of gas diffusion angles

The observed smaller angle of diffusivities for the samples taken below the basement compared to the samples taken from outside (fig.8) can be attributed to the high soil compaction below the building foundation.
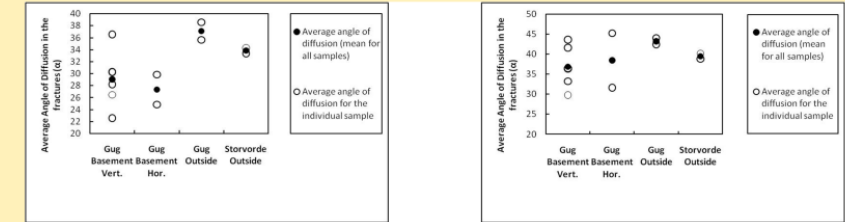
Fig.8 Average angles of diffusion in the fractures for the different samples: (left) Analyses without percolation threshold (right) Analyses with percolation threshold.

Merging the fingerprints together

Fracture Network

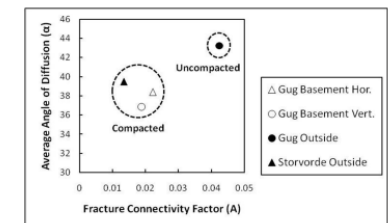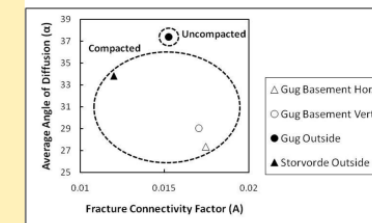Fracture Connectivity Factor (A) ↔ Average Angle of Diffusion (α)

Fig.9 Relation between the fracture connectivity and average angle of diffusion in the fractures (left) Analyses without percolation threshold (right) Analyses with percolation threshold.

Limestone matrix

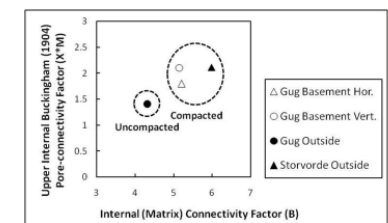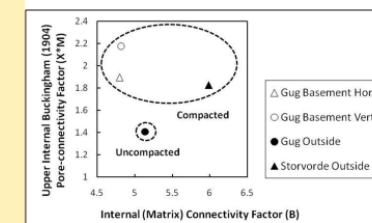Matrix Pore-connectivity Factor (B) ↔ Internal Pore-connectivity Factor (X*)

Fig.10 Relation between the matrix pore-connectivity and the internal pore connectivity (left) Analyses without percolation threshold (right) Analyses with percolation threshold.

Conclusions

The three presented fingerprints provided us with valuable insights into both the fracture connectivity and matrix pore-connectivity:

. The two-parameter exponential model showed that the diffusivity in the fracture network is related to the diffusivity within the limestone matrix; a lower diffusivity in the fracture network will result in a low diffusivity in the limestone matrix.

. The modified Buckingham (1904) connectivity factor X* gives a fingerprint of the limestone matrix. It shows that the tortuosity inside the limestone matrix is related to compaction. A higher tortuosity will cause a higher value for X*.

. The average angle of diffusion, α, gives a fingerprint of the fracture network in the limestone. Less compaction results in higher values for this parameter.

The difference in results for the three fingerprints when taking the percolation threshold into account, illustrates that the inactive porespace should not be neglected in the analyses.

References

Buckingham E (1904) 'Contributions to our knowledge of the aeration of soils'. *Bur. Soil Bull.* 25. (U.S. Gov. Print. Office: Washington, DC).

Kristensen, AH, Thorbjørn, A, Jensen, MP, Pedersen, M & Moldrup, P 2010, 'Gas-phase diffusivity and tortuosity of structured soils', *Journal of Contaminant Hydrology*, vol 115, no. 1-4, pp. 26-33.

Moldrup, P, Hamamoto, S, Kawamoto, K, Komatsu, T, de Jonge, LW, Schjønning, P, Jacobsen, OH & Rolston, DE (2010), 'Taking Soil-Air Measurements Towards Soil-Architectural Fingerprints', *this poster session at the CESAR conference* .